SURFACE COMPLEXATION MODELING OF COAL COMBUSTION RESIDUALS CONSTITUENTS ON NATURAL HYDROUS FERRIC OXIDE

by

Austin Michael Willoughby

A thesis submitted to the faculty of
The University of North Carolina at Charlotte
in partial fulfillment of the requirements
for the degree of Master of Science in
Civil Engineering

Charlotte

2018

Approved by:

_____
Dr. John Daniels

_____
Dr. William G. Langley

_____
Dr. Shubhashini Oza

© 2018
Austin Michael Willoughby
ALL RIGHTS RESERVED

ABSTRACT

AUSTIN MICHAEL WILLOUGHBY. Surface complexation modeling of coal combustion residuals constituents on natural hydrous ferric oxide. (Under the direction of DR. WILLIAM G. LANGLEY)

Coal ash impoundments, along with other industrial and natural processes, can be sources of constituents of concern (COCs) to human health including arsenic (As), chromium (Cr), selenium (Se), and vanadium (V). Attempts to model the fate and transport of these COCs within subsurface aqueous environments often rely on extensive laboratory batch experiments to develop distribution coefficients (K_d values) for model input. Surface complexation theory can also explain the partitioning of constituents between the liquid and solid phases, with hydrous ferric oxide (HFO) often acting as a dominant solid phase adsorbent. While useful, such model descriptions generally apply to pure mineral phases and do not investigate natural adsorbents. This study applies surface complexation theory in the form of the generalized two-layer model (GTLM) to natural soils from coal ash sites by modeling the laboratory batch experiments used to generate soil isotherms and soil K_d values.

Laboratory batch experiments equilibrated different ratios of soil solid phase with a synthetic groundwater solution liquid phase containing As, Cr, Se, and V, allowing for solution equilibrium and isotherm generation. Modeled batch solid phases were represented by surface concentrations of hydrous ferric oxide derived from two sequential extraction procedures: one utilizing a modified Citrate-Bicarbonate-Dithionite (CBD) method, and another using an acidified hydroxylamine (Chao) solution. Model liquid phases were input by creating representative synthetic groundwater solutions

within the model. The defined phases were then equilibrated within the model so that isotherms and K_d values could be generated for all COCs.

Experimental and modeled results were statistically analyzed and the relative error (RE) of the modeled K_d values to their experimental counterparts was calculated. Overall Chao extraction method showed little to no correlation with experimental results, shifting the focus of discussion to CBD method. Modeled CBD method As and Se results showed moderate correlations with experimental results; however, model K_d values tended to trend lower than experimental making them conservative. CBD method V results showed slight correlation with experimental data; however K_d values trended higher than experimental and were not conservative. CBD method Cr results indicated no correlation, with little apparent connection to experimental results and K_d values which were far larger and thus not conservative.

Probable reasons for inconsistencies between model and experimental data include discrepancies between actual HFO content in soils and HFO calculated from sequential extraction, the exclusion of adsorptive mineral phases from the component additivity model, PHREEQC database equilibrium constants derived from pure mineral phase isotherms rather than natural soils, and the potential introduction of unknown constituents into solution from soil samples. While the Cr and V models used are likely too inaccurate for practical use, As and Se models show potential. With reasonable modification, As and Se models can return conservative K_d value estimates representative of natural soils.

The main body of this work is supplemented with additional files including model and experimental isotherms, PHREEQC inputs and outputs, and the PHREEQC database

utilized herein. Model and experimental isotherms are presented in the form of a spreadsheet with a .xlsx file type. PHREEQC files include both the .pqi and .pqo file types, and require the PHREEQC software provided by the United States Geological Survey (USGS). The database is included as a .txt file and must be designated as the default database within PHREEQC. Additional supplemental file information can be found in Appendix C.

DEDICATION

I dedicate this work to my parents, Michael and Deanna Willoughby, whose encouragement and support have paved the way for my academic achievements.

ACKNOWLEDGEMENTS

I would like to extend a special thanks to those who made this work possible. To the UNC Charlotte Civil and Environmental Dept. for the use of its facilities and equipment; to my fellow research assistants for their dedication to our experiments; to my friends for distracting me when needed; to my thesis committee chair Dr. Daniels, for providing such high-caliber research projects to the department; and especially to Drs. Langley and Oza for their support, both intellectually and emotionally, in the creation of this work. Thank you all.

TABLE OF CONTENTS

LIST OF TABLES

LIST OF FIGURES

LIST OF SYMBOLS/ABBREVIATIONS

As	arsenic
CBD	citrate-bicarbonate-dithionite solution
CCR	coal combustion residual
Chao	acidified hydroxylamine solution
COC(s)	constituent(s) of concern
Cr	chromium
DDL	Diffuse Double Layer
DI	deionized
EPA	United States Environmental Protection Agency
FGD	flue gas desulfurization
GTLM	generalized two-layer model
HFO	hydrous ferric oxide
HDPE	highly dense polyethylene
Kd Values	soil batch distribution coefficients
LDL	lower detection limit
NCDEQ	North Carolina Department of Environmental Quality
RCRA	Resource Conservation and Recovery Act
RE	relative error
Se	selenium
USGS	United States Geological Survey
V	vanadium

CHAPTER 1: INTRODUCTION

1.1. Background

Over the past century, energy production in the United States has been dominated by the burning of fossil fuels like coal, natural gas, and petroleum. Coal has been the largest source of electricity with a 30% share of production attributed to it in 2017 (EIA 2018). This production occurs by combusting coal at a coal-fired steam station where the heat energy boils steam which in turn rotates turbines. Coal combustion inevitably leaves residuals in the forms of fly ash, bottom ash, boiler slag, and flue gas desulfurization (FGD) waste. These individual material streams are managed differently and are collectively described as coal combustion residuals (CCR). In 2014 it is estimated that 129,684,142 short tons of CCR were produced in the US (ACAA 2015). This enormous quantity of CCR has generally been stored in onsite unlined landfills or impoundments. In December, 2014 CCR storage practices changed when the EPA implemented legislation requiring coal ash waste be classified under Subtitle D of the Resource Conservation and Recovery Act (RCRA). This legislation classifies CCR as a non-hazardous industrial solid waste (EPA 2015).

While the new legislation requires the storage of CCR in lined enclosures, the pre-existing unlined ponds and landfills have contributed to environmental issues including impoundment dam stability, leachate generation, and groundwater contamination. Groundwater contamination is the primary focus of this study, and results from the leaching of COCs present in CCR impoundments or landfills.

Leached COCs have the capacity to enter aquifers and create groundwater concentrations above those standards set by the EPA and local agencies like the North

Carolina Division of Environmental Quality (NCDEQ). Once in the aquifer these COCs are transported through the subsurface environment by means of groundwater flow. The mobility of COCs is dependent on their solubility in groundwater which is controlled by the geochemistry of the subsurface system, as well as the properties of the COC. The four COCs examined within this study include As, Cr, Se, and V, and the main mobility factor of these COCs is adsorption through surface complexation. Adsorption occurs when a constituent has an affinity for the surrounding porous media and adsorbs onto the soil particle's surface. A constituent's affinity for a surface, and thus its mobility, will vary according to the surrounding system's geochemical properties, particularly pH and Eh. (Berkowitz et al. 2014)

COCs within an aquifer can be transported towards vulnerable areas like potable wells and areas of groundwater discharges into surface waters. COCs consumed at elevated concentrations can harm humans and natural organisms alike (Berkowitz et al. 2014). To avoid these deleterious effects, an understanding of constituent transport and the controls thereof is necessary. Specifically, accurate modeling of constituent transport within subsurface systems can be useful to those making CCR related decisions. This study is intended to expand on constituent transport models through exploration of practical uses for geochemical surface complexation models.

1.2. Scope of Research

The primary objective of this study was to describe the relationship between coal ash related COC K_d values obtained through laboratory experiments, and those obtained through surface complexation modeling of extracted HFO. Upon comparison, the modeled K_d values were evaluated for use in practical applications. Two HFO extraction

procedures were utilized to provide multiple independent concentrations as seen in Table 1. The first utilized an acidified hydroxylamine solution developed by Chao and Theobald to extract HFO from soil samples (Chao and Zhou 1983). The second HFO extraction procedure utilized a CBD extraction solution developed by M.L. Jackson which was modified slightly for project needs (Mehra and Jackson 1960). The modification entailed using 5 extra ml of sodium citrate solution and excluded the use of acetone. Surface complexation modeling was used to generate theoretical isotherms using the geochemical modeling software PHREEQC, and laboratory isotherms using the batch and analytical techniques in accordance with EPA Technical Resource Document EPA/530/SW-87/006-F. PHREEQC is a text based software developed by the US Geological Survey to computationally model aqueous systems.

Generated model isotherms were compared with experimental isotherms primarily through the correlation of their corresponding K_d values, but also through comparison of K_d value trends relative to sample HFO concentration. Model and experimental correlations were determined through use of the RE function, which shows the percent error of modeled values compared to those of experiments. Further statistical analysis was completed and resulting data was quantified and visualized to assist in the derivation of any trends.

CHAPTER 2: LITERATURE REVIEW

2.1. Adsorption

Adsorption plays a dominant role in subsurface trace element transport. The process can occur in any system which has both a liquid and solid interface and is a particularly important mechanism when considering the subsurface environment due to the high surface area of porous mediums. Adsorption is defined as the net accumulation of constituents on the solid phase at the aqueous or gaseous interface. When adsorption occurs, the solid phase is considered the adsorbent and the aqueous particle is the adsorbate (Berkowitz et al. 2014). This attraction or bond can occur between electrically charged particles, as well as nonionized surface sites and constituents. This is due to electrical and chemical interactions between the adsorbent and adsorbates (Dzombak and Morel 1990).

It is this attraction which causes a constituent to adsorb and thus become removed from the aqueous solution. The removal from the bulk phase is what makes adsorption significant to subsurface transport. Upon adsorption, a COC will either become part of the solid phase, or more likely desorb back into the bulk solution after a time. While adsorption is not necessarily a constituent sink, this time spent adsorbed to the solid phase will serve to attenuate the mobility of the constituent. This attenuation is known as retardation, and is a useful phenomenon to quantify when modeling groundwater systems (Berkowitz et al. 2014).

To quantify this retardation, one must first measure adsorption. This is done by carrying out lab experiments in which porous media and aqueous solutions can reach equilibrium. Upon equilibrium, the measured adsorption onto the solid phase is plotted

as a solid concentration against the concentration of adsorbate in the aqueous phase. The graph that results from this process is known as an adsorption isotherm and has been described mathematically by multiple adsorption models. These models include the simple K_d model, as well as the Langmuir and Freundlich models(Berkowitz et al. 2014). The GTLM of David Dzombak and François Morel is a more modern computational based adsorption model and is the basis for the modeling performed in this study. The GTLM and is described in depth within section 0.

2.1.1. Distribution Coefficient

The distribution coefficient (K_d value) is a simple but useful model used to describe the partitioning of COCs between the solid and liquid phases. It is the most common description of a COCs solid phase affinity within fate and transport models. Within a batch procedure, it is empirically derived by plotting the measured solution COC concentration versus the calculated adsorbed solid phase COC concentration for all liquid to solid batch ratios (i.e. an isotherm), and then determining the slope of the linear line of best fit (EPA 2004).

While useful, concerns have been raised that the intricate nature of COC-soil adsorption is too complex to be modeled with a K_d approach. Robust models that can further describe the dynamic interactions occurring between adsorbents and adsorbates can be useful; however situations favorable for K_d can still occur. Such circumstances include batch experiments entailing reversible reactions and linear isotherms. Evaluations of K_d based approaches to evaluate the transport of trace metals have in the past successfully held up against computational, laboratory, and field data. Due to this

ease of use and reasonable accuracy, K_d values are viable and practical means of describing trace metal mobility (Daniels and Das 2014).

2.1.2. Langmuir Isotherm

The Langmuir equation was originally derived from gas to solid interfaces and consequently has some strict assumptions. It assumes that the adsorbate bonds to the solid phase at a specific, homogeneous, localized site, creating a monolayer (one molecule thick layer). It also assumes there are no cross interactions between adsorbed molecules, equilibrium within the system is attained, the heat of adsorption is constant, and that temperature does not affect the energy of adsorption. The equation is as follows:

$$\frac{x}{m} = \frac{KCb}{1 + KC} = \frac{Kb}{\frac{1}{C} + K}$$

x = amount of adsorbed chemical
m = mass of adsorbent
C = equilibrium concentration
K = bonding strength constant
b = maximum possible adsorbent that can be adsorbed

These parameter values are determined by plotting the K_d value, which is the ratio between the amount of adsorbed constituent at equilibrium per mass of adsorbent (x/m) and the concentration of constituent in solution (C):

$$K_d = \frac{x/m}{C}$$

The Langmuir equation is applicable when plotting K_d values against x/m at a relatively low C yields a straight line; however the restrictive assumptions of the equation may make such a task difficult. When dealing with the heterogeneous materials present in a natural subsurface environment, one may find a large discrepancy between models and results. These can be resolved through corrections supplemented into the equations

which account for coupled adsorption-desorption reactions, and adsorption of trace elements on geosorbents. Other models may also be used in place of the Langmuir equation such as the Freundlich isorherm(Berkowitz et al. 2014).

2.1.3. Freundlich Isotherm

The Freundlich isotherm accounts for the decrease in adsorption energy due to the decrease in available adsorption sites over time. Unlike the Langmuir equation, the model was derived empirically and assumes multilayer adsorption. The model uses the equation

$$\frac{x}{m} = KC^{1/n}$$

to fit adsorption data from low concentrate solutions where *n* and *K* are constants. The Freundlich equation is limited in that it doesn't predict a maximum adsorption capacity. It instead models adsorption interactions of dilute solutions with low solute concentrations and low sorbent loading which appear to be linear. Despite this limitation the Freundlich equation is broadly used to describe constituent adsorption, especially on geosorbents. However, the model will require modifications when at least one of the component variables causes the isotherm to depart from linearity (Berkowitz et al. 2014).

2.2. Constituents of Concern

There are countless COCs within the realms of groundwater science. These constituents can range from complex organic pharmaceuticals, to heavy metals, to hydrocarbons. When in relation to coal ash waste, the primary COCs are metals with the potential to leach from the ash pond or landfill. The COCs discussed in this study can be classified as either heavy metals, metalloid, or nonmetal due to their placement on the periodic table. They are dense and are often toxic at relatively low concentrations. All of

the COCs are naturally occurring components of the Earth's crust which can neither be degraded nor eliminated, but can affect humans and wildlife alike through ingestion of contaminated food and water (Berkowitz et al. 2014).

While many of these COCs, (e.g. Se and copper) are used in biological processes such as catalytic functions, higher concentrations can harm biological organisms. Specifically, they can disrupt the metabolism through their ability to act as redox catalysts. This ability causes oxidative damage to cellular structure, DNA, and enzyme processes. As evident by these effects many heavy metals can result in both acute and chronic issues (Berkowitz et al. 2014).

While CCR is composed of and may leach many constituents, this study only considers a limited number of the most common. Laboratory experiments yielded isotherms for As, boron, cadmium, Cr, molybdenum, Se, thallium, and V; however the model only created isotherms for As, Cr, Se, and V due to their environmental significance and potential impact to humans and natural organisms alike. For these reasons it is useful to understand the health risks a constituent poses to humans, as well as their behavior within natural systems.

2.2.1. Arsenic

As is a heavy metaloid and natural trace element commonly found in subsurface environments. It is harmful to both human and animal health and has been a well-known poison for centuries. Large doses of As over 60,000ppb in water can result in death, while levels as low as 300ppb can lead to intestinal irritation and decreased production of blood cells. These health issues can lead to side effects such as nausea, vomiting, fatigue, and impaired nerve function. Aside from acute issues, As is also a well known

carcinogen, and can increase the risk of cancer throughout the body with extended contact (U.S. Department Of Health And Human Services 2007). Ingestions of As containing drinking water has affected the wellbeing of millions globally and caused thousands of deaths (Miller 2001). It is evident from these consequences, that As is a public health risk. It is thus useful to further understand As within the subsurface environment (U.S. Department Of Health And Human Services 2007).

Concentrations of As in the environment can increase due to natural and anthropogenic causes. These include mineral dissolution, pesticides, fly ash disposal, and geothermal discharge. When in natural conditions, As generally exists as inorganic species with redox states of arsenite (As(3)), or arsenate (As(5)). Of the two states, As(3) is significantly more toxic. Water quality standards in the United States establish that concentrations of As over 50ppb can be harmful to the public (Goldberg and Johnston 2001).

Depending on the pH, As(3) and As(5) will either exist as a neutral or anionic species. Both of these natural redox states can exist within a groundwater system due to the slow kinetics of the redox reactions involved. Regardless of the redox state, As species have been shown to have a strong affinity for metal oxides in soils. It is well documented in the literature that iron oxide, specifically ferrihydrite, surface complexation is the controlling factor for As transport (Miller 2001). It is also shown that reducing conditions may cause As to become more soluble, causing elevated concentrations of As and demonstrating the difference between adsorption capacity of the two redox states. Adsorption capacity variances occur in part because As(5) is suggested to bond to the solid phase through inner sphere complexes, allowing for a stronger bond

than As(3). This also explains why As(III) is more sensitive to ionic strength than As(5) (Goldberg and Johnston 2001).

Models of As behavior are currently useful in simple systems; however systems with excess geochemical variables have proven difficult to describe. Further research into As geochemistry is needed before accurate evaluation of natural As behavior can be understood (Miller 2001).

2.2.2. Chromium

Cr is another heavy metal which can occur naturally or through artificial means. High levels of Cr in the environment are usually a result of industrial activities. In natural groundwater conditions Cr will exist in two different oxidation states, Cr(6) and Cr(3). While composed of the same elements, these two oxidation states act very differently. When in contact with humans, Cr(6) is considered roughly 1000 times more toxic than Cr(3). It can cause symptoms like nausea, vomiting, diarrhea, internal hemorrhage, and liver and kidney damage (Kalhori et al. 2013). Due to Cr(6)'s high level of toxicity, it has become strictly regulated; however some of its inherent properties make regulatory control difficult.

In a groundwater system Cr(6) will exist in higher concentrations due to high solubility. This high affinity for the liquid phase makes Cr(6) much more mobile than its reduced state (Kalhori et al. 2013). Cr(3) on the other hand is the most stable of the two species under typical environmental conditions. This form of Cr has very low solubility and is considered highly adsorptive. Cr(3) thus has a low environmental mobility and is of concern only when conditions are favorable for oxidizing the constituent (Kent et al.

1994). Due to the geochemical controls involved in Cr toxicity it is deemed valuable to further understand subsurface systems containing Cr.

2.2.3. Selenium

Se is a relatively heavy metalloid which is found naturally in soil at trace amounts. It is an important element within human nutrition, with an adult daily recommended intake of 55 µg/day. While Se may be helpful to the body at low doses, daily levels above 400 µg/day are not recommended. Research has indicated that higher doses between 1.5 and 6 mg/kg of body mass can stunt developmental growth and prove mortally toxic to laboratory animals. Cases of excess Se consumption in humans have resulted in side effects including hair loss, weak nails, gastrointestinal problems, and neurological issues. Routes of human exposure generally include most foods, especially protein rich ones, and groundwater. Due to its deleterious effects on human health and its presence in groundwater, interest in Se's behavior within aquatic environments has risen (WHO 2011).

Within natural conditions Se will exist in the redox states Se(2-), Se(0), Se(4), and Se(6). Selenite (Se(4)) and selenate (Se(6)) are the most common redox states of Se in groundwater due to their relatively high solubility, aversion to redox speciation, and slow kinetics. Depending on the treatment process, it can be challenging to remove these constituents from solution. Selenate tends to be the more difficult of the two, with coagulation, lime clarifications, and filtration through activated carbon proving ineffective in the removal process. Instead, adsorption onto iron and aluminum coated particles proves to be more useful in the removal of both forms of Se (WHO 2011).

Within subsurface aquatic environments, Se(6) is generally the more mobile state of the two, with Se(4) exhibiting a higher affinity for the solid phase. Se speciation between the two is mostly a function of redox potential, with Se(4) existing as the dominant species in moderate groundwater redox conditions and Se(6) predominantly existing in high Eh conditions. It is thus evident that Se will increase its mobility within highly alkaline aquifers, creating a need to understand the geochemical processes relevant to Se (Fernández-Martínez and Charlet 2009).

2.2.4. Vanadium

V is another example of a naturally occurring element which is essential to life; however, it is chronically toxic at aqueous concentrations as low as 20ppb. At nominal levels, V plays a part in regulating sugar levels in the body, and is a part of enzyme systems (Bağda 2014). At higher levels of ingestion the metal can cause issues within the gastrointestinal tract and hematological system. Symptoms of these issues include nausea, diarrhea, stomach cramps, decrease in blood cells, and decrease in hemoglobin. V is generally released into the environment at excess levels through the burning of fossil fuels (U.S. Department of Health And Human Services 2012).

It is because of these adverse effects that V is listed on the EPA's Contaminant Candidate List 3. It is a complex constituent due to the large multitude of different molecular arrangements and chemical reactions which occur in subsurface environments. V has a high affinity for oxygen which allows it to chemically speciate into both oxycations and oxyanions. Within natural systems, V will exist in three oxidation states: V(5), V(4), and V(3). In a natural groundwater with oxygenated conditions, V(5) is the prevailing oxidative state, and will exist in the form of $H_2VO_4^-$ or HVO_4^{2-}. V(4) can exist

under slightly reducing conditions, and has a high affinity for surface oxides relative to V(5). In relatively extreme natural reducing conditions, V(3) will occur at many pH values; however according to studies it may not be as important in groundwater as the other two species (Wright et al. 2014).

Previous models have shown that V(5) species will not precipitate when in an oxic environment. This behavior points towards adsorption and desorption at surface oxide sites as the primary mechanism governing V solubility. With adsorption as the primary mechanism, it is expected that V concentrations will increase as pH increases. This is because the surface sites will deprotonate at higher pH's, thus gaining a negative charge. At high pH's it has been shown that V is mostly in the V(5) redox state, which will exist as an oxycation. The oxycation will in turn avoid adsorption with the negatively charged surface sites, causing the elevated concentration of V. At lower pH's V is expected to adsorb to the solid phase as the surface sites become protonated and more positive, like the anion adsorption described in the General Two Layer Model described by Dzombak. This adsorption is believed to be an inner sphere complexation (Wright et al. 2014).

V likely has a higher affinity for amorphous or poorly crystalized oxides. Once sorbed to Fe or Mn oxides, it can desorb through dissolution processes such as proton promoted, ligand-promoted, and reductive dissolution processes. Of these mechanisms, reductive dissolution is the most common; however the conditions required for reductive dissolution will generally make V precipitate. It has thus been hypothesized that V does not mobilize when oxic conditions become anoxic (Wright et al. 2014). Previous V adsorption isotherms have yielded no significant effect of pH on V adsorption. This

leads one to believe that the adsorption capability of the solid media is more important than small changes of pH (Wright et al. 2014).

2.3. Hydrous Oxides

Hydrous oxides are useful indicators of adsorption due to their prevalence within natural soils, their propensity to coat particles, and their affinity for trace metals. The combination of these factors generally makes hydrous oxides the dominant control, or at least a significant influence, of trace metal adsorption. In nature there are several common hydrous oxides, the most abundant of which include iron, aluminum, manganese, and silicon oxides. These oxides generally exist as a solid mixture rather than in their pure mineral phases and are amphoteric in nature (Dzombak ad Morel 1990). While adsorption data is often described through means of isotherm equations and partitioning coefficients, the adsorption of inorganic ions onto hydrous oxides relies heavily on factors such as pH, Eh, ionic strength, and competing ions (Berkowitz et al. 2014). With large quantities of thermodynamic data available, prevalent hydrous oxides can be used to model adsorption within a range of geochemical conditions rather than conducting laboratory experiments to quantify adsorption (Dzombak ad Morel 1990).

Surface complexation reactions which occur on similar hydroxyl groups such as gibbsite (HAO), goethite, and HFO generally demonstrate comparable surface complexation constants and reactivity for the same adsorbing ions. This similarity occurs because the reactive surface hydroxyl group determines the reactivity of the hydrous metal oxide surface. Hydrous manganese oxide (HMO) reactions and surface complexation constants have been more difficult to measure due to the many redox states at which HMO exists in nature. These multiple redox states make it difficult to

synthesize an HMO coated solid phase with consistent geochemistry in the lab, thus making HMO experimental data vary more widely than its mineral cousins. The end results are HMO complexation constants and reactions that are less consistent with those of HFO and HAO; however the modeling data is valuable nonetheless due to their similar order of affinity with HAO and HMO constants (Dzombak and Morel 1990).

2.3.1. HMO

Soils generally contain a much higher concentration of iron oxides than manganese oxides; however manganese oxides are still considered significant in contaminant transport due to their higher chemical reactivity, as well as their large multitude of mineralogical species. Mn oxides consist of over 30 different mineral species, while Fe oxides consist of about half a dozen. Mn oxides are typically more reactive than Fe oxides because they can exist in multiple oxidation states, form nonstoichiometric oxides with different valence states, exist in multiple crystalline and amorphous forms, and can form solid solutions with Fe oxides (Tonkin et al. 2004). Due to the complex nature of HMO and the desire for a simplistic model, HMO was not utilized in the development of this model.

2.3.2. HFO

Hydrous ferric oxide (HFO) is an abundant amorphous solid which commonly coats soil particles. It is formed by rapid hydrolysis of ferric iron solutions at common environmental temperatures and is denoted as ferrihydrite when found in nature. HFO gets its amorphous characteristic from the highly porous nature of its aggregated particles. The porosity allows for increased water content which in turn gives HFO a gel-like consistency rather than a solid structure (Dzombak and Morel 1990).

The actual bulk structure of the HFO solution is unclear; however its chemical composition is represented by the stoichiometric formula $Fe_2O_3 \cdot nH_2O$ where *n* varies from 0 to 3. Its surface area is large due to high porosity, and is estimated to be $600 m^2/g$. It is upon the HFO surface that adsorption occurs between constituents and adsorption sites. These sites can be segregated in to two different types. Type 1 sites are less common and are considered high-affinity cation binding sites. These sites are not utilized in this study due to the anionic nature of COC. Type 2 sites are far more abundant than type 1 and represent the total reactive sites available for adsorption of protons, cations, and anions (Dzombak and Morel 1990).

Estimates of the density of type 1 and 2 sites vary from 0.001 to 0.01mol/mol, and 0.1 to 0.3mol/mol respectively. These ranges are adequately close to allow for the use of only one defined site density for each site type. Type 1 site density is defined as 0.005mol/mol Fe, while type 2 sites are defined as 0.2mol/mol Fe. Since these defined values lie within a range of estimated values it is acceptable to adjust site densities to describe a particular sample of HFO (Dzombak and Morel 1990).

2.3.3. HAO

Aluminum (Al) is the most common element in the lithosphere and generally makes up about 7% of soils. In natural systems Al is mostly present in the form of oxides and aluminosilicates due to elemental Al's reactivity. These aluminum oxides and hydroxides, or HAOs, can both influence the chemistry of soil, sediment, groundwater, and surface water systems due to their sorptive properties. Similar to other hydrous metal oxides, HAO will adsorb ions and anions and plays a role in subsurface transport

(Karamalidis and Dzombak 2010). While HAO is important in surface complexation modeling, it is not considered within this model for simplicity.

2.3.4. Hydrous Oxide Extraction

To accurately model surface complexation onto hydrous oxides, one must have an accurate measurement of the hydrous oxide. These concentrations can be determined through different extraction procedures. The procedures used in this study include a modified version of the dithionite-citrate with sodium bicarbonate buffer (CBD) methods (Mehra and Jackson 1960), and the acidified hydroxylamine (Chao) method (Chao and Zhou 1983). These two procedures offer different ways of dissociating HFO from soil particles.

2.4. Generalized Two Layer Model

There are a multitude of different models which describe constituent complexation with hydrous oxides; however they all have a few things in common. Each model assumes that constituent adsorption on oxides occurs at particular coordination sites, uses mass law equations to quantitatively define adsorption reactions on oxides, considers surface charge a possible product of adsorption reactions, and uses the electric double-layer (EDL) theory to account for the effect of surface charge on adsorption by applying a correction factor to mass law constants for surface reactions (Dzombak and Morel 1990).

The EDL theory states that a charged surface, such as a clay particle, is composed of a charged solid layer with an adjacent layer of counter charged ions present due to the electrostatic attraction. In cases of solutes with high concentrations, these counter ion

layers can precipitate onto the surface, creating a solid solution on the surface layer (Dzombak and Morel 1990).

Of all the modern computer-based surface complexation models, the simplest is the GTLM developed by David Dzombak and Morel. This model defines adsorption as a chemical reaction between solutes and clearly defined oxide surface sites. It differs from the EDL theory in that the number of binding sites on a surface limit the surface charge of the solid phase to a finite value. This limited surface charge is an improvement to the Gouy-Chapman model because it accounts for sensible amounts of counterions in solution instead of EDL's elevated concentrations. This improvement was initially done by Stern and Grahame's modified EDL theory, the Double Layer Model. Double Layer Model took the initial steps of considering specific adsorption sites, thus paving the way for the GTLM (Dzombak and Morel 1990).

These surface site chemical reactions consist of acid/base proton exchange, cation binding, and anion binding by means of ligand exchange between solute and hydroxyl site. These adsorption reactions must also follow a mass law equation with the sorbent, sorbate, and surface site concentrations acting as the variables. The equilibrium constant which will result from this mass law equation is composed of two individual terms, the chemical free energy of binding, and coulombic free energy of binding. These terms are coined "intrinsic" and "coulombic" respectively. The intrinsic term represents the chemical free energy involved in binding to a specific site, while the coulombic term represents the binding energy present due to the electrostatic charge on the surface phase. Materials which are bonded due to the intrinsic term are dubbed specifically sorbed, and have the ability to give an uncharged surface a charge (Dzombak and Morel 1990).

It is impossible to experimentally separate the chemical and electrostatic forces involved in adsorption; however it is useful to separate them in theoretical terms. This allows the model to account for a chemical reaction that does not vary with surface charge. The electrostatic force is then added to this chemical force, allowing for a more accurate model which fits experimental data (Dzombak and Morel 1990).

The coulombic term is considered an activity coefficient, and is a result of the EDL concept theorized by Gouy-Chapman. A columbic correction factor must be applied to model the constant variation in the acidity constant at diverse pH values. It must also be applied to the mass law constants for surface complexation reactions. When applied to the mass law equation it will describe the effect of pH and ionic strength on adsorption (Dzombak and Morel 1990).

2.4.1. Surface Acidity

Within the model, a diprotic acid depiction of surface sites is generally used to explain surface charge. The depiction is also useful since it simple and easily describes zero proton charge at the surface. These oxide surfaces will act as both an acid and a base due to the following surface ionization reactions

$$\equiv XOH_2^+ = \equiv XOH^0 + H^+ \quad K_{a1}$$

$$\equiv XOH^0 = \equiv XO^- + H^+ \quad K_{a2}$$

where $\equiv XOH_2^+$, $\equiv XOH^0$, and $\equiv XO^-$ represent positive, neutral, and negative surface hydroxyl groups, and K_{a1} and K_{a2} represent their relevant acidity constants. It is thus intuitive that the magnitude of surface charge is variable with pH, making pH a significant factor when modeling surface complexation (Dzombak and Morel 1990).

2.4.2. Anion Surface Complexation

As mentioned previously, the GTLM describes anions as adsorbing to a surface through ligand exchange processes which involve the exchange of surface hydroxyl groups with the sorbing ion. This interaction can be described with complexation reactions like the following

$$\equiv XOH^0 + A^{3-} + H^+ = \equiv XA^{2-} + H_2O \quad K_{1A}$$

and,

$$\equiv XOH^0 + A^{3-} + 2H^+ = \equiv XHA^- + H_2O \quad K_{2A}$$

where A^{3-} is a trivalent anion. Anion complexation models generally require between one and three such complexation reactions to remain accurate. The ligand exchange reaction shown has the propensity to create a relatively negative surface charge on the solid phase. Since many anions of concern are di- or triprotic weak acids that have the capability to become fully deprotonated within a relatively small pH range, more information is required regarding surface site types. Usually two or three surface species must be known to model anion adsorption, whereas cations only require one (Dzombak and Morel 1990).

The GTLM considers all proton exchange sites as viable adsorption sites for anions. This anion adsorption exhibits Langmuirian properties, such as surface concentrations proportional to solution concentrations, within a wide array of pH's. These properties indicate that there is often one type of binding site. Thus, the ionizable proton site density should be equal to the maximum adsorption density of an anion (Dzombak and Morel 1990).

The model also takes anion surface precipitation into account. These precipitation processes will occur at high anion concentrations, while complexation is associated with

lower concentrations. When precipitation occurs, a solid solution with a composition between that of the original surface and pure precipitate is formed on the solid surface. The chemical model reaction of precipitation for a trivalent anion on a hypothetical oxide is as follows

$$\equiv XHA^- + X^{3+} + A^{3-} = XA_{(s)} + \equiv XHA^- \quad \frac{1}{K_{spXA}}$$

Where K_{sp} represents the surface precipitation coefficient. Precipitation models such as these are necessary in addition to complexation models to fully describe anion transport (Dzombak and Morel 1990).

2.4.3. Cation Surface Complexation

Cation species in solution also have an affinity to complex with surface sites. During this process the cation will deprotonate a hydroxyl site and bond with surface oxygen. Example models include,

$$\equiv XOH^0 + M^{2+} = \equiv XOM^+ + H^+ \quad K_M$$

or,

$$\equiv XOH^0 + M^{2+} + H_2O = \equiv XOMOH_2^+ + H^+ \quad K_M$$

Where M^{2+} signifies a divalent cation. The first equation above is the equation used to define cation complexation, while the second equation is used only in precipitation. Surface complexation reactions such as these, along with acid/base reactions, comprise the equilibrium model used in the General Two Layer Model (Dzombak and Morel 1990).

Due to the apparent movement of protons seen in the model reactions, the cation complexation reaction is very sensitive to pH. Cations have a much higher affinity for complexation when there is a higher pH due to the ease of surface site deprotonation that

will occur in such conditions. Similar to anions, cations will also change the net charge of a surface; however the resulting charge will be more positive than that of anion complexation. When modeling, cations require two site types; however the same surface stoichiometry can be used for both. The $\equiv XOH^0$ site species is thus usually the only site type considered when modeling cation complexation. The sum of all possible cation surface binding sites will, as with anions, add up to equal the number of proton binding sites (Dzombak and Morel 1990).

Cation precipitation will occur at higher concentrations of cations in solution, and can be considered a continuation of complexation. Once a cation is complexed, a new hydroxide group is formed that in turn can react with more cations. Once the old cations are no longer in contact with the liquid phase, the cation is considered part of the solid solution. In other words, once the surface sites are saturated precipitation becomes the dominant process (Dzombak and Morel 1990).

2.4.4. Other Factors Affecting Surface Complexation

There are numerous other factors which can affect complexation. The GTLM considers solution complexation, where cations and anions can complex while in the liquid phase. These complexes may have different affinities for surface sites than their parent ions and may cause different adsorption reactions. Another factor is the activity coefficient of a given solution. The double layer model's coulombic term is effectively an activity term which is designed to correct for long range surface charge effects. Other non-ideal properties in the liquid phase, such as ionic strength, are accounted for with the solution activity coefficient (Dzombak and Morel 1990).

2.4.5. Generalized Two Layer Model Overview

The GTLM utilizes the Gouy-Chapman diffuse layer model to create an equilibrium adsorption model. The model accomplishes the task of successfully fitting experimental acid-base titration and cation and anion adsorption data for oxide surface sites. All specific adsorption is assumed to occur on the surface layer in the diffuse layer model, while the liquid phase contains the diffuse layer of ions. While the Gouy-Chapman model is an integral part of the GTLM, it expands this understanding of surface interactions by including two site types for cation binding, and surface precipitation for anions and cations. The model can thus be considered a combination of the surface precipitation model, the diffuse layer model, and the multisite model (Dzombak and Morel 1990).

2.5. Redox Disequilibrium

During the course of this study, it was noted that As adsorption in laboratory experiments yielded isotherms considerably different than those generated in the computational models. Upon further exploration, it was discovered that model output was substantially more accurate when As existed in As(3) form. After additional research into the literature, it was noted that As can exist in a state of redox disequilibrium for extended periods of time.

Substantial redox disequilibrium between As species is associated with biologically controlled redox transformation, dynamic systems with rapid change and large energy flux, and redox pairs in low concentrations where equilibrium calculations are sensitive to analytical and sampling errors(U.S. Department of the Interior Bureau of Land Management 1991). Due to the nature of the laboratory batch experiments, where

rapid changes in water chemistry were induced by researchers, it is likely that any redox disequilibrium was a result of the dynamic laboratory system.

When in equilibrium As(3) is the dominant species in strongly reducing aquifers and will undergo oxidation to As(5) in mildly reducing waters. In contrast, a dynamic system's proportion of As(3) and As(5) can differ greatly due to large redox gradients, large redox variations, and variations in past redox history. Due to the different behaviors of As(3) and As(5), redox speciation becomes important when considering chemical transport (Smedley and Kinniburgh 2001). Geochemical models such as PHREEQC rely on equilibrium calculations to describe geochemistry; however the kinetics of a redox reaction may not allow for field and laboratory data to support equilibrium. This is evident in other studies where As(5)/As(3) ratios were found outside of their theoretical thermodynamic equilibrium.

In particular, oxygenation of As(3) to As(5) by dissolved oxygen is believed to be a kinetically slow reaction, with some As(3) half-life estimates lasting up to a year. Other research found that As(5)/As(3) ratios were stable for days to weeks when anti-oxidation methods were not employed and that oxygenation is slowest when slightly acidic conditions (near pH 5) are present. There is also contradiction in the literature as to whether or not As redox couple ratios can be used as redox indicators, leading one to acknowledge that using As couples in Eh calculations may be an unreliable method (Smedley and Kinniburgh 2001).

The experimental conditions of this study appear consistent with many of the qualities associated with dynamic systems in disequilibrium. As was moved from a highly acidic stock solution with water quality parameters favorable to As(3) into the

synthetic groundwater solution, representing a fairly drastic change in aquatic chemistry for As molecules. Once created, synthetic groundwater generally had a pH of about 6, which is close to the slightly acidic conditions favorable to disequilibrium. Synthetic groundwater was also fully utilized in a batch experiment within one week of its synthesis, only allowing As a small timeframe to reach redox equilibrium. While it is unknown how exactly As(3) would have undergone redox speciation, it is possible that the kinetically slow route of DO oxygenation could have been the dominant pathway and required long equilibrium times. Due to these experimental similarities, as well as model results compatible with As(3) adsorption, As redox disequilibrium is hypothesized to describe the behavior of As adsorption within the laboratory batch experiments.

2.6. PHREEQC

PHREEQC is a hydrogeochemical modeling program developed by the USGS capable of performing various aqueous geochemical computations. It is used to simulate processes and reactions which occur within industrial activities, natural or contaminated water systems, and laboratory experiments. The software bases its simulations on ion-association aqueous models which allow for (1) speciation and saturation-index calculations; (2) batch-reaction and one-dimensional (1D) transport calculations with both reversible and irreversible reactions, which include equilibria of gas, mineral, solid-solution, aqueous, surface-complexation, and ion-exchange processes; (3) inverse modeling (Parkhurst and Appelo 2013).

Batch reactions are the primary focus of this study. When simulating batch reactions, PHREEQC will account for total system equilibrium instead of just aqueous equilibrium. The simulation thus has a multiphase equilibrium that distributes all moles

of constituents between the gas phase, aqueous phase, pure phases, solid solutions, exchange sites, and surface sites. Mole balances on oxygen and hydrogen are employed to account for pe and water mass changes. This accounts for any water-consuming or –producing reactions in the system. Temperature effects can also be accounted for through the Van't Hoff equation, while pressure, gas solubility, specific volume, and adsorption can be considered as well (Parkhurst and Appelo 2013).

Adsorption and desorption are either modeled as neutral ion exchange reactions, or surface complexation reactions. Ion exchange reactions can be modeled using the Gaines-Thomas or Gapcon conventions; however are not implemented in this study. Surface complexation can be modeled using two individual models. The first is Dzombak & Morel's double layer model mentioned above. The second is the Charge Distribution MUltiSIte Complexation (CD-MUSIC) model. CD-MUSIC is a triple layer model that also allows for multiple binding sites. The double layer model is the only model used in this study, and supplies PHREEQC with surface complexation constants. These constants are input into two databases which the program utilizes in its simulations. These databases are *phreeqc* and *wateq4f*. A third database is also viable for use in surface complexation calculations. This database is *minteq* which was taken from MINTEQA2, an EPA model for geochemists (Parkhurst and Appelo 2013).

The batch simulation allows for the definition of any quantity of solution compositions, gas phases, pure-phases, solid-solutions, exchanges, or surface-complexation groups. It also allows for any of the aforementioned assemblages to be brought together and reacted in a closed system until equilibrium is reached. This equilibrium will have the lowest possible Gibbs energy for the system (Parkhurst and

Appelo 2013). The batch simulation within the PHREEQC model can offer insight to lab experiments such as those conducted in this study.

CHAPTER 3: EXPERIMENTAL METHODS AND PROCEDURES

The methods of this study can be categorized into two main parts, laboratory experiments and computational modeling. Both experimental and computational aspects of the study performed identical processes independently of each other in order to assess the feasibility of computational strategies in comparison to experimental ones. A computational sensitivity analysis was also completed in an effort to more thoroughly understand the effects of pH and Eh on model output.

3.1. Laboratory Experiments

All laboratory investigations occurred at the University of North Carolina at Charlotte's state of the art environmental laboratory located within the Energy Production and Infrastructure Center. Experimental methods were generally identical to, or modified versions of the authoritative standards of which they were derived. Laboratory and modeling activities and methods are as follows:

3.1.1. Sample Storage and Preparation

In accordance with the groundwater assessment plan requested by the North Carolina Department of Environmental and Natural Resources (NCDEQ), Duke Energy provided soil samples from 14 NC coal ash sites to UNC Charlotte for K_d values determination. Between 8 and 14 samples were chosen for analysis for each site. Samples were meant to provide a suitable representation of the saturated zone surrounding and downgradient of the ash basin. Samples taken from the field were preserved in sealed plastic bags and stored on ice until they could be stored in a cold storage refrigeration unit at 4° C. Prior to testing the samples were disaggregated, homogenized, and air-dried at room temperature in aluminum pans. Once dried, samples

were sieved through a #10 U.S. standard mesh to attain a maximum grain size of 2 mm (Langley et al. 2015).

Samples were then weighed and placed in 250 mL wide-mouth high density polyethylene (HDPE) bottles with polypropylene screw tops (in accordance with U.S. Environmental Protection Agency (EPA) Technical Resource Document EPA/530/SW-87/006-F). Each individual sample was weighed out in five masses of 10, 25, 50, 75, and 100 grams, all of which were added into separate HDPE bottles (Langley et al. 2015).

3.1.2. Selective Extraction of Metal Oxy-hydroxide Phases

Selective extraction was necessary to determine concentrations of HFO present in soil samples without interference from other Fe containing minerals. HFO concentrations were determined through two different analytical methods adapted from the Chao (Chao and Zhou 1983) and CBD (Mehra and Jackson 1960) methods.

The Chao method for selective extraction of HFO called for shaking the soil sample with a 0.25*M* $NH_2OH{\cdot}HCl$-0.25M HCl combined solution as the extractant at 50° C for 30 minutes at a soil/liquid ratio of 0.1g/25mL. Extraction samples were shaken in a heated deionized (DI) water bath and run through a centrifuge. All samples were decanted and filtered through a 0.45-µm filter, as shown in Figure 1, and stored in 15mL centrifuge tubes at 4° C until analyzed. Extraction samples were analyzed using atomic adsorption spectroscopy (AAS) and Inductively Coupled Plasma Mass Spectroscopy (ICP-MS) to determine concentrations of extracted metals in solution (Langley et al. 2015).

The CBD method for selective HFO extraction called for the stirring of the soil sample with a combined 22.5 mL 0.3 M $C_6H_5Na_3O_4{\bullet}2H_2O$ (sodium citrate) and 2.5 mL 1

M $NaHCO_3$ (sodium bicarbonate) solution at 75° C with a soil/liquid ratio of 0.1g/50mL. During the heated stirring 0.2g of $Na_2S_2O_4$ (sodium dithionite) powder was added once the solution reached the desired temperature. After 15 minutes of periodic stirring, another 0.2g dose of sodium dithionite powder was added with periodic stirring occurring for 10 additional minutes. The addition and stirring of sodium dithionite powder continued until the soil samples turned gray. Upon completion, samples are cooled and centrifuged before they were removed by pipette, filtered through a 0.45-µm vacuum filter, and stored in 50mL centrifuge tubes at 4° C until analyzed. Extraction samples were analyzed using ICP-MS to determine concentrations of extracted metals in solution.

3.1.3. Batch Synthetic Groundwater Solution

To conduct the batch experiments, a synthetic groundwater, with chemical composition shown in

Table 2, was prepared using reagent grade chemicals and 18 MΩ water. Target COC concentrations were attained through dilution of a concentrated reference standard to their desired levels. Actual synthetic groundwater COC concentrations used in calculations were derived from analytical measurements of synthetic groundwater. Consequently,

Table 2 only represents the theoretical concentrations produced in the lab, while actual concentrations varied for each synthetic groundwater. Upon the addition of COCs synthetic groundwater pH was increased to levels between 6.5-7.5 by means of titrating with 0.1N sodium hydroxide solution. These synthetic groundwater solutions were prepared and stored in 10 liter LDPE carboys (Langley et al. 2015).

3.1.4. Batch Experiment

For each batch experiment, 200 mL of synthetic groundwater solution were added into five 250 mL HDPE bottles containing soil masses of either 100, 75, 50, 20, or 10g. This addition yielded soil mass to solution ratios of 50, 125, 250, 375, and 500g/L, as well as a HDPE bottle filled with synthetic groundwater solution which acted as a blank. Two sets of these soil mass to solution ratios were created for each sample so that two trials could be run. The soil-solution mixtures were then equilibrated through end over end mixing using a rotary mixer operating as 30 rpm for 24 hours. The experimental batch set-up and filtration method are shown in Figure 2 and Figure 3. After equilibration, water samples were taken, filtered, acidified with two drops of concentrated nitric acid, and stored at 4° C in a refrigeration unit. Samples were later analyzed for constituent concentration using ICP-MS for the four COC's studied in this study, as well as others according to the requirements of the specific coal ash site (Langley et al. 2015).

3.1.5. Experimental Batch Isotherms

After the batch experiments reached equilibrium, the COC concentration in solution were reduced due to adsorption onto the soil surface. This reduction can be shown with the equation

$$\frac{x}{m} = [(Co - C)/m] * V$$

where, x/m is the soil concentration (μg/g), Co is the initial solution concentration (μg/L), C is the final solution concentration, m is the soil sample mass, and V is the volume of solution. Once the measured solution concentration and calculated soil concentration were known, they were plotted against each other to create an isotherm for each individual sample. Each isotherm has five data points representing the five different ratios equilibrated for each sample (Langley et al. 2015).

3.2. Geochemical Modeling

Geochemical modeling was conducted to evaluate (1) its utility in predicting experimentally observed behavior, (2) its ability to predict sorption behavior under a wider set of Eh and pH conditions and (3) the role of specific minerals in the sorption of specific contaminants. In order to accurately model the adsorption reactions, the GTLM created by Dzombak and Morel was chosen to model surface complexation. The model was implemented using the geochemical modeling software, PHREEQC. Modeling procedures were generally inferred from similar studies, the PHREEQC User's Manual, and limited collaboration with one of the PHREEQC creator, Dr. David Parkhurst. The entire model input and output can be found in APPENDIX C.

3.2.1. Model Database

The GTLM requires inputs in the form of reaction constants which have been defined through acid-base titrations, pH edges, and isotherm data found in literature (Dzombak and Morel 1990). These reaction constants have been compiled from literature into multiple databases by the USGS, and are included with the PHREEQC software package. To account for all COC reactions the database utilized in this study was a combination of the *phreeqc*, *wateq4f*, and *minteq* databases, as well as arsenic reaction constants from literature (Gustafsson and Bhattacharya 2007). The collective databases included HFO complexation reactions from Dzombak and Morel and represent the most reputable equilibrium constants found in literature to date.

3.2.2. Model Solid Phase

Soil samples were selected for geochemical batch modeling from samples used in the laboratory batch experiments; however modeled samples were limited to seven coal

ash sites (e.i. Allen, Belews Creek, Buck, Cliffside, Dan River, Marshall, and Riverbend steam stations). The roster of samples designated for geochemical modeling was as extensive as possible and only excluded samples if they either did not have valid synthetic groundwater data, or did not have valid HFO concentration data. A total of 79 samples were used in the modeling of samples with HFO data derived from the CBD method, and a total of 80 when modeling samples with HFO values derived from the Chao method.

Input parameters were needed for the model solid phase to accurately represent the chosen soil samples. To define the surface phase, the total moles of strong and weak HFO surface sites within a sample, HFO surface areas, and total sample HFO masses were all input into the model, as seen in Appendix C. HFO surface areas were taken from literature and were set constant at 600m^2/g, for all samples (Dzombak and Morel 1990). The moles of strong and weak HFO surface sites, as well as total HFO mass were unknown and had to be determined on a sample by sample basis. This could be done since weak HFO adsorption sites can be estimated as 4% of its extractible iron (HDR Engineering 2016), and sample HFO mass was determined during sequential extraction analysis as shown in Table 1. The extracted iron values derived from the HFO extraction procedure were thus used in this calculation. The derived value was converted into moles of Fe per gram of solid. 4% of the total molar iron concentration was then assumed to be iron adsorption sites. The equation can be written as follows:

$$[\equiv FeOH] = [Solid] * [HFO] * \frac{1g}{1000mg} * \frac{mol\ HFO}{55.845g} * \frac{0.04\ mol \equiv FeOH}{mol\ HFO}$$

and was utilized to compute the total moles of weak adsorption sites (HDR Engineering 2016). Once the moles of weak HFO sites were determined, total moles of strong sites

could be determined due to the 1:40 strong to weak HFO site ratio (Dzombak and Morel 1990). An example of model solid phase input is noted in Figure 4**.**

3.2.3. Model Liquid Phase

Once all the PHREEQC surface parameters were defined and input, the model surface phase was considered fully defined. The next step in modeling a batch experiment was to define a liquid phase. A liquid phase for each sample was generated within the model by defining model solutions with identical quantitative water quality parameters to those of the synthetic groundwater used in the laboratory batch experiments. Solution parameters such as total solution mass, chemical concentration and water quality parameters like pH, pe, and temperature were input into the model. An example of model solution input is noted in Figure 4.

3.2.4. Mixing Model Batches

Once the solid and liquid phases were defined within the model, a batch mixing process was defined. This was done by using the MIX command within PHREEQC to mix specified amounts of the solid and liquid phases for each sample. Unlike the experimental batches, the amount of solution was varied within the model to achieve the desired liquid to solid ratio, rather than varying the amount of solid. This modification was done to allow for simpler inputs, and was determined to output identical results to models that varied the solid phase mass instead.

Five liquid to solid ratios identical to those used in the laboratory batch experiments were used in the model batch mixing in order to develop comparable batch isotherms. In addition to the isotherm points, a model curve was developed by means of

mixing eleven additional liquid to solid ratios of the solid and liquid phases. These eleven points were later developed into a model curve within excel.

3.2.5. Model Constraints

With the phases and batch mixing defined, the model would generally be ready to run; however due to PHREEQC's assumption of redox equilibrium, and the redox disequilibrium assertion described in section 2.5, model constraints were input as well. Model constraints included the restriction of both As and V to their respective As(3) and V(5) redox states in order to account for the hypothesized redox equilibrium. This restriction was accomplished by means of the SOLUTION_SPECIES command in PHREEQC, which allows one to define the properties of a constituent within PHREEQC. The As(3) to As(5) and V(4) to V(5) redox reactions were defined with a log_k of 100 and -100 respectively. This definition effectively caused the speciation of As(3) to As(5) and V(5) to V(4) to cease entirely. Since the initial solution input only included As(3) and V(5), the constraints effectively made these two redox states the only possible states for As and V within the model. Model surface complexation reactions were thus able to occur in a simulated redox disequilibrium state.

In addition to disequilibrium constraints, the model was adjusted to account for the saturation of Cr on HFO. Such adjustments were necessary due to the Cr saturation displayed in 34 of the 159 models created in for study. While consistent with the GTLM, experimental results did not show any sign of reaching maximum Cr adsorption capacity. In order to account for this disparity the amount of strong sites were increased until Cr no longer displayed saturated behavior.

3.2.6. Model Batch Isotherms

Once solid phases, liquid phases, batch mixing processes, and model constraints were all input, the model was run and an output dataset was generated. Output constituent data was then used to create isotherms in the same manner as the laboratory batch isotherms described in section 3.1.5. In addition to the steps taken in experimental isotherm generation, model isotherms required the additional model curve points to be processed in the same manner as the five isotherm points. Experimental and model isotherms are found in Appendix C.

3.3. Data Analysis

Once both experimental and model isotherms were generated, K_d values were calculated by defining a line of best fit through the five isotherm points using the least square method with a y intercept of zero. The resulting line represents a linear line of best fit, with the slope of the line representing the K_d value. Experimental and model K_d values of the same sample were then compared by determining the RE of the model K_d value with respect to the experimental. The relative error function is written as:

$$RE = \frac{K_{d(model)} - K_{d(experimental)}}{K_{d(experimental)}} \times 100$$

where RE represents relative error and K_d represents the adsorption coefficient of the respective model or experimental isotherm. With relative error acting as a quantifiable metric of model accuracy, a histogram of all sample relative error values was created to gauge model accuracy with a large sample size. Relative error histograms for each constituent and each extraction method are displayed between Figure 5 - Figure 12.

As an additional means of visualizing model accuracy, model and experimental K_d values were plotted directly against each other to visualize their correlation. A 1:1

line is included to visualize the actual trends compared to a perfect correlation. Model vs experimental plots are shown between Figure 13 - Figure 20.

In addition to visualizations of model accuracy, the K_d versus HFO concentration correlation was observed. K_d values of both modeled and experimental data were plotted against each soil sample's corresponding HFO concentration. These plots allow for the visualization of the correlation between HFO concentrations and K_d values, as well as correlations between model and experimental results. Linear regression lines with R^2 values were created on these plots to observe the strength of HFO vs K_d correlations as seen in Figure 21 - Figure 28.

Lastly, HFO versus K_d value graphs for each COC were developed on a site by site basis for all COCs, as seen in Figure 29 through Figure 42. This effort was conducted after the main body of this study was completed, in response to insight gained from additional literature review used to supplement the discussion section. As a result, the trend was not investigated as thoroughly as its significance deserves. The author has instead described the general trends observed herein, and leaves further in depth analysis to future research.

3.4. Sensitivity Analysis

To better understand geochemical controls within the model, multiple sensitivity analyses were completed. The first analysis further develops the understanding of the effect of water parameters on trace metal adsorption through the variation of pH and redox conditions; while the second analysis observes the effect of ion competition on COC adsorption.

3.4.1. pH and Redox Analysis

In order to create pH and redox sensitivity models, input constituents and HFO concentrations from every CBD model were averaged together and used as inputs for the sensitivity model so as to represent the entire population of batch experiments. Within PHREEQC, the PHASES and EQUILIBRIUM PHASES commands were used to enable solution pH and pe manipulation. Solutions were varied by inputting identical solution constituent concentrations, but with varying water quality parameters. Parameter values were maintained during solid and liquid phase equilibrium by adding either HCl or NaOH to fix pH, or O_2 to fix pe.

To understand the full scope of sensitivity, the effects of changing water quality parameters were observed throughout the entire natural pH & pe range. pH was varied between 5 and 9, while pe was varied between -1.69 and 6.76. pe values corresponded with an Eh range of -100mV to 400mV. Constituent isotherms were generated for every individual pH and pe pair as seen in Figure 43 - Figure 86.

3.4.2. Competition Analysis

The effect competing ions and trace metals have on an adsorbing COC is valuable when modeling natural and laboratory conditions that contain a variety of background constituents. In order to measure the effects of competition on COCs a base batch model was created and compared with multiple single COC batch models. Base model inputs included an average of constituent and HFO concentrations from every CBD model so as to represent the entire population of batch experiments. The single COC models included the same average HFO value; however the solution input only contained average values of either As, Cr, Se, and V respectively. Model batch isotherms were created using these

inputs in the same manner as previously mentioned model batches, with base and single COC isotherms contrasted in Figure 87 through Figure 90.

In addition to the observing the differences between batch experiments with no competition and average competition, the effects of ionic strength were also observed. In order to do so, 8 model batches were created with the background constituents $CaSO_4 \cdot 2H_2O$, $MgSO_4$, and $Na(HCO_3)$ all varied in concentration from their respective 20ppm, 5ppm, and 10ppm base model concentrations. These 8 batches each consisted of initial solutions with ionic strengths either 0, 0.001, 0.01, 0.1, 1, 10, 100, or 1000 times the concentration of the base model, but with identical concentrations of As, boron, cadmium, Cr, molybdenum, Se, thallium, and V to the base model. The results allowed for the visualization of a solution's ionic strength on the adsorption of the relevant COCs, as seen in Figure 91 through Figure 94.

3.5. Adsorption Capacity Analysis

In an effort to further understand COC interactions with HFO, a model was created to observe HFOs adsorption capacity with regards to the four COCs observed in the study. Input HFO concentrations from every CBD model were averaged together and used as surface inputs so as to represent the entire population of batch experiments. The liquid phase solution input into the model consisted of only a single COC for each analysis, so as to get a clear understanding of maximum adsorption without constituent competition. To determine the input COC concentration, the model was run with different concentrations, until the proper magnitude required for breakthrough was found. Once all of the input variables were determined the model was run and an isotherm was generated in excel for each COC as seen in Figure 95 through Figure 98.

3.6. Diffuse Double Layer vs No Electrostatics Models

Further exploration of the GTLM was conducted by comparing isotherms developed using a PHREEQC model incorporating the Diffuse Double Layer (DDL) model and a PHREEQC model that did not utilize the DDL. The DDL model was the base model with HFO and COC averages used section 3.4.2, while the non-DDL model was the same model, but with no DDL option implemented. Isotherms were generated and compared for both models, as seen in Figure 99 through Figure 102.

CHAPTER 4: RESULTS

4.1. CBD Extraction Method Isotherms

Models generated with HFO concentrations derived from the CBD extraction method showed medium to no correlation with experimental results; however correlations varied considerably between COCs. A summary of data analysis results comparing model and experimental data is presented in Table 3.

4.1.1. Arsenic

Of the four COCs and two extraction methods studied, modeled As concentrations derived from CBD extraction data showed the best overall correlation with experimental results. As visualized in the RE histogram shown in Figure 5 and data analysis results summarized in Table 3, analysis shows that 26.6% of CBD method As K_d values were within a factor of 2 of experimental K_d values (i.e. between an RE of -50% to 100%), while 86.1% were within an order of magnitude (i.e. between an RE of -90% and 900%). While not perfectly accurate, the As model with CBD extraction techniques displayed the least amount of error out of all other constituent and extraction method combinations, as shown in Figure 103 and Figure 104.

In addition to describing model and experimental correlation, the GTLM's premise that a soil's HFO concentration has a causal effect on its adsorptive capacity was investigated. Figure 21 demonstrates the relationship between a sample's HFO concentration and its corresponding As K_d value for both modeled and experimental isotherms. Out of all the COCs and extraction methods, experimental As K_d values and CBD HFO concentrations exhibited the best correlation, with a linear regression R^2 value

of 0.34. Model K_d values naturally showed a strong correlation to HFO, with an R^2 of 0.98, due to the use of HFO as a model input.

Along with quantifying accuracy, adsorption trends between model and experimental results could be observed. The relative error histogram in Figure 5 exhibits that the large majority of As batch K_d values are below zero. With a median K_d RE value of -63.6%, approximately 81% of modeled As K_d values were below those of experimental values. These results signify that the modeled As isotherms represented conservative estimates of K_d values. This study considers higher liquid COC concentrations, and thus lower K_d values to be conservative due to the general undesirability of COCs in groundwater.

Model conservatism is also evident in Figure 21 where the two plots, as well as their linear regression lines, depict model and experimental HFO's effect on adsorption. Regression slopes indicate that a unit of HFO displays about 3.5x more adsorptive effect in experimental isotherms than modeled isotherms do. While this higher experimental affinity may indicate a model that underestimates As's affinity for HFO, additional explanations are explored in the discussion below.

4.1.2. Chromium

When considering RE, modeled Cr concentrations showed little to no correlation with model results, with no Cr K_d values falling within an order of magnitude of experimental Cr results as seen in Figure 103 and Figure 104. The overall accuracy of the CBD Cr model can be visualized through the relative error histogram shown in Figure 6. Upon a more qualitative evaluation, one will observe that the strong majority of model Cr isotherm concentrations fell well below the lower detectable limits (LDL) of the ICP-

MS equipment used to determine experimental isotherm concentrations. In addition, most experimental Cr isotherms contained concentrations below the LDL, which were rounded up to 1ppb as shown in Figure 105. Due to these laboratory precision limitations, experimental K_d values of Cr are lower than true values. Had experimental Cr concentrations been measured with greater precision, the correlation between modeled and experimental isotherms would have been stronger.

Modeled K_d results for Cr also did not appear to be conservative, with 97% of modeled K_d values exceeding experimental values and a median RE of 217,603% as noted in Figure 6. Figure 22 further demonstrates inflated model K_d values through the model and experimental HFO vs K_d plots and linear regression lines. Regression slopes indicate that a unit of HFO displays drastically more adsorptive effect in model isotherms than in experimental. The extremely high RE values can again be partially attributed to laboratory measurement limitations; however experimental Cr isotherms with concentrations above LDL still yield drastically lower K_d values, as seen in Figure 106, suggesting that the model still greatly underrepresents Cr in groundwater regardless of analytical limitations.

Cr concentrations did not appear to be correlated to input HFO concentration. Figure 22 also demonstrates the relationship between a sample's HFO concentration and its corresponding Cr K_d value for both modeled and experimental isotherms. Of the four COCs, experimental Cr K_d values exhibited the least correlation with HFO concentrations of all CBD models, as seen in Table 3, with an R^2 value of -0.185. As with As, model K_d values showed a strong correlation to HFO, with an R^2 of 0.89, due to the use of HFO as a model input.

4.1.3. Selenium

After As, modeled Se concentrations showed the second strongest correlation to laboratory generated isotherms out of the 4 COCs studied, including all Chao method isotherms. Figure 7 illustrates the accuracy of the modeled Se isotherms relative to the experimental isotherms. Data analysis demonstrates that 23.1% of Se K_d values were within a factor of 2 from experimental K_d values, while 79.5% were within an order of magnitude as seen in Figure 103 and Figure 104. While still not perfectly accurate, the CBD derived Se and As results indicate the two most promising constituent models.

Experimental Se concentrations were moderately correlated to input CBD HFO concentrations. Figure 23 demonstrates the relationship between a sample's HFO concentration and its corresponding Se K_d value for both modeled and experimental isotherms. Out of all the COCs and extraction methods, experimental Se K_d values with CBD HFO concentrations exhibited the second best correlation, as tabulated in Table 3, with an R^2 value of 0.23. Model K_d values showed a strong correlation with an R^2 of 0.90.

Modeled Se isotherms generally represented conservative estimates of K_d values, similar to As. As visualized in Figure 7, approximately 63% of modeled Se K_d values were below those of experimental values, with a median RE of -52.2%. Model conservatism is also apparent in Figure 23 where the two plots, as well as their linear regression lines, depict HFO's effect on adsorption. Se regression slopes indicate that one unit of HFO displays about 3.5x more adsorptive effect in experimental isotherms than in modeled isotherms, similar to As. While this higher experimental affinity may

indicate a model that underestimates As's affinity for HFO, additional explanations are discussed below.

4.1.4. Vanadium

V model isotherms did not show as strong of a correlation with experimental results as As and Se; however they contained significantly less error than Cr isotherms. Figure 8 illustrates the accuracy of the modeled V isotherms relative to experimental isotherms through a relative error histogram. In total, 15.4% of V K_d values were within a factor of 2 from experimental K_d values, while 52.6% were within an order of magnitude, as tabulated in Table 3. With barely half of the modeled K_d values falling within an order of magnitude, the V model is not considered to be well correlated with experimental results.

Experimental V concentrations showed minimal to no correlation with input CBD HFO concentrations, while model concentrations exhibited a nonlinear quadratic trend as seen in Figure 24. The poor correlation of V K_d values with CBD HFO concentrations only had an R^2 value of 0.0036. Model K_d values showed a strong correlation with an R^2 of 0.80.

Further data analysis revealed that V isotherms were generally not conservative. With a median RE of 410%, as seen in Figure 8, and approximately 29% of modeled V K_d values below those of experimental values, it is evident that model computations tend to favor more V in the liquid phase than real world data suggests. This trend is further observed in Figure 24 where the two plots, as well as their linear regression lines, depict HFO's effect on adsorption. V regression slopes indicate that one unit of HFO displays

about 0.073x the adsorptive effect in experimental isotherms than in modeled isotherms, similar to Cr.

4.2. Chao Extraction Method Isotherms

Models generated with HFO concentrations derived from the Chao extraction method (Chao model) did not show as strong of a correlation with experimental results as CBD method results did, as seen in Figure 103 and Figure 104. Chao method HFO concentrations also showed little to no observable trend when plotted against experimental K_d values as exhibited in Figure 25 through Figure 28.

4.2.1. Arsenic

As isotherms generated from models using HFO concentrations derived from Chao method extraction data did not show as strong of a correlation with experimental isotherms as those created with CBD data; however they showed the best correlation with experimental results with regards to other constituents modeled which Chao extraction data, as seen in Figure 103 and Figure 104. The overall accuracy of the Chao As model can be visualized through the relative error histogram shown in Figure 9. The analysis results tabulated in Table 3 show that 16.3% of CBD method As K_d values were within a factor of 2 from experimental K_d values, while 48.8% were within an order of magnitude.

Similar to CBD method concentrations, COC concentration correlations with Chao derived HFO measurements were evaluated. Figure 25 demonstrates the relationship between a sample's HFO concentration and its corresponding As K_d value for both modeled and experimental isotherms. No COC K_d vs Chao HFO plots showed any significant correlation, with the As regression returning an R^2 value of -0.55. As expected, model K_d values still showed a strong correlation to HFO, with an R^2 of 0.97.

Similar to CBD derived As isotherms, As isotherms derived from Chao method data represented conservative estimates of K_d values with a median RE of -85.4% as seen in Figure 9. Approximately 83% of modeled As K_d values were below those of experimental values, indicating that Chao method isotherms were slightly more conservative than their CBD counterparts. Model conservatism is also evident in Figure 25 where the two plots, as well as their linear regression lines, depict HFO's effect on adsorption. While regression slopes are not very useful due to poor correlation, it is still visually evident that experimental K_d values are higher than model generated K_d.

4.2.2. Chromium

Similar to CBD model results, Chao model Cr concentrations showed little to no correlation with model results. Again, no Cr K_d values fell within an order of magnitude of real world results, as inferred from Figure 103 and Figure 104. The overall accuracy of the Chao Cr model is visualized through the relative error histogram shown in Figure 10. Just as with the CBD model and exemplified in Figure 107, most Chao model Cr isotherm concentrations fell well below laboratory LDL. In addition, most experimental Cr isotherms required their concentrations be rounded up to meet the 1ppb LDL. These limitations once again caused inherent inaccuracies when comparing modeled and real world results, causing less correlation than would have occurred had exact precision been employed. Despite experimental flaws it is believed that the GTLM exhibits more adsorptive Cr behavior than experimental results suggest, as evident by comparisons of model isotherms with real world isotherms that have concentrations about the LDL, as seen in Figure 108.

Chao model Cr results similarly did not appear to be conservative, with 99% of modeled K_d values exceeding experimental values and a median RE of 85,467% as seen in Figure 10. Figure 26 demonstrates inflated model K_d values through model and experimental HFO vs K_d plots. Unlike CBD models, regression lines were poor metrics due to the lack of correlation between Chao HFO and Chao model K_d values. The extremely high RE values can again be partly attributed to laboratory measurement limitations; however Cr isotherms with concentrations above LDL suggest that the model still greatly underrepresents Cr in groundwater regardless of experimental limitations.

Cr concentrations did not appear to be correlated to Chao HFO concentrations. Figure 26 demonstrates the relationship between Chao HFO and experimental Cr K_d. The two parameters don't appear to show any meaningful correlation, with Table 3 showing an R^2 value of -0.185; however the data still makes it apparent that Cr model K_d values are calculated well above experimental values. Model K_d values showed a strong correlation to HFO, with an R^2 of 0.89, due to the use of HFO as a model input.

4.2.3. Selenium

Modeled Chao Se concentrations showed less correlated yet comparable trends to those of As. Figure 103 and Figure 104 reveal that 11.4% of CBD method Se Kd values were within a factor of 2 from experimental Kd values, while 41.8% were within an order of magnitude. The histogram of Se RE values shown in Figure 11 offers a visualization of the overall accuracy of the Chao Se model.

The relationship between a sample's HFO concentration and its corresponding As K_d value for both modeled and experimental isotherms is demonstrated in Figure 27. Se K_d vs Chao HFO plots did not reveal any significant correlation, with the Se regression

returning an R^2 value of -0.55. Model K_d values still showed a strong correlation to HFO, with an R^2 of 0.97.

Similar to CBD derived Se isotherms, Se isotherms derived from Chao method data represented conservative estimates of K_d values with a median RE of -87.7% as seen in Figure 11. Approximately 71% of modeled Se K_d values were below those of experimental values, indicating that Chao method isotherms were slightly more conservative than their CBD counterparts. Model conservatism is also evident in Figure 27 where the two plots, as well as their linear regression lines, depict HFO's effect on adsorption. While regression slopes are not very useful due to poor correlation, it is still visually evident that experimental K_d values are higher than model generated K_d.

4.2.4. Vanadium

V model results derived from Chao method exhibited little correlation with experimental results, as inferred from Table 3. The resulting data revealed that 16.4% of V K_d values were within a factor of 2 from experimental K_d values, while 43.0% were within an order of magnitude as seen in Figure 103 and Figure 104. The model and experimental correlation is further visualized in Figure 12 as a histogram of RE values.

Experimental V concentrations showed minimal to no correlation with input Chao HFO concentrations, while model concentrations exhibited a nonlinear quadratic trend as seen in Figure 28. The poor correlation of V K_d values with Chao HFO concentrations only had an R^2 value of -0.086. Model K_d values showed a strong correlation with an R^2 of 0.63.

Similar to CBD model Se results and evident in Figure 12, Chao model concentrations were not consistently conservative, with approximately 52% of modeled

V K_d values falling below those of experimental values. The median RE was conservative at -46.0; however the histogram displayed exhibits high RE variation, making the consideration of the median rather impractical. Results were conservative only at relatively low HFO solid concentrations as seen in Figure 28 where the two plots, as well as their linear regression lines, depict HFO's effect on adsorption. Similar to Cr, V regression slopes indicate that one unit of HFO displays about 0.054x the adsorptive effect in experimental isotherms than in modeled isotherms.

4.3. Site Specific Trends

The comparison of HFO to K_d values on a site by site basis revealed significant trends in both As and Se isotherms, as seen in Figure 29 through Figure 42. Site specific Cr and V trends are not included due to the lack of any trend. As K_d values show high correlation with the extracted HFO values measured in the laboratory, with an average regression line R^2 value of 0.805. These As site by site correlations are significantly higher than the combined site HFO versus K_d value R^2 value of 0.343, as seen in Figure 21. Se showed less of a site specific correlation than As, with an average R^2 value of 0.294; however, the site by site average was still higher than the combined site HFO versus K_d value R^2 value of 0.229 seen in Figure 23.

4.4. Sensitivity Analysis

4.4.1. pH and Redox Analysis

The pH and redox sensitivity analysis yielded the isotherms shown in Figure 43 through Figure 86, which enhanced the conceptual understanding of model COC trends within PHREEQC. Changes in pH with constant Eh generally resulted in incrementally different isotherms, while isotherms generally remained static after changes in Eh. With

pH held constant, Eh changes often tended to yield identical isotherms throughout a large range of values, with large changes occasionally occurring on the outer bounds of the pH range.

4.4.1.1. Arsenic

The sensitivity analysis of As was carried out similar to other COCs, but included the additional redox disequilibrium limitations mentioned in section 2.5. Due to the lack of any model As(5) redox speciation, it is likely that As concentrations were not as sensitive to Eh as one would expect. Instead, As(3) was shown to respond to changes in pH, as seen in Figure 50. As generally became more soluble at lower pH, with As(3) generally existing as the neutral species H_3AsO_3 between a pH range of 5 to 8. At pH 9 As concentrations became more dominated by anionic species. Anions generally have less affinity for the solid phase at higher pH, and pH 9 results were in line with such trends (Dzombak and Morel 1990). At low Eh and pH, such as the pH 5 & Eh -100 isotherm seen in Figure 48, it appeared that solution complexation may have made As(3) less adsorptive. In these conditions the As(3) species $H_2As_3S_6^-$ was dominant and appeared to have a different adsorption affinity than other As(3) species.

The lack of As(3) Eh sensitivity became evident when step changes were performed for Eh at constant pH. As seen in Figure 43 through Figure 47, As did not display significant sensitivity to changes in Eh, except in the singular case mentioned above, where the solution with an Eh of -100 and pH of 5 yielded large concentrations of $H_2As_3S_6^-$ in the liquid phase.

4.4.1.2. Chromium

Unlike As, the sensitivity analysis of Cr did not include any model limitations to Cr redox speciation. The pH step change in Figure 60 shows how Cr complexation increased between pH 5 and 7, but began to steadily decrease at higher pH between 7 and 9. The increase from pH 5 to 7 occurs when Cr(3) cations are dominant in solution. This increase is to be expected since cation complexation generally increases as pH increases (Dzombak and Morel 1990). The decrease in complexation at pH higher than 7 is likely attributed to the neutral and negative Cr species which form in higher pH conditions. Anions adsorption is typically greatest at lower pH (Dzombak and Morel 1990). Overall Cr was highly adsorptive due to Cr(3)'s affinity for strong binding sites.

Similar to As, Cr was fairly unresponsive to Eh, likely due to the fact that Cr(3) exists in a wide range of natural groundwater chemistries, as seen in Figure 61. The only solution conditions where Cr isotherm concentrations significantly diverged occurred at pH 9 and Eh 400 where the more soluble Cr(6) was the dominant species as seen in Figure 58. Cr(6) was shown to be much less adsorptive than Cr(3) within the model, which is also what is expected in natural conditions. Cr(6) however, does not play much of a role in model results, due to Cr(3) favorable solution conditions within the laboratory experiment.

4.4.1.3. Selenium

Just as with Cr, Se was also modeled without any constraints to redox speciation and was responsive to incremental changes in pH as seen in Figure 70 through Figure 75. Se(4) (e.i. H_2SeO_3, $HSeO_3^-$, and SeO_3^{2-}) was the dominant species throughout most of the pH and redox conditions; however, deprotonation of Se(4) appeared to affect adsorption throughout different pH values. Se appears to be the most adsorptive around

pH 6, while consistently losing affinity for the solid phase the farther away from pH 6 a solution became.

Se was more responsive in regards to changes in Eh relative to the other COCs examined. As seen in Figure 69, Se(6) became dominant over Se(4) at pH 9 and Eh 400, while lower pH isotherms allowed Se(-2) to become dominant as seen in Figure 65. In situations where either Se(-2) or Se(6) were dominant, Se displayed much lower affinity for the solid phase; however Se(4) was the most common dominant redox state throughout the analysis. While these effects are apparent in the sensitivity analysis, it is unlikely that Eh played much of a role in modeled batch isotherms due to experimental solution parameters generally falling within ranges of Se(4) dominance. Isotherms with dominant Se(4) redox states displayed more sorptive characteristics and are seen in Figure 65 through Figure 69.

4.4.1.4. Vanadium

Similar to As, V was limited within the model in order to constrain V redox states to account for the hypothesized redox disequilibrium. While V naturally speciates between V(2), V(3), V(4), & V(5) in common groundwater Eh & pH conditions, model constraints only allowed for V(5) to exist in solution. When modeled with constant Eh, V was shown to be responsive to changes in pH as seen in Figure 83. While the lack of redox speciation likely reduced more dramatic changes in isotherm concentrations, speciation within redox states still allowed for nuances. In particular, speciation of V(5) between $H_3V_2O_7^-$ and $H_2VO_4^-$ seemed to influence V(5) adsorption. The less sorptive $H_3V_2O_7^-$ was prevalent in lower pH isotherms, as can be seen in the pH 5 and Eh 300 isotherm in Figure 85. Aside from the occurrence of $H_3V_2O_7^-$ at low pH, model analysis

showed V as otherwise very adsorptive, with trends indicating that higher pH yielded higher adsorption.

V was not very sensitive to changes in Eh, with isotherms that only significantly diverged at low pH and low Eh (e.i. pH 5 & Eh -100), as seen in Figure 76. Aside from the single extreme, all V isotherms had similar concentrations despite Eh changes as seen in Figure 77 through Figure 80. This lack of sensitivity to changing redox conditions is to be expected due to the V redox speciation constraints implemented into the model.

4.4.2. Competition Analysis

The competition analysis yielded the isotherms shown in Figure 87 through Figure 94, which help demonstrate the role competition played in the generation of model batch isotherms. With the exception of Cr, COCs experienced higher adsorption affinity when in solution by themselves than compared to the base solution with average concentrations. General ionic strength also played a role, with increasing concentrations of $CaSO4 \cdot 2H2O$, MgSO4, and Na(HCO3) causing COC adsorption to decrease incrementally, as seen in Figure 91 through Figure 94.

4.4.2.1. Arsenic

As displayed a higher affinity for HFO when present as the only constituent within the liquid phase. As seen in Figure 87, a solution phase composed of only 400ppb As resulted in a K_d value of 0.46L/g, while the base model solution resulted in 0.25L/g. Similar results were displayed when ionic strength was varied up and down by multiple orders of magnitude, as depicted in Figure 91. When background concentrations fell below those of the base model As adsorption increased, but only slightly. Ionic strengths lower than base levels by one order of magnitude or less tended to exhibit little to no

effect on As adsorption. This is evident by the overlap of isotherms yielded from the 0.1x, 0.01x, 0.001x, and 0x background concentration runs. More significant competitive effects occurred once ionic strength was increased by orders of magnitude. Figure 91 visualizes a moderate decrease in adsorption with an order of magnitude increase to background constituent concentrations (i.e. 10x Ions isotherm), with more significant decreases in isotherm K_d values as concentrations approach a 3 order of magnitude increase (i.e. 1000x Ions isotherm).

4.4.2.2. Chromium

Cr was the only COC which did not display a higher affinity for HFO when isolated from competing ions, with adsorption magnitude mostly unchanged. As seen in Figure 88, a solution phase composed of only 59ppb Cr resulted in a K_d value of 497L/g, while the base model solution resulted in 493L/g. Similar results were displayed when ionic strength was varied up and down by multiple orders of magnitude, as depicted in Figure 92. Cr adsorption was largely unimpeded until ionic strengths were increased by a factor of 100 (i.e. 100x Ions isotherm) or more. Ionic strengths lower than 100 times the strength of the base model allowed Cr to remain highly adsorptive, with little change in total adsorption. Even with a 1000 fold increase (i.e. 1000x Ions isotherm) Cr remained highly adsorptive, as seen by the relatively low dissolved Cr remaining in solution after equilibrium.

4.4.2.3. Selenium

Similar to As, Se displayed a higher affinity for HFO once isolated from competing constituents in the liquid phase. As seen in Figure 89, a solution phase composed of only 519ppb Se resulted in a K_d value of 2.5L/g, while the base model

solution resulted in 0.21L/g. Similar results occurred when solution ionic strength was varied, as depicted in Figure 93. When background concentrations fell below those of the base model Se adsorption increased; however ion competition became negligible once background concentrations decreased by an order of magnitude or more. This is evident by the overlap of the 0.1x, 0.01x, 0.001x, and 0x Ions isotherms. More significant competitive effects occurred once ionic strength was increased. Figure 93 displays significant decreases in Se adsorption once ionic strength was increased tenfold, with little to no adsorption occurring at higher concentrations.

4.4.2.4. Vanadium

Similar to As and Se, V displayed a higher affinity for HFO once isolated from competing constituents in the liquid phase. Figure 90 displays a solution phase composed of only 211ppb V resulted in a K_d value of 148L/g, while the base model solution resulted in 2.3L/g. Similar results occurred when solution ionic strength was varied, as depicted in Figure 94. When background concentrations fell below those of the base model V adsorption increased; however ion competition became negligible once background concentrations decreased by an order of magnitude or more. This is evident by the overlap of the 0.1x, 0.01x, 0.001x, and 0x Ions isotherms. More significant competitive effects occurred once ionic strength was increased. Figure 94 displays significant decreases in V adsorption once ionic strength was increased tenfold, with little to no adsorption occurring at higher concentrations.

4.5. Adsorption Capacity Analysis

The adsorption capacity analysis yielded the isotherms shown in Figure 95 through Figure 98. These isotherms all exhibit the asymptotic behavior expected from batches with COC concentrations high enough to saturate HFO binding sites.

4.5.1. Arsenic

In order to generate a saturation exhibiting As isotherm, a 30ppm As solution was used as the solution input. The generated isotherm, as seen in Figure 95, exhibits a lowercase r-like curve, with a horizontal asymptote occurring near 243ug/g. This asymptote represents the maximum adsorption density of modeled As for an average soil sample utilized in this study.

4.5.2. Chromium

Cr only required a 200ppb solution in order to generate a saturation isotherm, as seen in Figure 96. As with As, Cr also displayed the lowercase r-like isotherm indicative of a saturation asymptote. HFO's Cr maximum adsorption capacity thus appears to be about 4ug/g; notably lower than the adsorption capacity of the other COCs.

4.5.3. Selenium

Se required the highest solution concentration in order to recreate saturation conditions, with a 500ppm solution utilized within the model as seen in Figure 97. The saturation isotherm did not exhibit the smooth lowercase r asymptote-like isotherm like other COCs, and instead displayed varying slopes until an asymptote was reached. Se saturation was reached near 126ug/g, with notably more Se present in the liquid phase than required for As, Cr, and V.

4.5.4. Vanadium

V saturation was reached using an initial groundwater solution of 10ppm, as seen in Figure 98. It did not transition as suddenly from unsaturated to saturated conditions, exhibiting a subtler transformation from unsaturated to saturated conditions. V saturation was reached around 35ug/g.

4.6. Diffuse Double Layer vs No Electrostatics Model

The comparison of the DDL and no electrostatics models yielded the results shown in Figure 99 through Figure 102. As was least affected by the lack of the DDL model, with Cr, Se, and V becoming increasingly more sensitive respectively. All COCs displayed high affinity for the solid phase when the DDL was incorporated into the model.

CHAPTER 5: DISCUSSION

5.1. General Model Error

All models attempting to predict the results of complex systems will have a certain amount of error associated with their results. The GTLM is no exception, as seen by the lack of correlation presented in this study. While results will likely never be perfect, the error associated with them can be attributed to certain criteria, and potentially mitigated in the future. Model error is likely a result of: model simplicity not reflecting the complexity of real world processes, incorrect assumptions regarding HFO stoichiometry, large type 2 surface site density ranges, an imperfect database, low precision extraction techniques, and measurement precision.

With regards to model simplicity, the PHREEQC model used can be considered an incomplete component additivity model which only utilizes one surface site mineral phase. A component additivity model is a model that predicts adsorption by quantifying surface mineral phases such as HFO and modeling their interactions with ions using stability constants and stoichiometries developed in prior studies. While the model used in this study only contains the surface mineral phase HFO, other mineral phases such as HAO, HMO, and goethite could have also been implemented into the surface phase of the model. Any surface complexation that would have occurred with additional mineral phases would then have affected to total adsorption (Davis et al. 1998). Since the chosen model only uses HFO, it is possible that the implementation of these additional mineral phases would have resulted in different adsorption rates.

Additional simplicity error arises due to the use of linear K_d values to describe the entire population of isotherms. While a majority of experimental isotherms were linear in

nature, modeled isotherms tended to express nonlinear qualities. Some nonlinear modeled isotherms were subtle enough to be accurately described by a K_d value, as seen in Figure 109; while others displaying stronger nonlinear qualities were less accurately described, as seen in

Figure 110. While K_d values will not describe these nonlinear isotherms perfectly, they do provide a practical and meaningful quantification of a COC's adsorption affinity. They also provide quantitative consistency between the mostly linear experimental isotherms, and the less linear modeled isotherms. Due to their practicality and the need for consistent means of quantifying adsorption affinity between experimental and model isotherms, K_d values were utilized for all isotherms.

Further error can arise from assumptions made within the GTLM itself. Dzombak and Morel assume HFO stoichiometry of $Fe_2O_3 \cdot H_2O$ which is in turn used when calculating total HFO sites from the iron extracted in Chao and CBD methods. While useful for consistency, the stoichiometry can vary between Fe_2O_3 and $Fe_2O_3 \cdot 3H_2O$. Further assumptions are made when attempting to define the site density of surface sites. Previous studies showed that type 2 surface sites represent anywhere between 0.1 and 0.3mol/mol Fe, while type 1 sites represent between 0.001 and 0.01 mol/mol Fe. These assumptions are acknowledged by Dzombak and Morel, and are considered necessary in order to develop practical and consistent models. While justified, such assumptions nonetheless have the potential to contribute to model error (Dzombak and Morel 1990).

Aside from assumptions within the model, issues also arise when contemplating how the equilibrium constants within the database are derived. Equilibrium constants are often derived in laboratory experiments which utilize an assortment of pure mineral

phases to study ion adsorption. These experiments occur in controlled environments and have the advantage of utilizing homogeneous solid phases with far fewer variables than present in natural soils. Natural solid phases offer complications such as determining the composition of surface mineral phases, as well as the potential introduction of a multitude of unknown constituents into solution during equilibrium. With such complications introduced in models containing natural soils, it is likely that database equilibrium constants will have amplified amounts of error relative to those describing pure mineral phases (Davis et al. 1998).

While error was present within the model input in the form of the equilibrium constants, it was also present in input data derived from laboratory experiments. Laboratory data and procedures were developed with great diligence; however equipment precision and the complexities of describing sample heterogeneity can cause error. Of note are the concentration disparities between the results of the two HFO extraction procedures. It is evident by the differences in HFO extraction concentrations between the CBD and Chao methods, seen in Figure 111, that there is considerable room for error between such procedures. While the CBD method was assumed more accurate due to favorable results, the quantity of error within either method's results is unknown. Thus CBD method results could still contain enough inaccuracies to affect results. Further exploration of sequential extraction error is explored in section 5.2.

While never completely removed, all the aforementioned error sources can be mitigated through further research and understanding of their respective causes. While the results in this study did not achieve perfection, the data was nonetheless gathered using best practices and informed by large quantities of literature review. The author

considers the data adequate to describe the trends in surface complexation modeling defined herein.

5.2. Extraction Method Comparison

When considering extracted HFO concentrations it becomes evident that inaccuracies are present, as inferred from the differences in concentrations displayed in Figure 111. When considering entire COC datasets, CBD selective extraction method showed stronger correlation between extracted HFO and experimental K_d values than the Chao method did, as seen in Figure 103 and Figure 104, as well as in Table 3. R^2 values for K_d vs HFO linear regression lines were more favorable for CBD method than Chao method for As, Se, and V, as seen in Figure 21 through Figure 28. V regression lines displayed poor correlation in both methods that comparing the accuracy of the two trends becomes arbitrary. Similarly, while Chao method R^2 values were slightly better for Cr, results were poorly correlated in both instances that any comparison between correlations was meaningless. Further Chao method inadequacies become evident when comparing model K_d values with experimental ones. In all cases but Cr, CBD method yielded significantly more K_d values within an order of magnitude of experimental results than Chao did, with Cr models returned no K_d values within this range for either method. Due to the more favorable accuracy of its results, CBD method was chosen as the preferred HFO extraction procedure and is the focus of discussion in this section.

The Chao method may not have correlated as well with experimental results due to the complexities inherent to sequential extraction in natural soils. Prior research has indicated that different sequential extraction methods may not yield comparable results to each other. In addition, mineralogical differences between samples, such as the

dissimilarities prevalent between separate sites, can affect the resulting Fe measurements. Further evidence suggests that even the geochemical conditions in which a sample originally resided in can affect extracted Fe (MacDonald 2013).

These difficulties in accounting for natural heterogeneity can be caused by the extraction of multiple mineral phases during the sequential extraction process. Prior examinations of different mineral phases dissociated by a variety of common sequential extraction techniques showed that none of the methods consistently target a single individual mineral phase. Instead, the Chao method was found to dissociate HFO, siderite, and lepidocrocite, while CBD method dissociates significant amounts of HFO, lepidocrocite, goethite, hematite, and magnetite (MacDonald 2013).

The extraction of Fe from non-HFO mineral phases during the Chao and CBD methods has the potential to affect the calculated HFO concentrations, and in turn model results. In addition, the heterogeneity between natural samples makes any potential trend in error difficult to quantify. Such difficulties appear to be inherent in most common extraction methods utilized today (MacDonald 2013). Error due to natural complexity was expected within this study due to the use of natural soils. While future refinement of extraction procedures will be helpful, this study's goal of quantifying the utility of the CBD and Chao methods paired with HFO surface complexation modeling is nonetheless useful in assessing today's techniques.

5.3. CBD Method Modeling

While the CBD method proved to yield more favorable model results, the different COCs within the model yielded a variety of different trends. As mentioned in section 5.2 and seen in Figure 22 and Figure 24, Cr and V K_d values showed little to no

correlation with HFO values as evident by their low R^2 values. Thus when considering all HFO vs K_d trends, only CBD extraction with As and Se displayed any statistically significant inclinations, as seen in Figure 21 and Figure 23. In addition, comparison of model and experimental Cr and V K_d values indicated a significant divergence of model values from experimental ones, as seen in Figure 6 and Figure 8. Due to these divergences, and low correlation to HFO levels, As and Se CBD method models described herein are likely the only models with the potential for practical application.

5.3.1. Arsenic

As had the strongest correlation to experimental values, with 86.1% of respective modeled As K_d values falling within an order of magnitude of experimental values, as seen in Figure 104. With reasonably high accuracy, As modeling has the most potential for real world application out of all four COCs examined in this study. Higher As model correlation is likely the result of higher experimental K_d correlation with extracted HFO, as well as the abundance of research on the topic of As adsorption. Of all the COCs described in this study, As is generally considered to be the most thoroughly researched, likely leading to more accurate surface complexation constants in the database.

Along with higher levels of accuracy, 81% of modeled Kd values fell below experimental values, making the model conservative. While conservative results are generally favorable in real world modeling, experimental results tended to have higher K_d values than model results did. The model's skew towards lower K_d values may be a result of the aforementioned exclusion of non-HFO mineral phase adsorption sites from model inputs, or the built in model limitation which only allowed for the As(3) redox state due to hypothesized redox disequilibrium. While disequilibrium implies that the

ratio of As(3) and As(5) redox states is different than what the theoretical equilibrium calls for, it does not necessarily imply negligible As(5) concentrations. It is possible that disequilibrium within the batch experiments was more subtle (e.i. had higher concentrations of As(5)) than the extreme disequilibrium allowed in the model. A disequilibrium with meaningful concentrations of As(5) would cause higher K_d values similar to the experimental data; however such a disequilibrium was not practical to implement into the model. Thus due to the conservatism and practicality of only using As in the As(3) redox state, the lower K_d skew of the model results is deemed acceptable from a theoretical standpoint.

While the results seem to make sense when accounting for redox state and mineral phase limitations, a model which is only conservative for 81% of soils may not be desirable in a real world project where higher confidence is required. For further certainty, model generated K_d values may be decreased by a factor of 5 (e.i. $K_d * 0.2$) to become more conservative than 96% of all experimental Kd values. A 96% confidence rate may fall within the acceptable range of confidence for a project; however further decrease can occur for even more confidence. With the correct confidence level, As K_d values for input into fate and transport models can potentially be generated through HFO sampling and geochemical modeling rather than expensive and time consuming experimental batch experiments.

5.3.2. Chromium

Cr modeling showed the worst correlation out of any COC. With little to no correlation and only 3% of modeled K_d values falling below experimental values, modeled Cr K_d values are likely not viable for real world application in their raw form.

While As and Se K_d values could be reasonably modified to achieve desired levels of conservatism, Cr results require much more modification. In order to modify Cr K_d values so that 95% of modeled Kd values are more conservative than experimental values, modeled values would need to be decreased by more than 4 orders of magnitude (e.i. K_d * 0.0001). This level of modification is likely too high to justify; therefore this Cr model does not appear viable for real world application.

While the laboratory precision issues described in section 4.1.2 can explain some of the error seen in Cr modeling, it is possible that the GTLM predicts more sorptive Cr behavior than evident in experimental results. This overestimation trend becomes evident when comparing the model isotherms with real world isotherms that have their concentrations above the LDL, as seen in the isotherms in Figure 106. These experimental Cr isotherms allow for the visualization of experimental results without the limitation of the ICP-MS's LDL due to the higher concentrations of Cr in the liquid phase, and support the conclusion that the model overestimate Cr adsorption.

Reasons for the model's overestimation of Cr adsorption affinity are unknown; however there are a multitude of potential reasons, of which many are described in section 5.2. Of interest is Cr's exclusive binding with type 1 adsorption sites. As mentioned previously, type 1 sites are calculated as 0.005 mol HFO/mol Fe; however this value ranges in literature from 0.001 to 0.01 mol HFO/mol Fe (Dzombak and Morel 1990). This is a large range which could greatly affect the quantity of type 1 sites used to model Cr adsorption. In addition to adsorption site calculation issues, it is possible that Cr equilibrium constants are inaccurate. Further research is likely needed to determine accurate Cr equilibrium constants, especially as they relate to HFO in natural soils.

Pending more accurate constants, it is concluded that Cr modeling is not viable using the methods described in this study.

5.3.3. Selenium

Se modeling resulted in the second-best correlation with experimental results after As, with 79.5% of respective modeled Se K_d values falling within an order of magnitude of experimental values, as seen in Figure 104. Just as with As, relatively high model correlation is likely somewhat a consequence of Se's higher experimental K_d correlation with extracted HFO as seen in Figure 23. With moderate correlation and 63% of modeled Kd values falling below experimental values, the Se model is slightly conservative. Just as with As, the model's skew towards lower K_d values is potentially a result of the exclusion of the HAO, HMO, and goethite mineral phase adsorption sites from the model, on top of the other sources of error mentioned in section 5.1.

The exact reason for the Se model's conservative results is unknown and requires further research to understand; however, the model may have enough correlation with experimental results to be considered for real world application after some modification. Just as with As, Se K_d values would likely need to be adjusted lower to obtain a conservative enough confidence level for real world application. For further certainty, model generated K_d values can be decreased by an order of magnitude (e.i. $K_d * 0.1$) thus becoming more conservative than 94% of all experimental K_d values. A 94% confidence rate may fall within the acceptable range of confidence for a project; however further decrease can occur if even more confidence is desired. With the correct confidence level, Se K_d values for input into fate and transport models can potentially be generated through HFO sampling and geochemical modeling.

5.3.4. Vanadium

V showed some correlation to experimental results relative to other COCs, with 53% of modeled K_d values falling within an order of magnitude of experimental results as seen in Figure 104. With less correlation with HFO, as seen in Figure 24, and only 29% of modeled K_d values falling below experimental values, modeled V K_d values are not considered particularly accurate or conservative in their raw form. While As and Se K_d values could be reasonably modified to achieve desired levels of conservatism, V results require much more modification. To modify V K_d values so that 95% of modeled Kd values are more conservative than experimental values, modeled values would need to be decreased by 2 orders of magnitude (e.i. $K_d * 0.01$). This level of decrease in K_d will greatly increase V's affinity for the liquid phase within a fate and transport model. While these two order of magnitude decrease in K_d is small compared to the required Cr modification, it still greatly exceeds the K_d adjustments required for As and Se models. This level of modification is likely too high to justify, therefore this V model does not appear viable for real world application.

Reasons for V model inaccuracies include all those discussed in section 5.1; however it is also possible that the hypothesized redox disequilibrium played less of a role in V than it did in As. Due to poor model results, it was hypothesized that the solution was displaying V redox disequilibrium, with V(5) existing as the dominant redox state due to improved fit. While the V(5) redox state appeared to exhibit the best fit and was consistent with water quality conditions present in its stock solution, it may be possible that disequilibrium was skewed towards other redox states, or was not present at all. While initial investigations provided enough evidence to suggest that V(5) had the

highest correlation with experimental results, further investigation into modeling with V may prove useful in developing practical models. Pending more accurate V models, it is concluded that V modeling is not viable using the methods described in this study.

5.4. Site Specific Trends

The site specific analysis was conducted after this paper was completed in order to explore the site specific correlations discussed in section 5.2. The resulting site by site correlations seen in Figure 29 through Figure 42 proved to be very significant for As, and somewhat significant for Se. The As correlation was particularly strong, showing that As modeling can likely be calibrated on a site by site basis in order to achieve fairly accurate results. Se was less correlated; however, site by site analysis still revealed a better average HFO versus K_d R^2 value than those generated when all site data was lumped together. Cr and V results did not display an increase in correlation when controlling for sample sites, and are not included. The author considers the high site specific As and slightly higher Se correlations to have significant implications in regards to the modeling of these COCs, and recommends further investigation into such trends.

5.5. Sensitivity Analysis

5.5.1. pH and Redox Analysis

The pH and redox sensitivity analysis was enlightening with regard to small changes within model solution that effect adsorption. The big takeaway from the analysis was that model adsorption was affected by small changes in pH, but would not be affected by Eh until conditions became favorable for redox speciation to change the dominant species. Other trends in COC behavior were also observed such as solution complexation.

The common occurrences of adsorption change with respect to pH are partially the result of changes in surface charge on the solid phase due to the protonation and deprotonation of surface sites, and due to non-redox speciation or protonation which affected molecular charge. The surface charge theoretically affects the electrostatic columbic binding force which, along with the intrinsic chemical binding force, comprises the adsorptive activity of a COC and surface site (Dzombak and Morel 1990).

It is difficult to determine general trends for each metal due to their inclination to speciate or protonate and deprotonate, causing different dominant species in different conditions. While cations and anions should generally show defined trends, COCs will often speciate into a new form with a different charge before a large and definable trend arises. While all metals showed moderate sensitivity to pH, occasional changes in dominant species, both redox and non-redox speciation, could lead to larger sensitivity.

COCs in the GTLM were shown to be less sensitive to Eh than they were to pH, with little to no change in isotherm concentration when Eh changed and pH was held constant. While Eh indifference was usually the case, occasional but more drastic changes occurred when water quality conditions were favorable for redox speciation. These redox changes are generally observed within the Eh sensitivity analysis isotherms as big jumps, instead of small incremental changes like in the pH sensitivity isotherms. These jumps indicate that an isotherm curve is more sensitive to Eh when it is near a point of equal redox species distribution (e.g. the conditions at which a solution is composed of 50% As(3) and 50% As(5)); however these areas of sensitivity generally exist within a relatively small range of Eh conditions, and would require a smaller observational step change than were considered in this analysis.

As one would expect, COCs which were locked into a particular redox state (i.e. As(3) and V(5)) did not exhibit high levels of isotherm variability due to Eh and displayed low levels of isotherm variation during Eh step changes. In contrast, Se display more elevated levels of sensitivity to Eh, as seen in Figure 67 and Figure 69, which is unsurprising with a COC with so many redox states. Unlike Se, Cr was generally not as sensitive to Eh even though it was not constrained to an individual redox state. This was likely the case due to Cr's limited number of naturally occurring redox states, Cr(3) and Cr(6). While Cr(6) did make an appearance within the sensitivity analysis at pH 9 and Eh 400, as seen in Figure 58, Cr(3) is generally dominant throughout a wide range of natural conditions, making it by far the most prevalent Cr redox species in the sensitivity analysis.

Most of the changes observed in the sensitivity analysis can be explained by changes in surface charge, adsorbate charge, and adsorbate redox state; however another phenomenon was prevalent in one instance. At the lower pH and Eh levels of pH 5 and Eh -100, as seen in Figure 43, As experienced solution complexation with sulfur. In these conditions the As(3) species $H_2As_3S_6$- was dominant, and appeared to have a different adsorption affinity than other As(3) species. This complexation with another solution constituent likely caused As to have a lower affinity for the solid phase, largely changing its adsorption characteristics.

The trends seen in the sensitivity analysis give insight into what type of water quality conditions are favorable or unfavorable to COC adsorption. Such insight can be useful in understanding potential COC mobility changes brought about by future changes in the geochemistry near or within CCR sources. Anthropogenic activities significant

enough to affect site-wide geochemistry may include impoundment closure activities such as capping and excavation; however geochemical variation may also naturally occur within a site. In capping or removal situations, the flow of CCR leachate is expected to either attenuate or cease altogether. With decreased leachate flow, the pH within the impoundment's area of influence is expected to slowly converge with background levels. Since CCR leachate may exhibit a pH as acidic as 4, or as alkaline as 12, there exists the potential for nearby groundwater to exhibit dynamic geochemical behavior as it reaches equilibrium with background levels. Such a situation may also occur before capping or excavation, when geochemical conditions near a CCR source slowly change as groundwater flows outwards and parameters equilibrate back to background conditions (Roy and Berger 2011).

As inferred from Figure 48 through Figure 53 and Figure 81 through Figure 86, As(3) and V(5) will likely become less mobile if site pH trends toward more common background pH levels (i.e. pH 6-8) from both initially acidic and alkaline conditions. While the acidic trend is realistic, the existence of As(3) is unlikely in alkaline leachates and will likely exist in the As(5) state not considered in this study. Similarly, V(5) will likely not exist in real world acidic conditions, with the V(4) and V(3) species not considered here being more likely. Similar to As and V, both Cr and Se would also become less mobile as both acidic and alkaline site conditions become more neutral, as seen in Figure 59 through Figure 64 and Figure 70 through Figure 75, with some exceptions depending on Eh conditions.

Redox conditions in subsurface areas near CCR sources may also experience gradients near CCR sources, as well as changes during closure. Reducing conditions can

occur near CCR in situations where enough sulfate is released from the source to stimulate microbial driven reduction. Additionally, there is concern that redox conditions can be affected when a site is caped in place (Schwartz et al. 2016). In such instances when a redox gradient exists in either time or space, Eh becomes important parameter to consider. The effects of redox on As and V were difficult to observe in this study due to the assumption of redox disequilibrium and the fixed redox states used within the model; however insight can be found in relevant literature. Evidence suggests that the more adsorptive As(5) will exist in more aerobic states; however soluble As(3) will exist in elevated levels within groundwater in reducing conditions. This trend suggests that extra consideration of redox effects should be taken when capping a CCR in place or when working with high sulfate CCR (Schwartz et al. 2016). On the other hand, the more soluble V(5) species exists in aerobic conditions, while the more adsorptive V(4) exists in reducing conditions (Wright et al. 2014). This trend would suggest that V concentrations in groundwater will decrease if reducing conditions occur due to capping source material of elevated sulfate concentrations.

Cr and Se redox effects were much easier to describe due the redox speciation freedom allotted to them within the model. As seen in Figure 54 through Figure 58, Cr displays a high affinity for HFO in most geochemical conditions. Only when Cr(6) becomes the dominant species in relatively high aerobic and alkaline conditions do Cr concentrations in groundwater become elevated. This trend suggests that CCR sources high in Cr content may need to avoid highly oxidative treatments. Se was shown to exist in the highly soluble S(-2) form at low pH and Eh levels, as seen in Figure 65 through Figure 69. Once redox conditions became more aerobic the more adsorptive Se(4)

became dominant; however in relatively high alkaline and oxidizing conditions, Se(6) would become dominant and cause elevated Se concentrations. These results suggest that CCR sites with Se concerns will find moderate redox conditions more favorable, with Se concentrations in groundwater increasing should reducing conditions occur due to capping source material of elevated sulfate concentrations

While the geochemical effects of pH and redox are significant and useful when considering changes to a CCR source, they are not the only geochemical controls. Further expansion of the analysis could be conducted by varying additional variables other than Eh and pH. Additional investigations could vary parameters like solution ion composition to explore the effects of ion adsorption site competition, HFO concentrations to as to observe the effects of adsorption site availability, and COC concentrations to evaluate the behaviors of high and low concentration solutions.

5.5.2. Competition Analysis

The competition sensitivity analysis was informative with regards to the significance of ion competition with COC adsorption; however the investigation was only limited to average pH and pe conditions observed in the CBD and Chao experiments. The main trend observed in Figure 87 through Figure 94 was that higher background constituent concentrations in solution led to a decrease in COC adsorption to HFO. This behavior is expected since the dominant control with relation to an adsorbent is the availability of adsorption sites, making decreased site availability due to the addition of competing ions significant. In addition to adsorbent effects, higher concentrations of ions can also affect the activity of adsorbates through either ion pairing or electrostatic interactions. These interactions will generally make activity coefficients smaller and can

decrease a COCs adsorption affinity; however activity can occasionally be raised, causing the opposite effect (Zhang et al. 2019).

When observing the effect of competition on COCs in the base model by comparing it to the single COC batch runs, it becomes evident that competition affects each COC differently. For instance, the effect of competition in the base model appeared to be negligible in regards to Cr adsorption, somewhat significant in regards to As, and very significant in regards to Se and V, as seen in Figure 87 through Figure 90. These differences indicate that trace metals such as Se and V are relatively sensitive to background constituents and other trace metals, while As is moderately, and Cr only negligibly sensitive.

With regards to ionic strength differences caused by increases in Na^{+}, Ca^{2+}, and Mg^{2+}, and SO_4^{2-}, all COCs became less adsorptive as background concentrations increased. While this trend held steady for all COCs, individual COCs again displayed different sensitivities to changes in ionic strength. As seen in Figure 92, Cr was still able to strongly adsorb to the solid state due to its existence as Cr(3) in such conditions. This high level of adsorption in the face of very high ionic strengths is evidence of Cr(3)'s ability to outcompete common background ions for HFO adsorption sites. While the case, it is evident that these increases in concentration still have an effect on Cr(3), making it slightly mobile, rather than immobile.

The rest of the COCs observed exhibited sensitivities to ionic strength changes more similar to each other rather than to Cr. Model conditions and assumptions caused As, Se, and V to exist in the redox states As(3), Se(4), and V(5) respectively. As with the base model vs single COC solution comparison, As was moderately affected by the

increases in ionic strength, while Se and V were more significantly affected, as seen in Figure 91, Figure 93, and Figure 94 respectively. This is evident since all three COCs were effectively fully dissolved in the liquid phase when ionic concentrations were 1000 times larger than base model concentrations; however only Se and V were fully dissolved at 100x concentrations.

These sensitivities can have implications in both experimental and natural systems, where a wide range of groundwater chemistries and trace metal concentrations can exist. When considering competition's effects on trace metals derived from CCR, a multitude of potential consequences arise. In particular, brine solutions associated with CCR wastewater have the potential to affect COC adsorption through ion competition. Should these brines enter into natural systems the large concentrations of dissolved ions within these solutions would cause higher trace metal mobility. While such solutions will likely decrease in ionic strength as dilution occurs through mixing, higher concentrations near source materials likely should be taken into account when considering the transport of COCs.

Additional implications arise when considering the competition of other trace metals on COCs. Se and V in particular may be fairly sensitive to the existence of other trace metals, as inferred from the results displayed in Figure 89 and Figure 90. Such sensitivities could make the trace metal composition of CCR leachate significant with respect to the adsorptive affinity and mobility of these COCs. For instance, CCR sources which leach relatively high concentrations of trace metals may not only experience high COC levels within groundwater, but may also experience higher levels due to COC

competition. With implications as such, special note should be given to adsorption site competition when considering groundwater quality associated with CCR sources.

5.6. Adsorption Capacity Analysis

The adsorption capacity analysis gave insight into the quantity of COC which can be adsorbed by the solid phase, and the relevancy of such a limit to the concentrations utilized in this study. In all cases except Cr, the magnitude of solution concentration required to cause COC saturation on the solid phase was significantly higher than the concentrations used in the study, as seen in Figure 95, Figure 97, and Figure 98. This sizable concentration variation provides confidence that the lower concentrations modeled in this study could not approach the theoretical maximum adsorption capacity due to As, Se, and V adsorption alone. Instead, saturation would only be able to occur due to the occupation of adsorption sites by background constituents such as calcium, magnegsium, sodium, and sulfur.

Unlike the other COCs, the HFO's adsorption capacity for Cr was much lower, and occurred at the far lower solution concentration of 200ppb, as seen in Figure 96. This lower capacity is the result of Cr's adsorption to HFO's strong sites, rather than the weak sites favored by As, Se, and V. Due to the smaller availability of strong sites in the GTLM, as described in section 3.2.2, it is expected that Cr would reach its saturation capacity at lower solution concentrations than those COCs binding with weak sites. With such low Cr solution concentrations causing solid phase saturation, HFO's adsorption capacity for Cr becomes relevant within the model, with such saturation events occurring within 34 of the 159 models created in this study, as corrected for and discussed in section 3.2.5.

5.7. Diffuse Double Layer vs No Electrostatics Models

As displayed in Figure 99 through Figure 102, the use of DDL within a model can have a wide range of impact on COC adsorption depending on the COC. The main difference between a model with a DDL and one without is that the consideration of the change to electrostatic surface charge due to constituent complexation on the surface phase is only considered when the DDL is modeled. In addition, a charged surface will cause an equal amount of opposite charges to build up in the solution, instead of existing as a part of the DDL. This solution charge buildup is likely what causes the difference in the models, as models without a DDL require more ions in solution to balance the charge of the surface (Parkhurst and Appelo 2013). As such, the use of the DDL model is recommended when modeling surface complexation.

REFERENCES

(ACAA 2015)
ACAA (2015) "2014 Coal Combustion Product (CCP) Production & Use Survey Report." (n.d.). ACAA-USA, American Coal Ash Association, <https://www.acaa-usa.org/Portals/9/Files/PDFs/2014ReportFinal.pdf> (Apr. 15, 2016).

(Berkowitz et al. 2014)
Berkowitz, B., Dror, I., and Yaron, B. (2014) *Contaminant Geochemistry: Interactions and Transport in the Subsurface Environment*. 2nd Ed., Springer, Heidelberg.

(Bağda 2014)
Bağda, E. (2014). "Determination of vanadium in groundwater samples with an improved kinetic spectrophotometric method." Environmental Technology, 35:9, 1165-1174, DOI:10.1080/09593330.2013.864337

(Chao and Zhou 1983)
Chao, T.T., and Zhou, L. (1983). "Extraction Techniques for Selective Dissolution of Amorphous Iron Oxides from Soils and Sediments." Soil Science Society of America Journal, 47(2), 225-232.

(Daniels and Das 2014)
Daniels, J.L., and Das, G.P. (2014). "Practical Leachability and Sorption Considerations for Ash Management." *Geo-Characterization and Modeling for Sustainability*, (GSP 234) ASCE Reston/VA 362-376

(Davis et al. 1998)
Davis, J., Coston, J., Kent, D., & Fuller, C. (1998). "Application of the surface complexation concept to complex mineral assemblages." Environmental Science & Technology, 32(19), 2820–2828.
<http://search.proquest.com/docview/230116581/>

(Dzombak and Morel 1990)
Dzombak, D., and Morel, F. (1990). *Surface complexation modeling: hydrous ferric oxide*, John Wiley & Sons, Inc., New York

(EIA 2018)
EIA (2018), *Electricity in the United States*. (n.d.).
<https://www.eia.gov/energyexplained/index.php?page=electricity_in_the_united_states>
(Oct. 19, 2018)

(EPA 2004)
EPA (2004) *Understanding Variation in Partition Coefficient, K_d Values*. Vol 3., EPA, Environmental Protection Agency

(EPA 2015)
EPA (2015). “Final Rule: Disposal of Coal Combustion Residuals from Electric Utilities.” (n.d.). EPA, Environmental Protection Agency, <https://www.epa.gov/coalash/coal-ash-rule> (Apr. 15, 2016)

(Fernández-Martínez and Charlet 2009)
Fernández-Martínez, A. & Charlet, L. (2009) “Selenium environmental cycling and bioavailability: a structural chemist point of view.” Rev Environ Sci Biotechnol 8: 81. https://doi.org/10.1007/s11157-009-9145-3

(Goldberg and Johnston 2001)
Goldberg, S., and Johnston, C. (2001). “Mechanisms of Arsenic Adsorption on Amorphous Oxides Evaluated Using Macroscopic Measurements, Vibrational Spectroscopy, and Surface Complexation Modeling.” Journal of Colloid and Interface Science, 234, 204-216

(Gustafsson and Bhattacharya 2007)
Gustafsson, J., and Bhattacharya, P. (2007). “Geochemical modelling of arsenic adsorption to oxide surfaces.” Trace Metals and Other Contaminants in the Environment, 9, 159–206. https://doi.org/10.1016/S1875-1121(06)09006-7

(Kalhori et al. 2013)
Kalhori, E., Yetilmezsoy, K., Uygur, N., Zarrabi, M., and Shmeis, R. (2013). “Modeling of adsorption of toxic chromium on natural and surface modified lightweight expanded clay aggregate (LECA).” Applied Surface Science, 287, 428-442

(Karamalidis and Dzombak 2010)
Karamalidis, A., and Dzombak, D. (2010). Surface complexation modeling: gibbsite, John Wiley & Sons, Inc., New York

(Kent et al. 1994)
Kent, D., Davis, J., Anderson, L., and Rea, B. (1994). “Transport of chromium and selenium in the suboxic zone of a shallow aquifer: Influence of redox and adsorption reactions.” Water Resources Research, 30(4), 1099-1114

(Langley et al. 2015)
Langley, W., Daniels, J., Oza, S. (2015) *Sorption Evaluation Mayo Power Plant*, UNC Charlotte

(HDR Engineering 2016)
HDR Engineering Inc. of the Carolinas, (2016) *Corrective Action Plan Part 2 Allen Steam Station Ash Basin*, Charlotte, NC

(MacDonald 2013)
MacDonald, K. (2013). *Evaluation of Selective Iron Extraction Techniques to Quantify Iron-Bound Phosphorus in Sediments* (master's thesis). University of Hawai'I at Mānoa, Honolulu, HI

(Mehra and Jackson 1960)
Mehra, O., and Jackson, M. (1960). "Iron Oxide Removal From Soils and Clays by Dithionite-Citrate Systems Buffered With Sodium Bicarbonate" Clays and Clay Minerals, 7(1), 317-327

(Miller 2001)
Miller, G.P. (2001). "Surface Complexation Modeling of Arsenic in Natural and Sediment Systems" Doctoral dissertation. UNCC Interlibrary Loan 443066

(Parkhurst and Appelo 2013)
Parkhurst, D., and Appelo, C. (2013). *Description of Input and Examples for PHREEQC Version 3—A Computer Program for Speciation, Batch-Reaction, One-Dimensional Transport, and Inverse Geochemical Calculation: U.S. Geological Survey Techniques and Methods*, book 6, chap. A43, 497 p., <https://pubs.usgs.gov/tm/06/a43/>

(Roy and Berger 2011)
Roy, W., and Berger, P. (2011). "Geochemical Controls of Coal Fly Ash Leachate pH." Coal Combustion and Gasification Products, 3(1), 63-66

(Schwartz et al. 2016)
Schwartz, G., Rivera, N., Lee, S., Harrington, J., Hower, J., Levine, K., Vengosh, A., Hsu-Kim, H. (2016). "Leaching potential and redox transformations of arsenic and selenium in sediment microcosms with fly ash." Applied Geochemistry, 67, 177-185

(Smedley and Kinniburgh 2001)
Smedley, P.L., Kinniburgh, D.G. (2001). "A review of the source, behaviour and distribution of arsenic in natural waters." Appl. Geochem. 17, 517–568

(Tonkin et al. 2004)
Tonkin, J., Balistrieri, L., & Murray, J. (2004). "Modeling sorption of divalent metal cations on hydrous manganese oxide using the diffuse double layer model." Applied Geochemistry, 19(1), 29–53. <https://doi.org/10.1016/S0883-2927(03)00115-X>

(U.S. Department Of Health And Human Services 2007)
U.S. Department Of Health And Human Services. (2007). *Toxicological Profile For Arsenic*.

(U.S. Department Of Health And Human Services 2012)
U.S. Department Of Health And Human Services. (2012). *Toxicological Profile For Vanadium*.

(U.S. Department of the Interior Bureau of Land Management 1991)
U.S. Department of the Interior Bureau of Land Management. (1991). *Environmental Impact Statement Betze Project*, B-6-6 p., <https://books.google.com/books?id=WwYzAQAAMAAJ&pg=SL18-PA54&lpg=SL18-PA54&dq=redox+disequilibrium+as(III)+As(V)&source=bl&ots=L72z0V2ZQo&sig=Tn_GYadiDV6EWYJ6xQ6-_IhWpXo&hl=en&sa=X&ved=0ahUKEwiMvfO5osPVAhWGCMAKHSL8DQoQ6AEIYTAI#v=onepage&q=redox%20disequilibrium%20as(III)%20As(V)&f=false>

(WHO 2011)
WHO (2011). "Selenium in Drinking-water." WHO Press, World Health Organization, < http://www.who.int/water_sanitation_health/dwq/chemicals/selenium.pdf > (Oct. 15, 2018)

(Wright et al. 2014)
Wright, M., Stollenwerk, K., Belitz, K. (2014). "Assessing the Solubility controls on Vanadium in Groundwater, Northeastern San Joaquin Valley, CA." Applied Geochemistry, 48, 41-52

(Zhang et al. 2019)
Zhang, Y., Zhu, C., Liu, F., Yuan, Y., Wu, H., and Li, A. (2019). "Effects of ionic strength on the removal of toxic pollutants from aqueous media with multifarious adsorbents: A review." Science of The Total Environment, 646, 265-279

APPENDIX A: TABLES

Table 1: HFO concentrations derived from Chao and CBD extraction methods

HFO Extraction Concentrations			
Site	Sample Name	CBD	Chao
		(mg/Kg)	(mg/Kg)
Allen	AB-20S	2546	3934
	AB-20D	450	2204
	AB - 28D	2398	1889
	AB - 29D	543	3691
	AB - 31D	3613	2014
	AB - 33S	2979	1209
	AB - 34S	1803	161
	AB - 35S	1955	1785
	AB - 35R	257	2129
	GWA - 3BR	883	4698
	GWA - 7S	1595	1016
	GWA - 9S	472	1490
Belews Creek	AB - 2D	486	1257
	AB - 9S	939	1246
	BG - 3S	2060	NA
	GWA - 2D	224	1085
	GWA - 3D	1235	2156
	GWA - 5S	450	2005
	GWA - 8S	NA	4060
	GWA - 11D	1888	2446
	GWA - 12	1857	412
	MW - 200BR	191	3830
Buck	AB – 2BR	3149	384
	AB – 5D	313	306
	AS – 2D	3595	353
	BG – 3D	3334	338
	GWA – 3D	1563	884
	GWA – 4D	822	559
	GWA – 6D	1205	2695
	GWA – 9D	3873	513
	GWA – 10D	580	1190
	GWA – 12D	436	364
Cliffside	AB − 1D	3148	153

	AB − 2D	1838	225
	AS − 3BR	58	231
	GWA − 55	640	283
	GWA − 1BRU	440	1535
	GWA − 2D	578	809
	GWA − 10D	1135	600
	GWA − 23D	1953	302
	GWA − 20S	1503	266
	GWA − 24S	930	509
	IB − 3SB	1618	531
	MW − 22BR	2735	697
	US − 3D	2540	176
Dan River	AB – 30 BR (32-34)	3534	232
	AB – 30 BR (43-44)	2683	383
	AB – 105 L	3076	360
	AS – 2D	1696	269
	AS – 10D	3811	461
	GWA – 10	NA	676
	GWA – 5BR	1878	322
	GWA – 4D	2295	689
	GWA – 11D	2444	488
	GWA – 12D	2002	992
	GWA – 1S	3405	351
	GWA – 3S	3168	257
Marshall	AB – 1 BR	699	353
	AB – 1 S	103	666
	AB – 2 S	445	127
	AB – 4 D	182	466
	AB – 6 BR	501	685
	AB – 8 D	860	682
	AB – 11 D	674	358
	AB – 16 D	1105	601
	AS – 1 D	43	148
	GWA – 1 S	504	243
	GWA – 2D	156	254
Riverbend	AB - 4D	741	268
	AB - 6S	3973	774
	AB - 7S	1356	558

	GWA - 1BRU	43	438
	GWA - 7D	96	501
	GWA - 8D	5880	419
	GWA - 1S	1389	611
	GWA - 2S	916	651
	GWA - 4S	274	107
	GWA - 5S	1652	271
	GWA - 6S	2044	365
	GWA - 7S	1033	568
	GWA - 10S	2080	266

Table 2: Synthetic groundwater constituents and trace metals concentrations

Chemical	Concentration	Units
$CaSO_4 \cdot 2H_2O$	20	ppm
$MgSO_4$	5	ppm
$Na(HCO_3)$	10	ppm
Arsenic	500	ppb
Boron	500	ppb
Cadmium	500	ppb
Chromium	500	ppb
Molybdenum	500	ppb
Selenium	500	ppb
Thallium	500	ppb
Vanadium	500	ppb

Table 3: Overall data analysis result summary

	Arsenic		Chromium		Selenium		Vanadium	
	CBD	Chao	CBD	Chao	CBD	Chao	CBD	Chao
Average RE	19.06	435.13	785066.3	382732.6	138.702	714.66	1925.681	8571.58
Median RE	-63.6	-85.44	217602.5	85466.54	-52.1698	-87.66	409.7704	-45.99
% RE w/in factor of 2	26.6	16.25	0	0	23.1	11.4	15.4	16.5
% RE w/in order of magnitude	86.1	48.75	0	0	79.5	41.8	52.6	43
% RE conservative	81	82.5	2.7	1.3	62.8	70.9	29.5	51.9
R^2 of Model Kd vs HFO regression	0.978	0.974	0.8889	0.842	0.902	0.8417	0.805	0.6311
R^2 of Experimental Kd vs HFO regression	0.343	-0.549	-0.185	-0.048	0.229	-0.213	0.0036	-0.086
Model Kd vs HFO regression slope	0.0002	0.0002	0.3869	0.3596	0.0002	0.0002	0.0096	0.0074
Experimental Kd vs HFO regression slope	0.0007	0.0005	0.0001	0.0002	0.0007	0.0005	0.0007	0.0004
M/E Regression Slope Ratio	0.285714	0.4	3869	1798	0.285714	0.4	13.71429	18.5

APPENDIX B: FIGURES

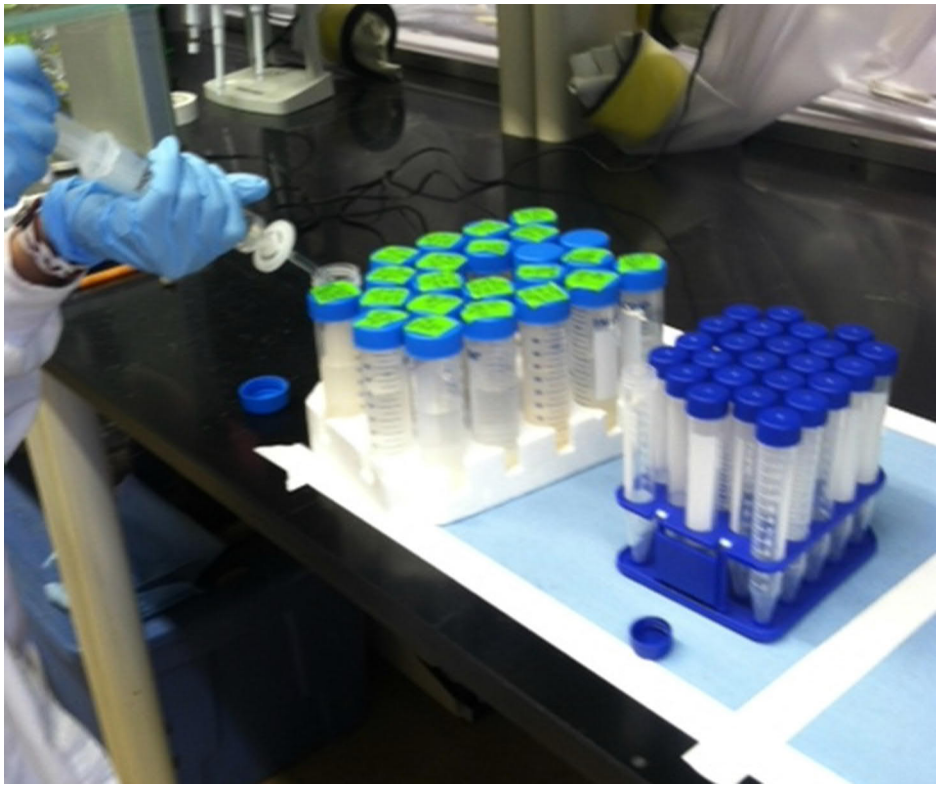

Figure 1: Syringe filtration for both Chao and CBD HFO extraction methods

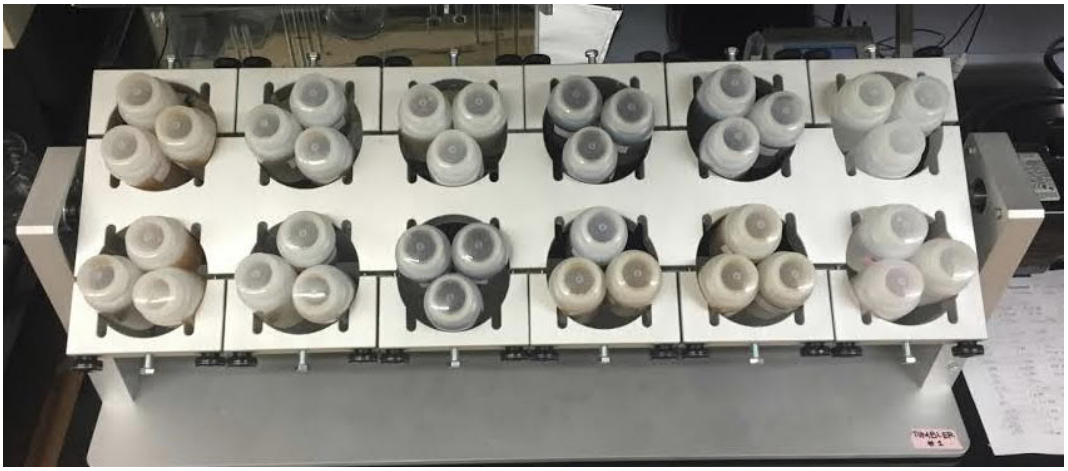

Figure 2: Tumbler for batch K_d

Figure 3: Batch filtration set-up

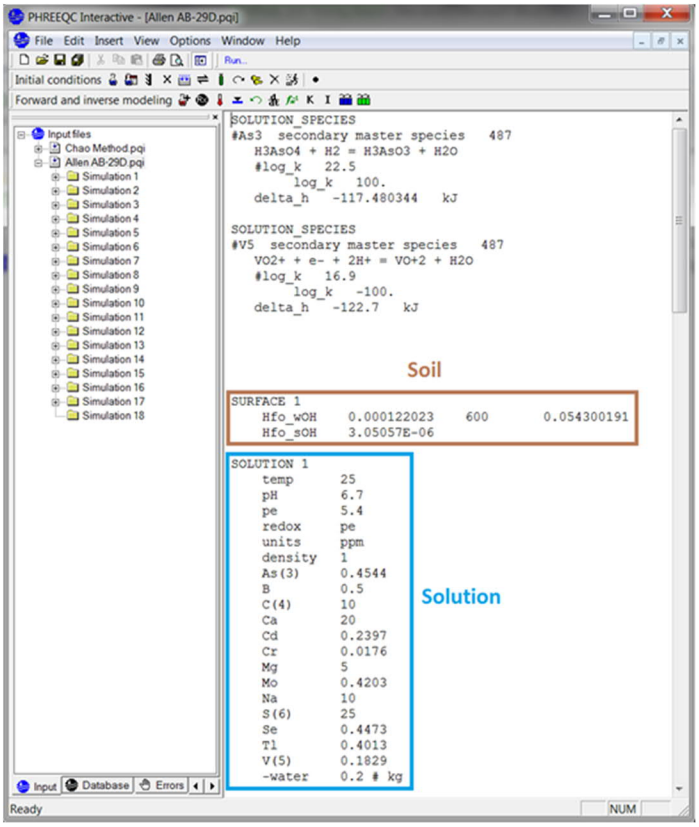

Figure 4: PHREEQC solid and liquid phase input

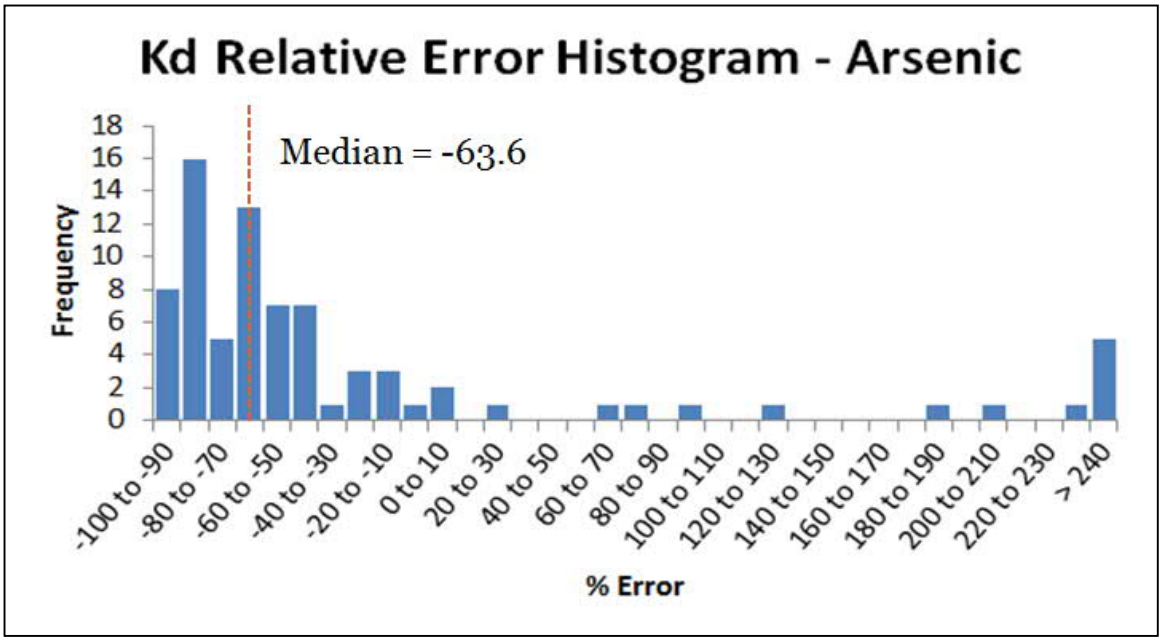

Figure 5: Histogram of Modeled CBD Method As K_d RE

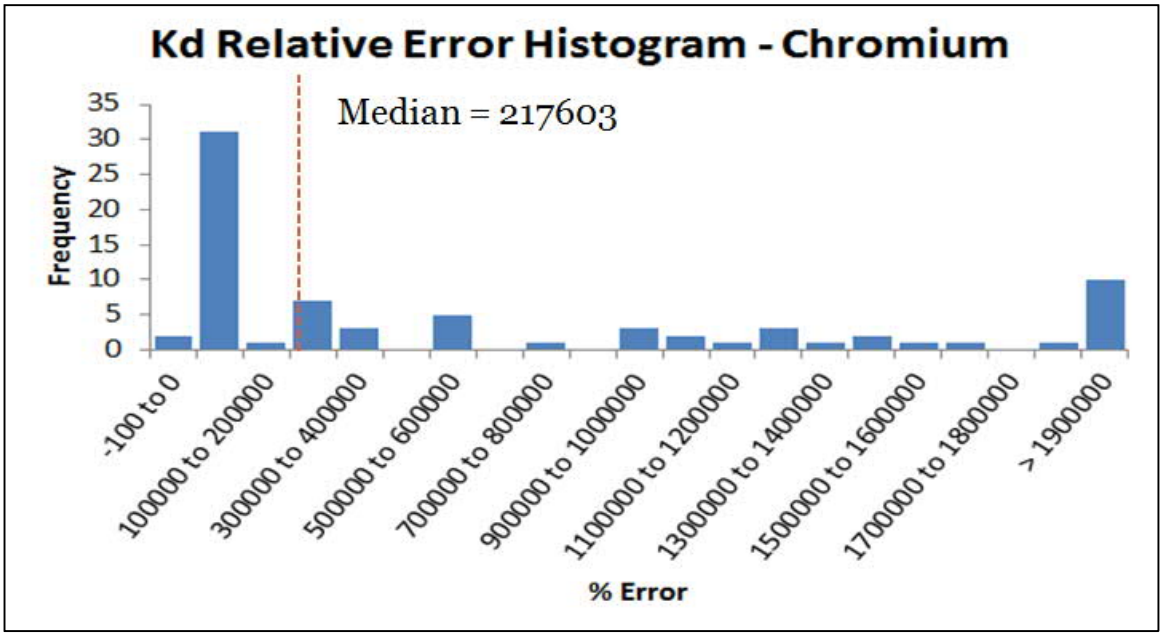

Figure 6: Histogram of Modeled CBD Method Cr K_d RE

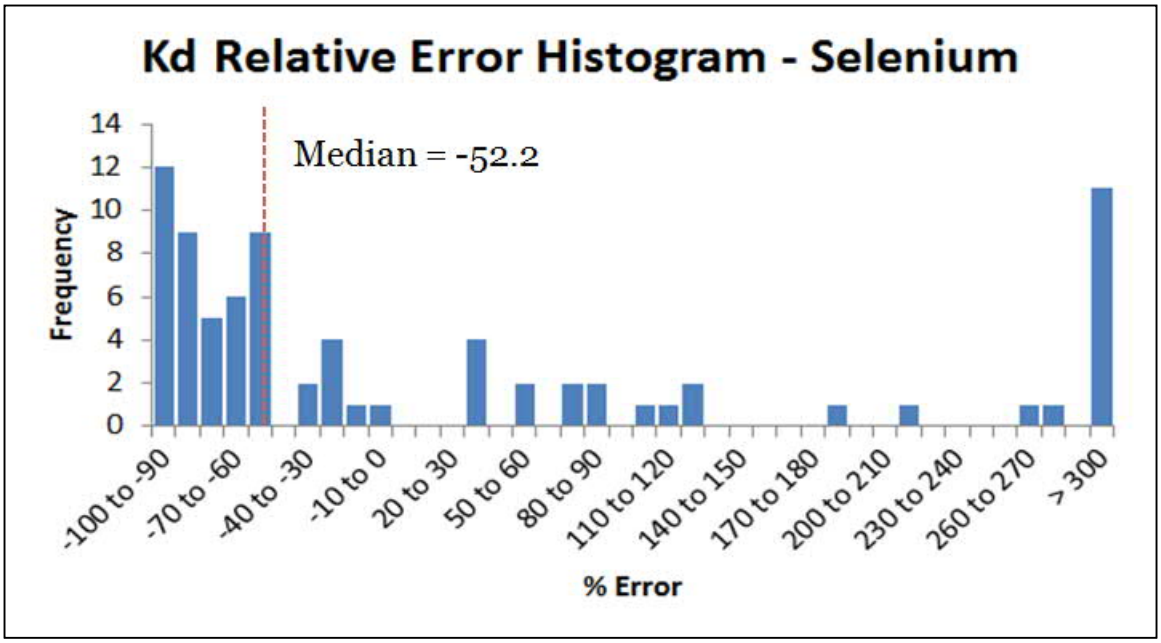

Figure 7: Histogram of Modeled CBD Method Se K_d RE

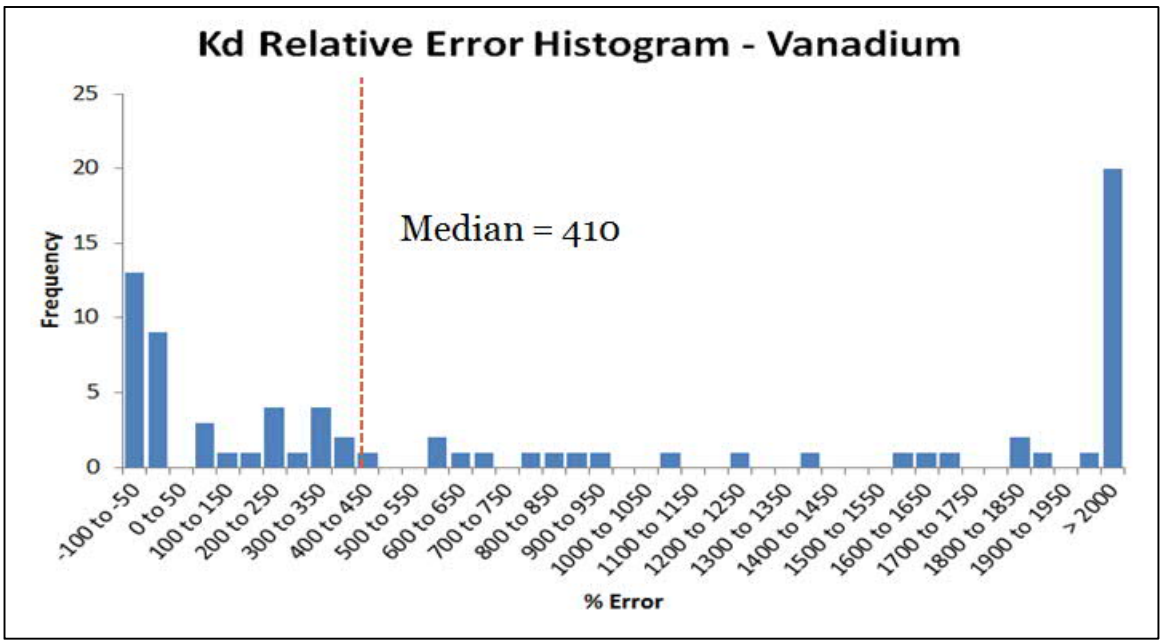

Figure 8: Histogram of Modeled CBD Method V K_d RE

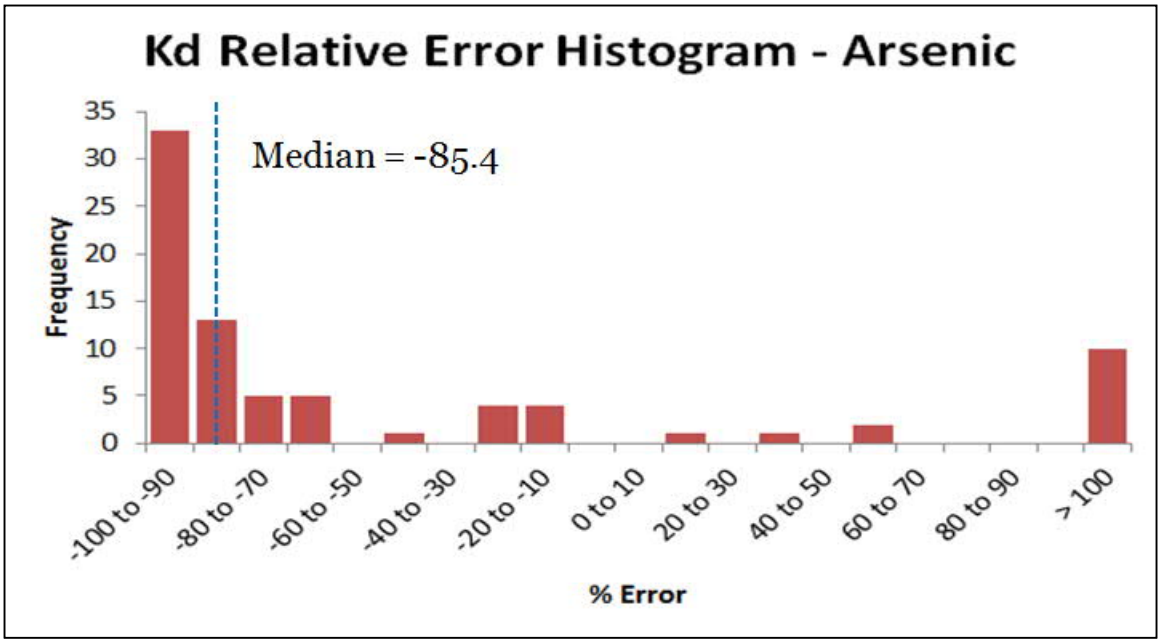

Figure 9: Histogram of Modeled Chao Method As K_d RE

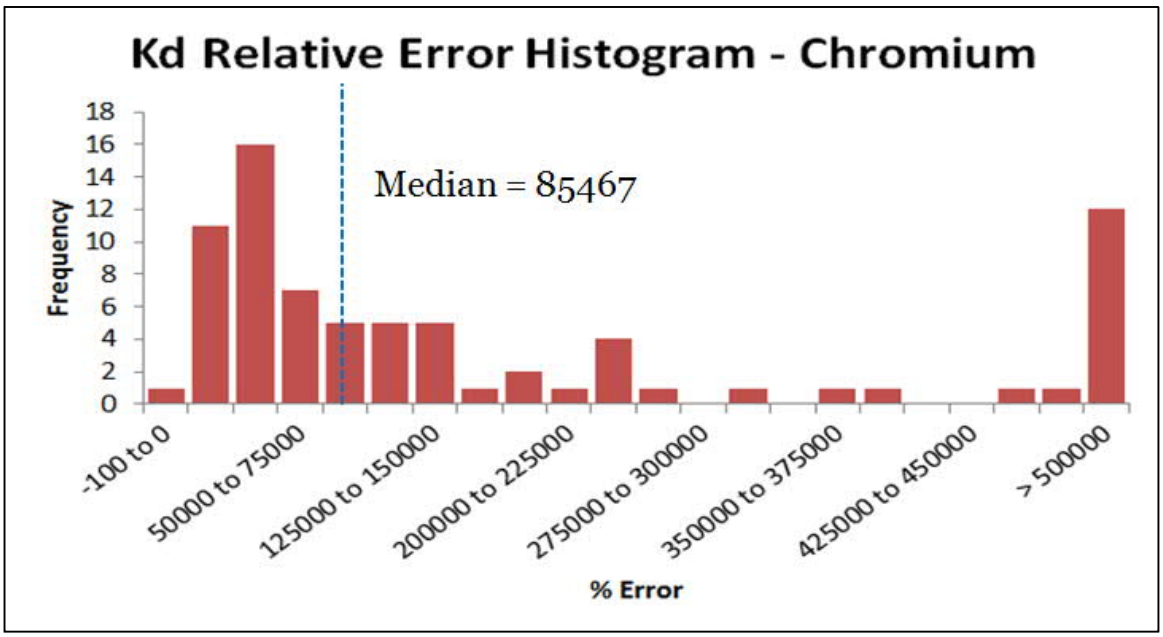

Figure 10: Histogram of Modeled Chao Method Cr K_d RE

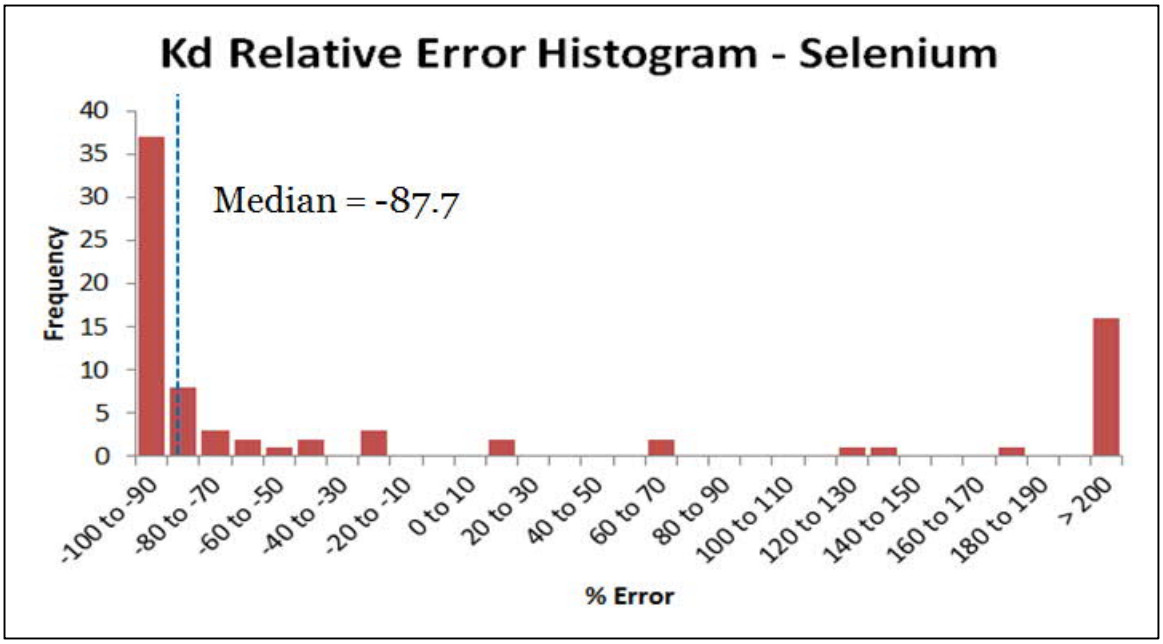

Figure 11: Histogram of Modeled Chao Method Se K_d RE

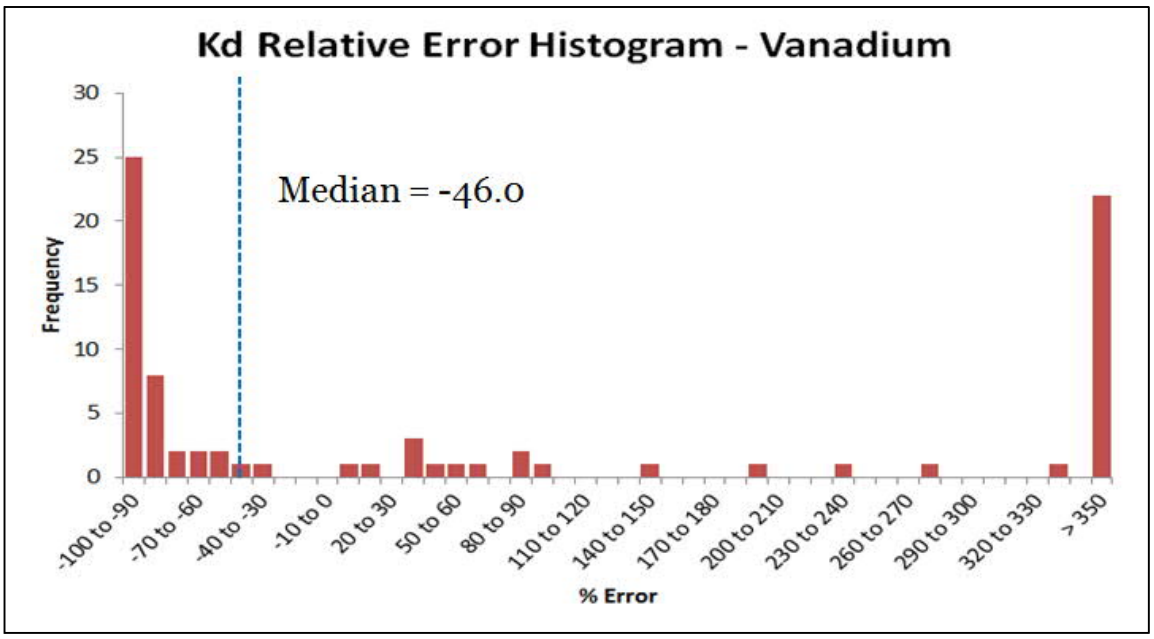

Figure 12: Histogram of Modeled Chao Method V K_d RE

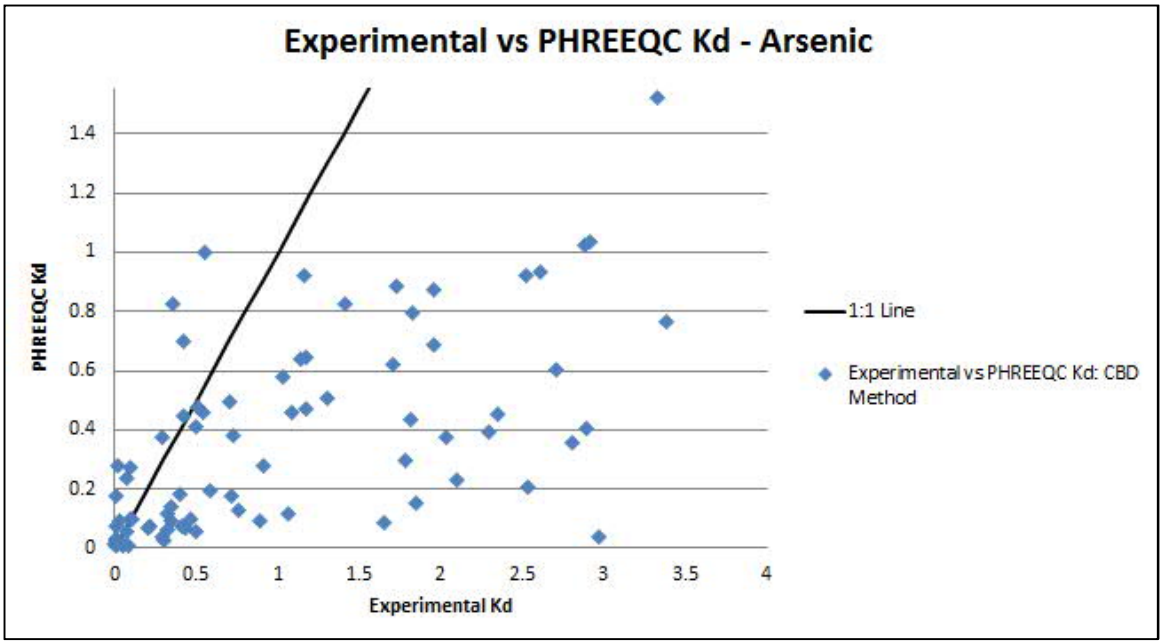

Figure 13: Experimental vs CBD method Model As K_d with 1/1 line

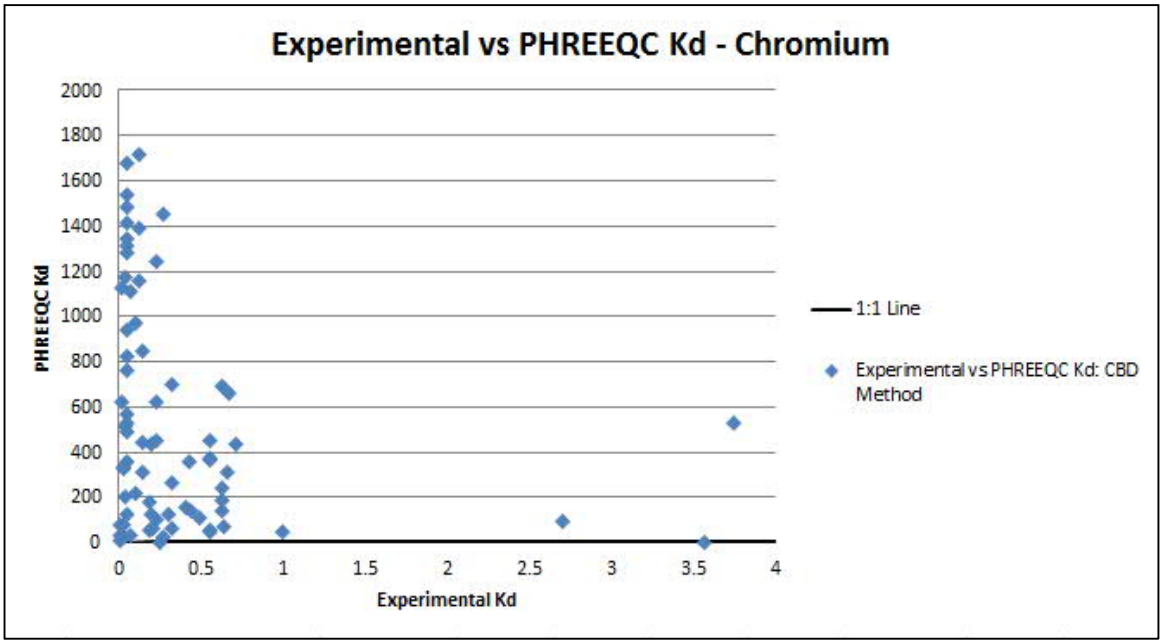

Figure 14: Experimental vs CBD method Model Cr K_d with 1/1 line

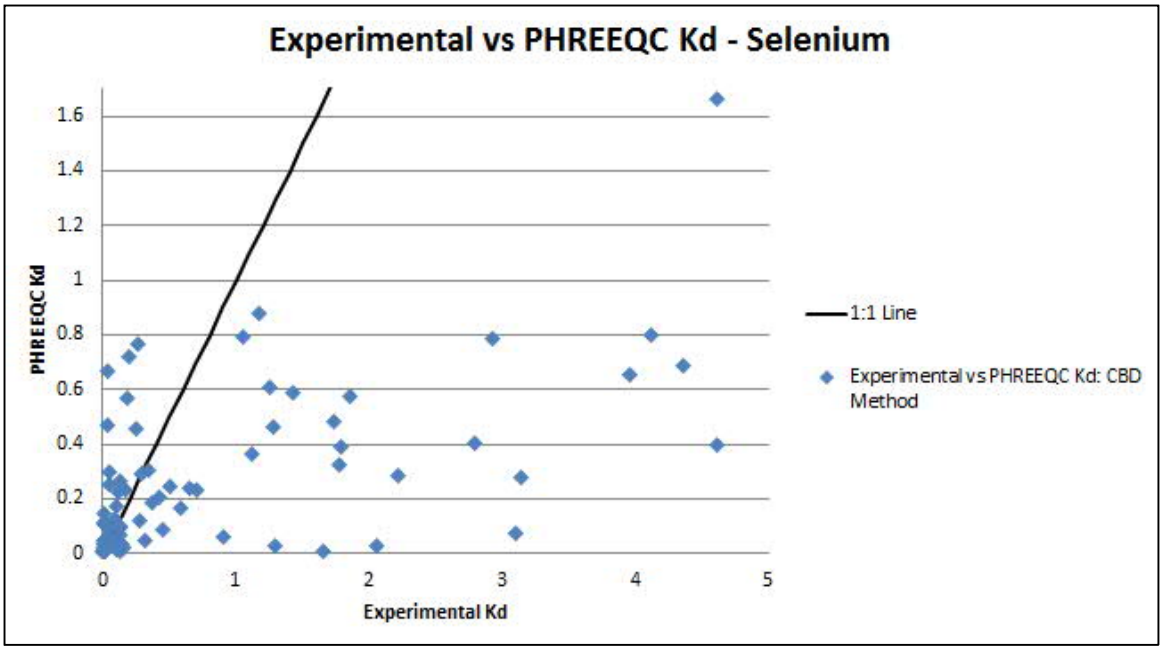

Figure 15: Experimental vs CBD method Model Se K_d with 1/1 line

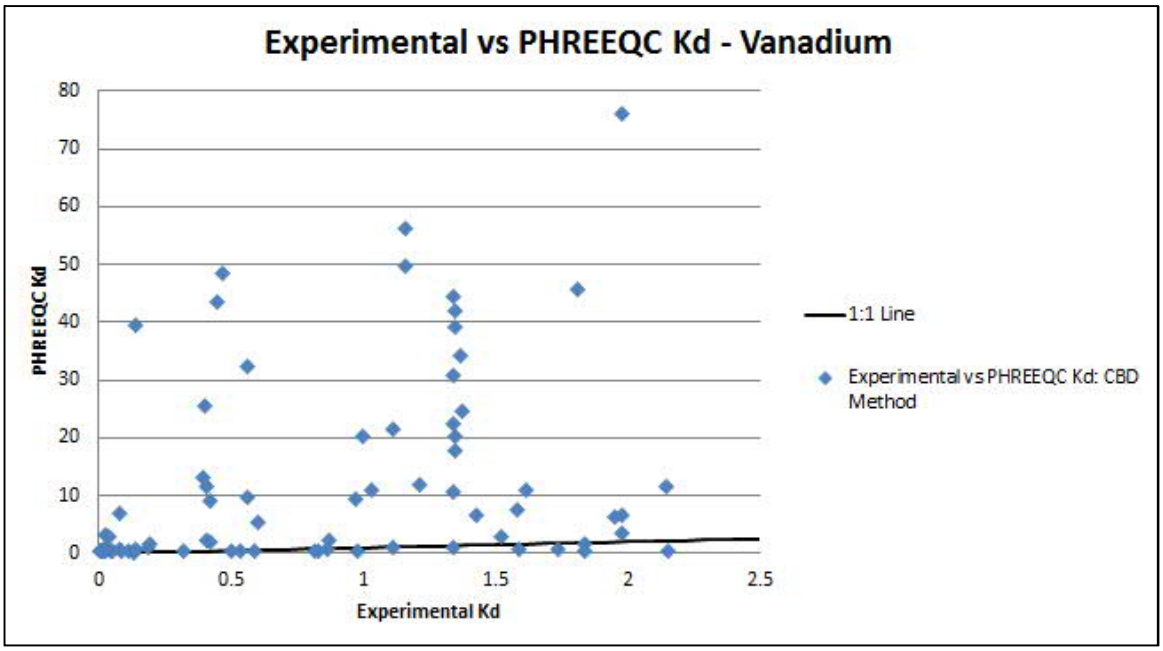

Figure 16: Experimental vs CBD method Model V K_d with 1/1 line

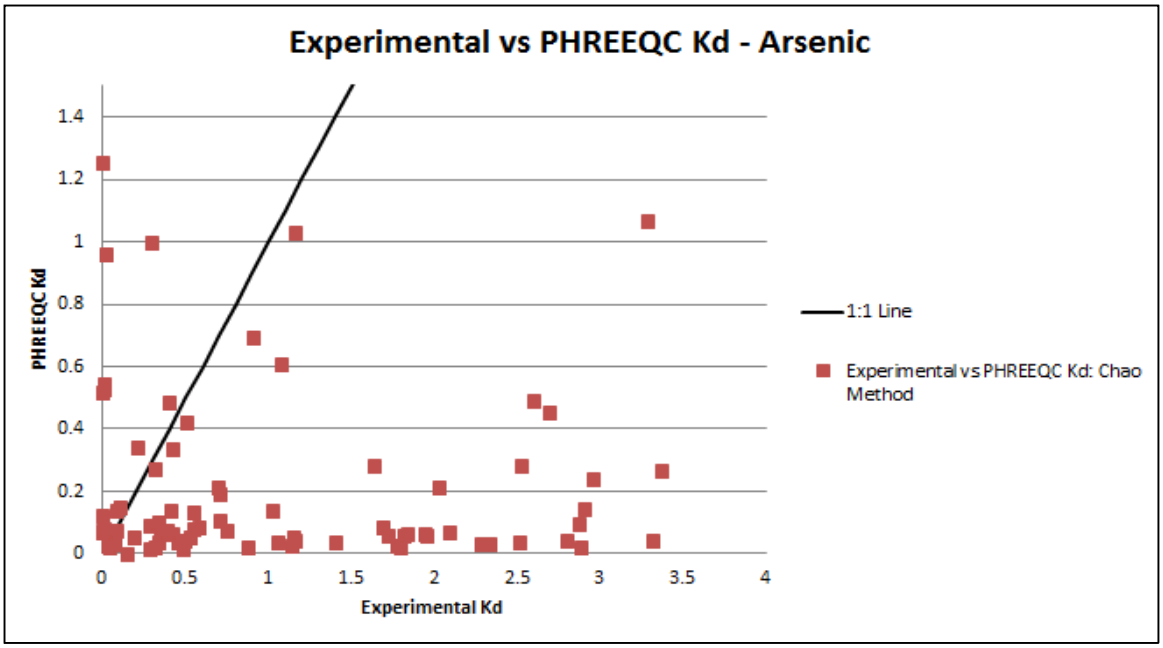

Figure 17: Experimental vs Chao method Model As K_d with 1/1 line

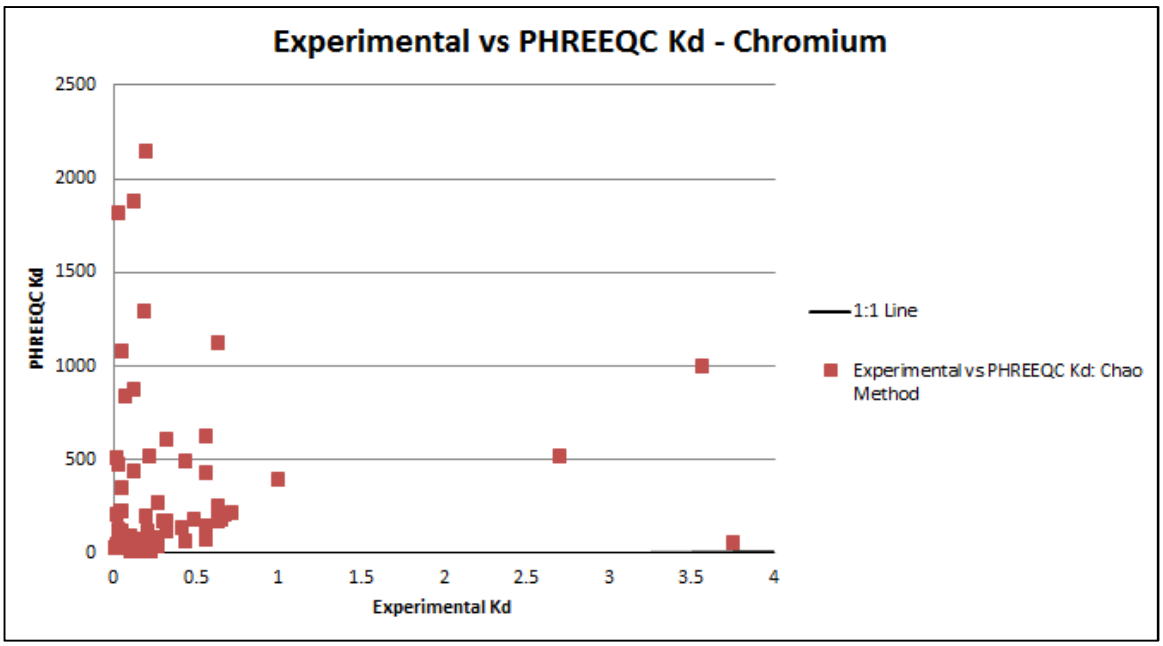

Figure 18: Experimental vs Chao method Model Cr K_d with 1/1 line

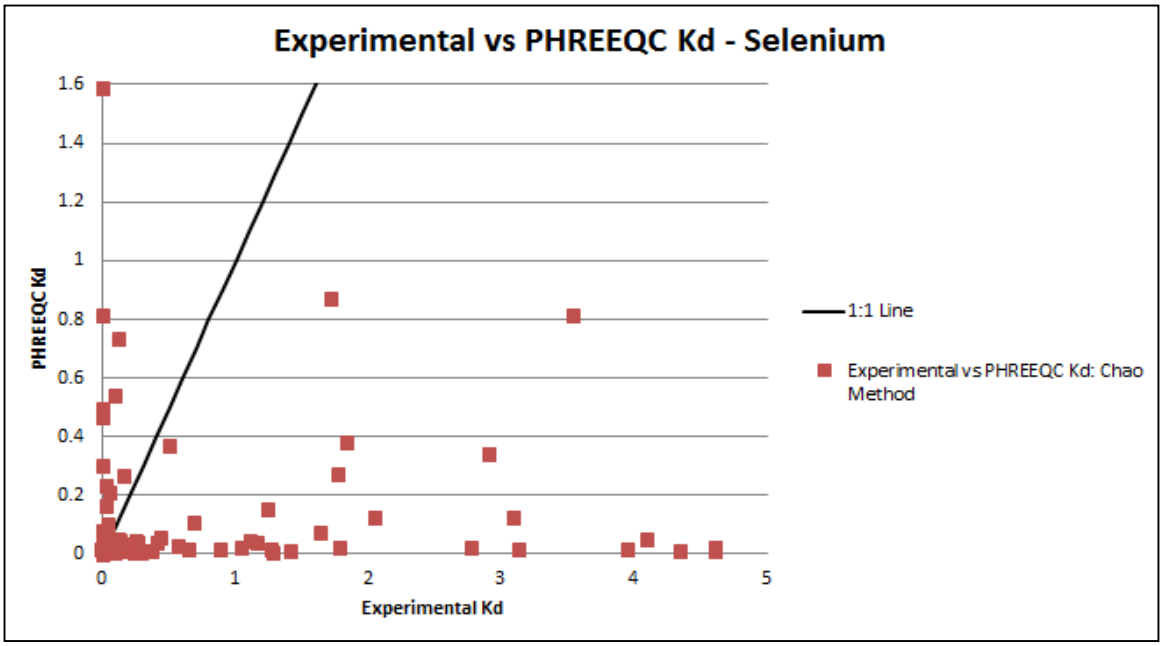

Figure 19: Experimental vs Chao method Model Se K_d with 1/1 line

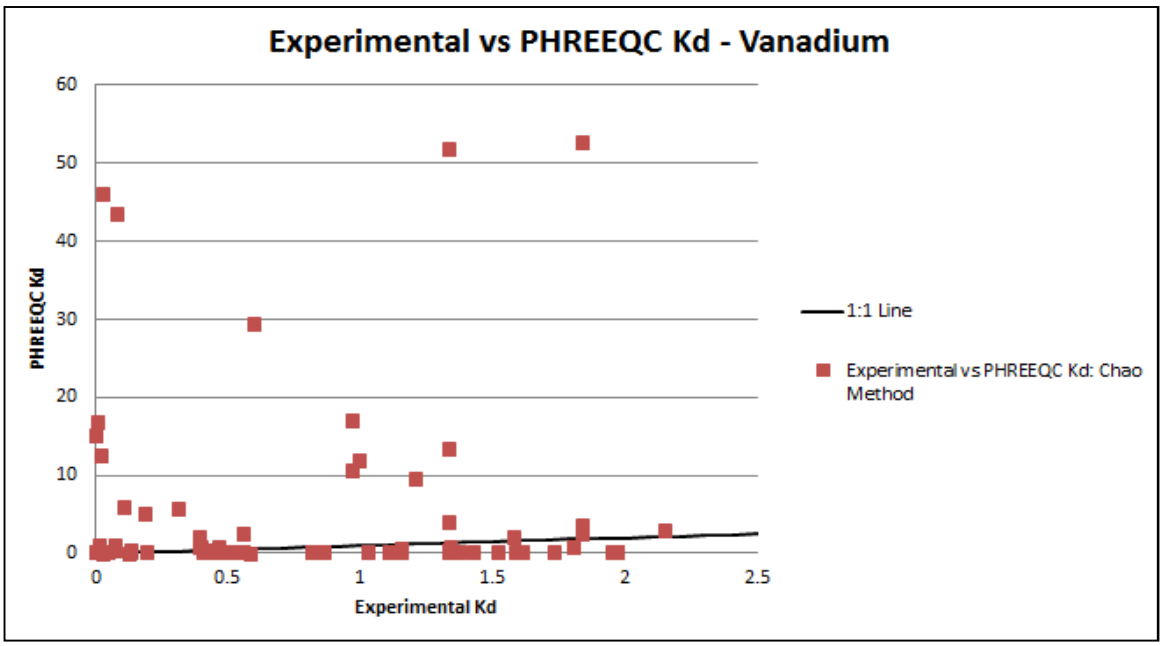

Figure 20: Experimental vs Chao method Model V K_d with 1/1 line

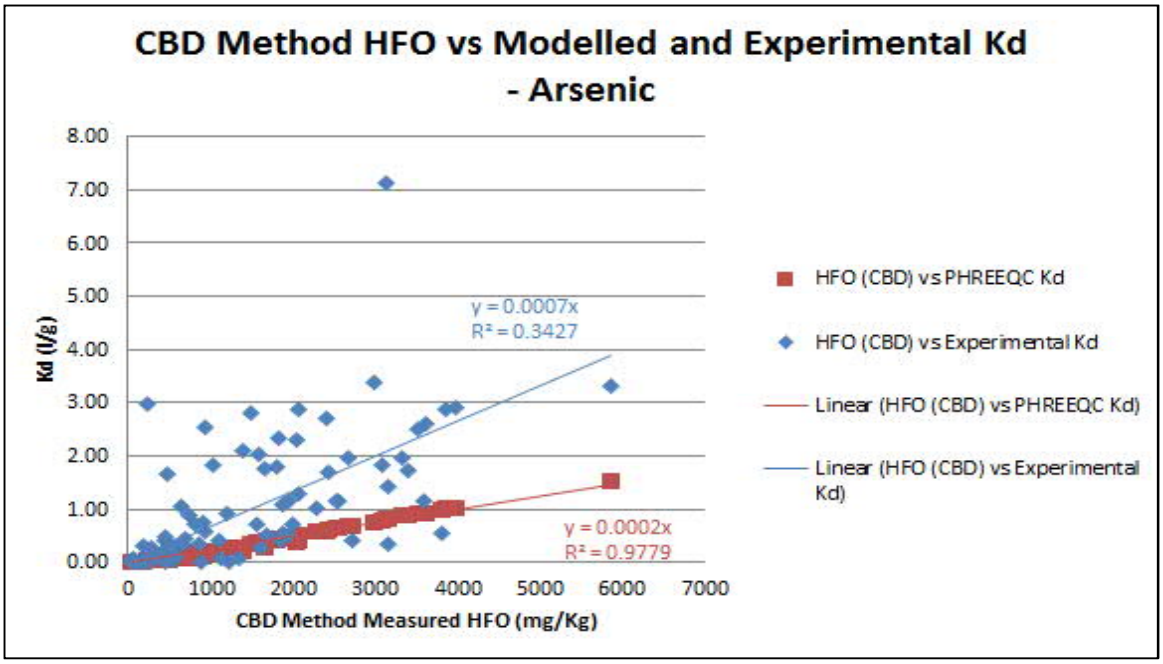

Figure 21: Experimental and model CBD method HFO vs As K_d plot

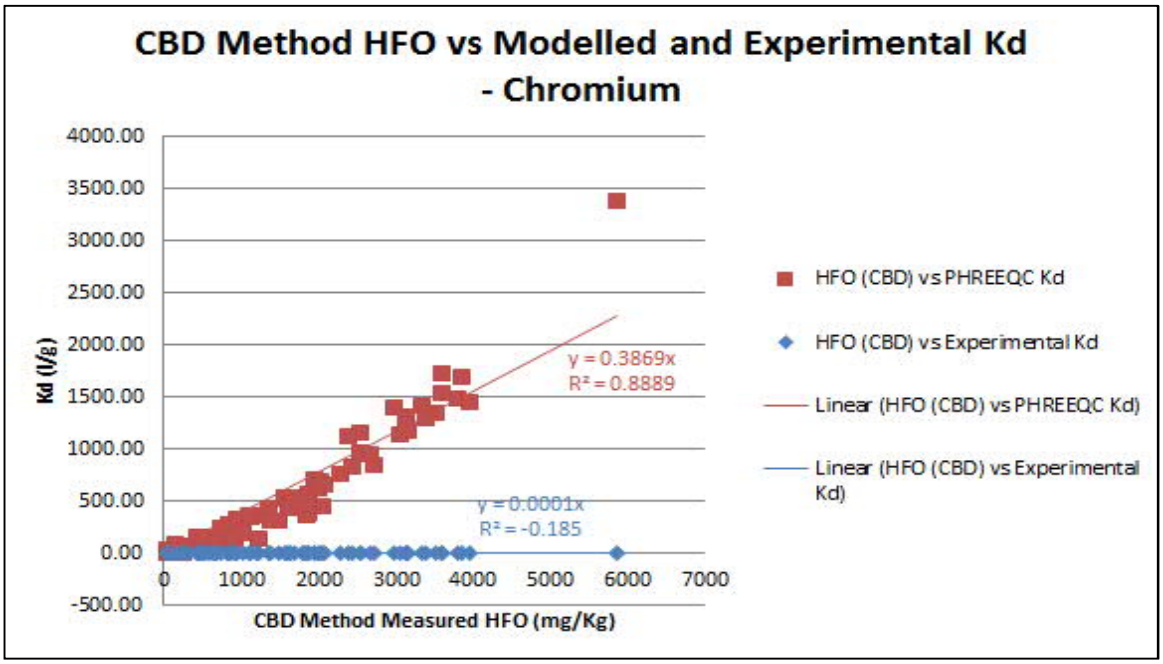

Figure 22: Experimental and model CBD method HFO vs Cr K_d plot

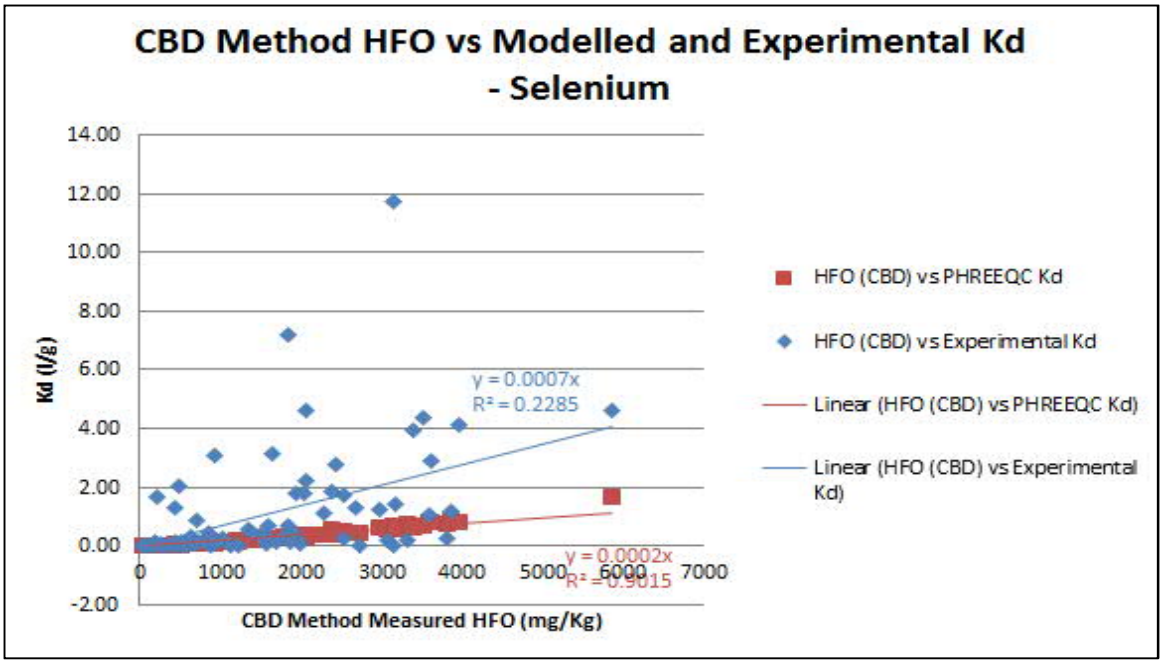

Figure 23: Experimental and model CBD method HFO vs Se K_d plot

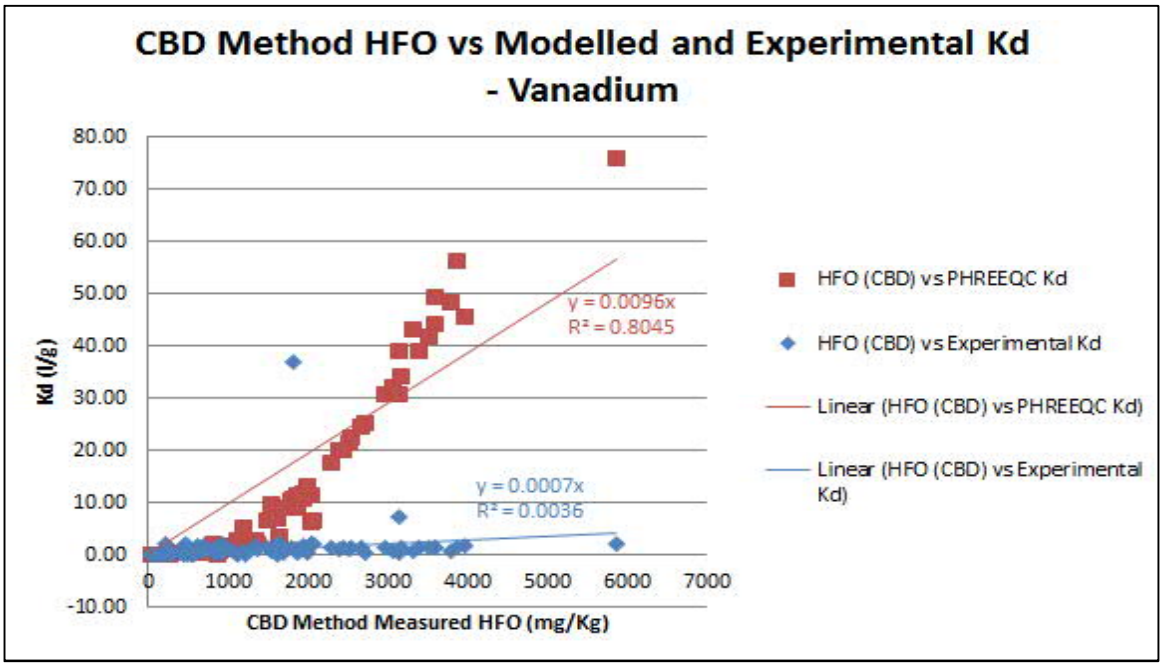

Figure 24: Experimental and model CBD method HFO vs V K_d plot

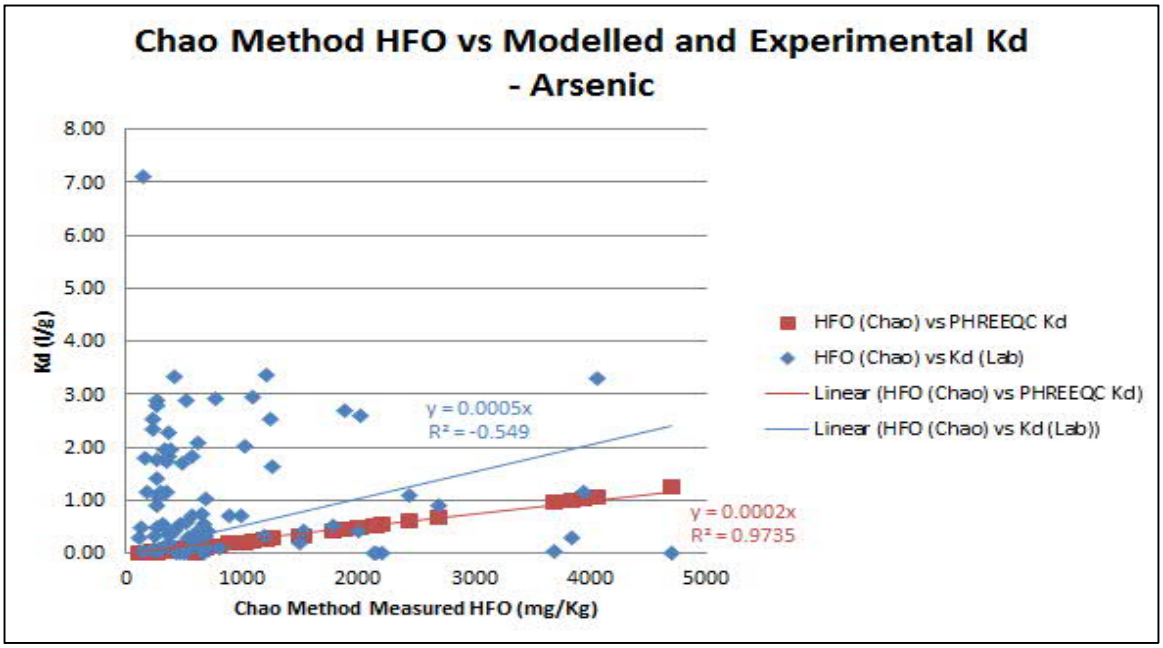

Figure 25: Experimental and model Chao method HFO vs As K_d plot

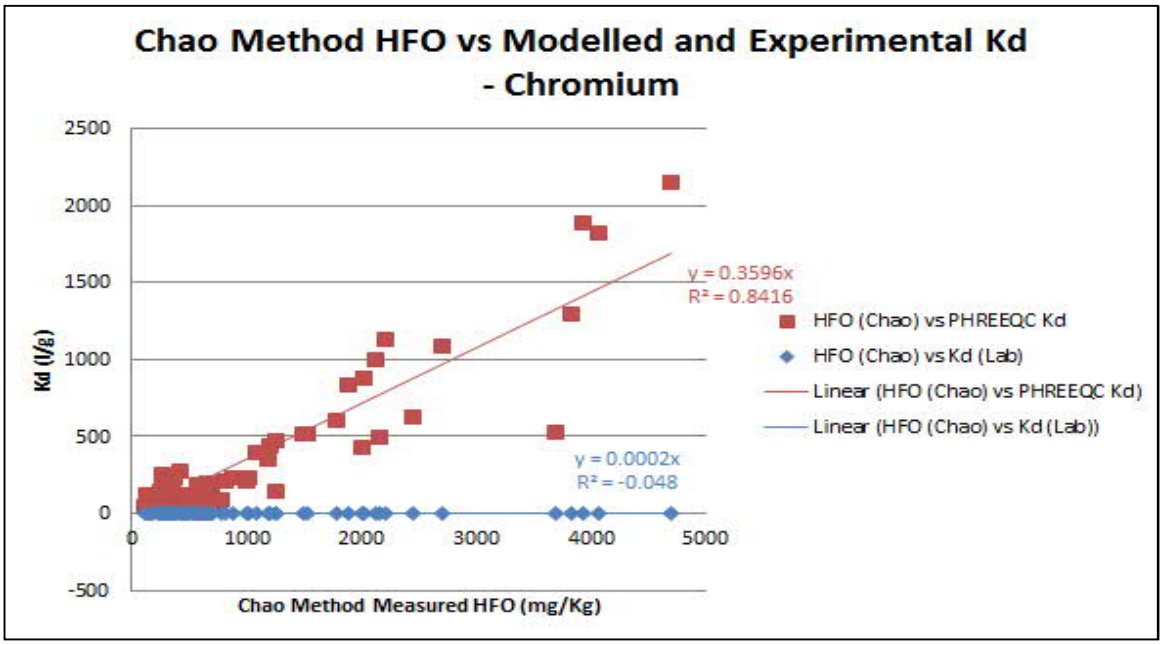

Figure 26: Experimental and model Chao method HFO vs Cr K_d plot

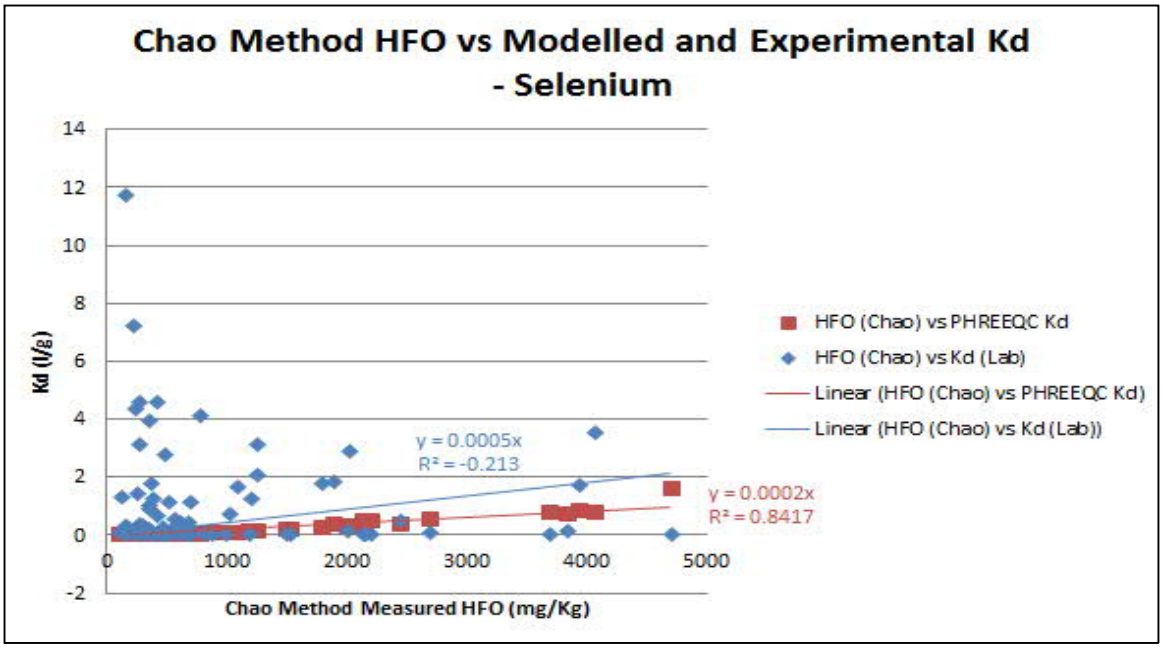

Figure 27: Experimental and model Chao method HFO vs Se K_d plot

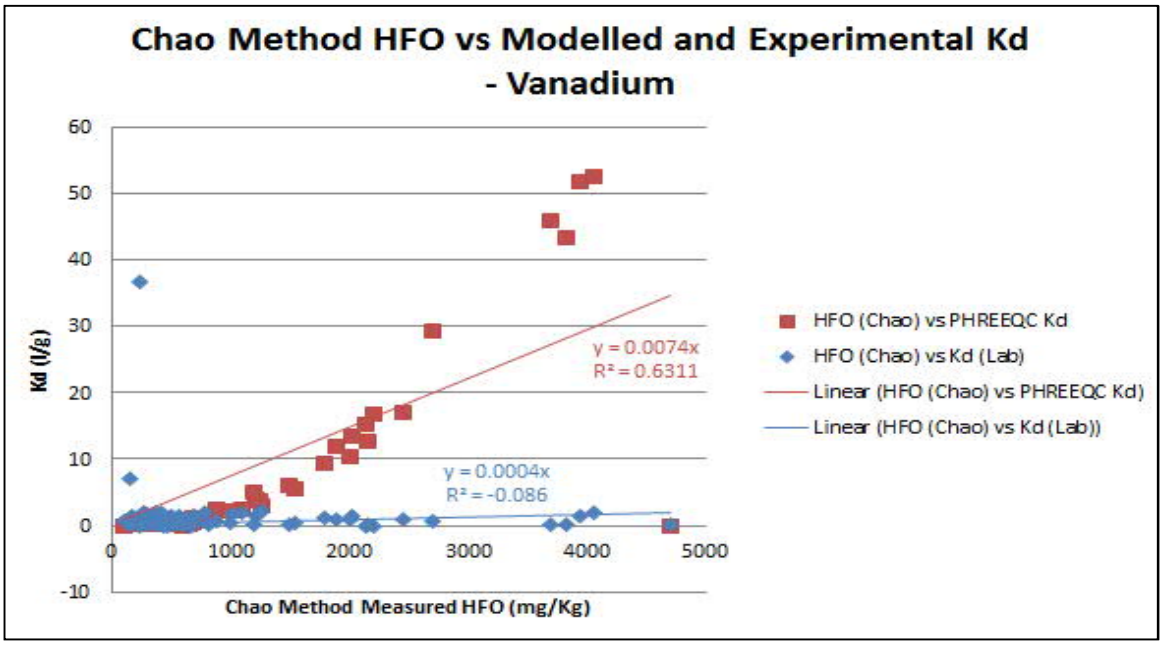

Figure 28: Experimental and model Chao method HFO vs V K_d plot

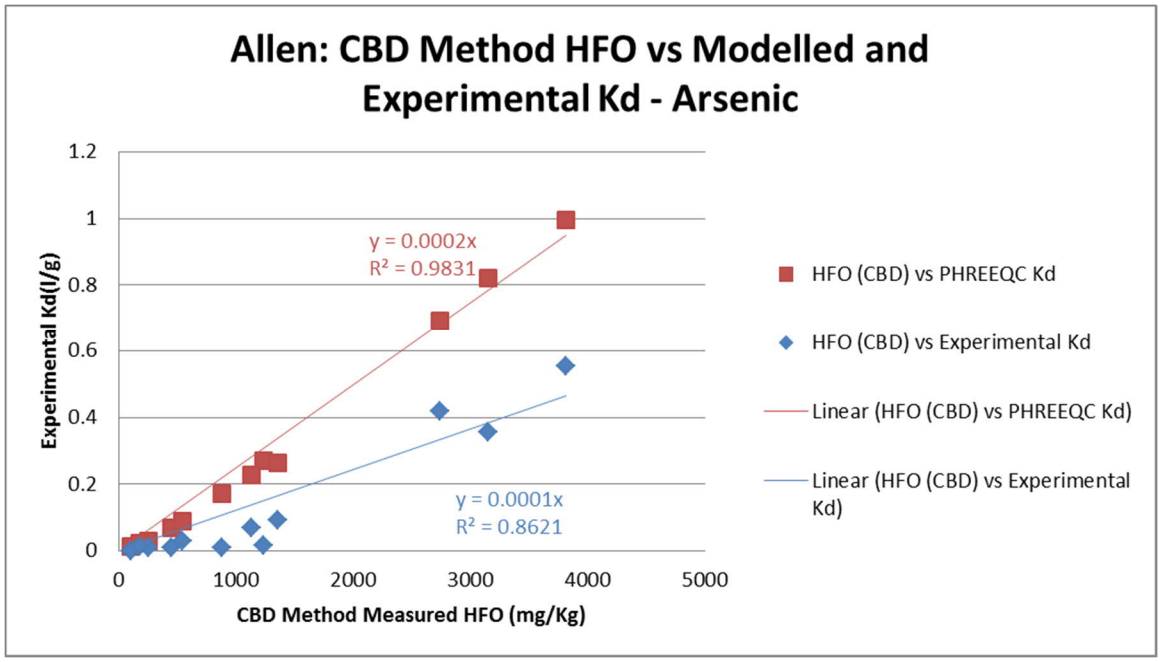

Figure 29: Experimental and model CBD method HFO vs As Kd plot - Allen

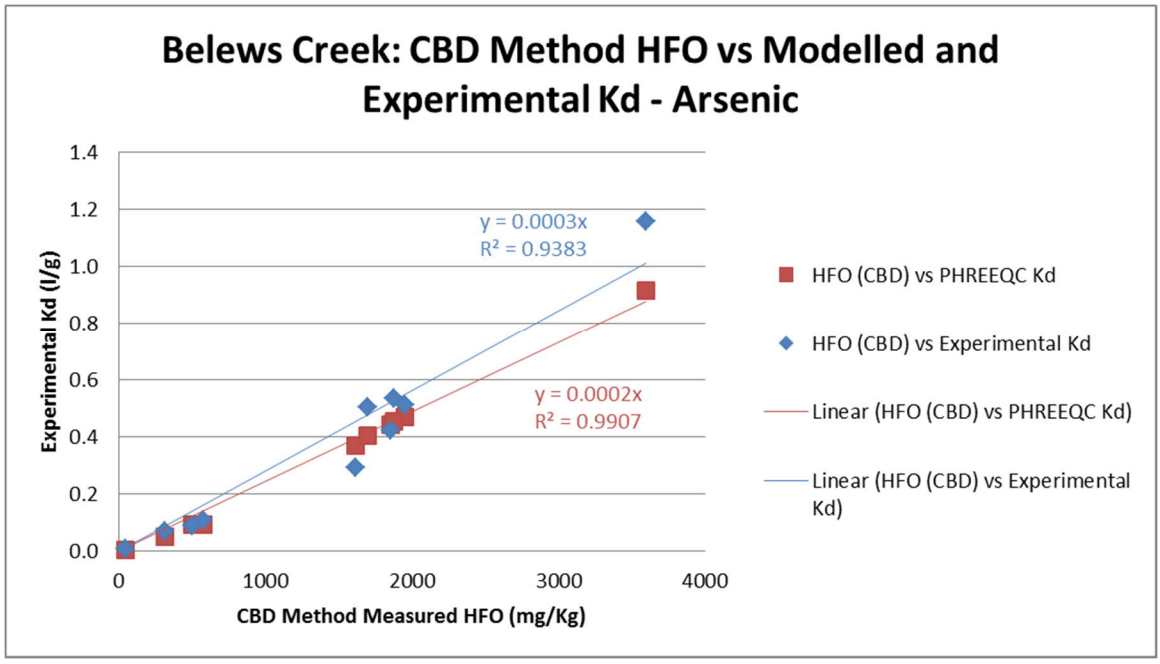

Figure 30: Experimental and model CBD method HFO vs As Kd plot - Belews Creek

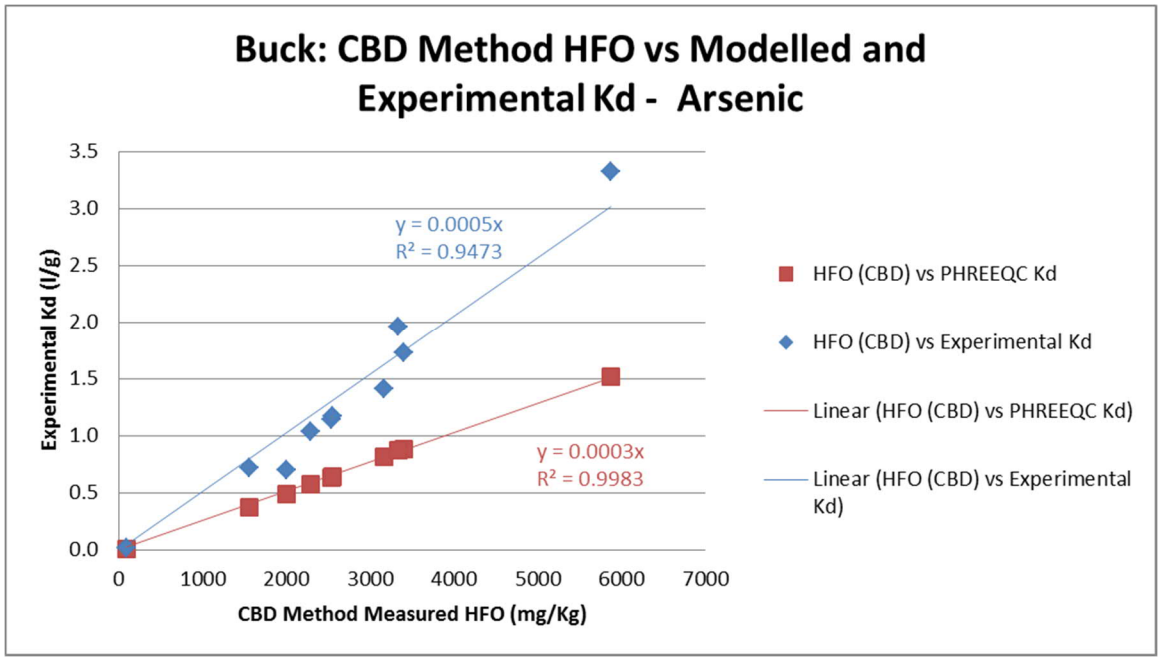

Figure 31: Experimental and model CBD method HFO vs As Kd plot - Buck

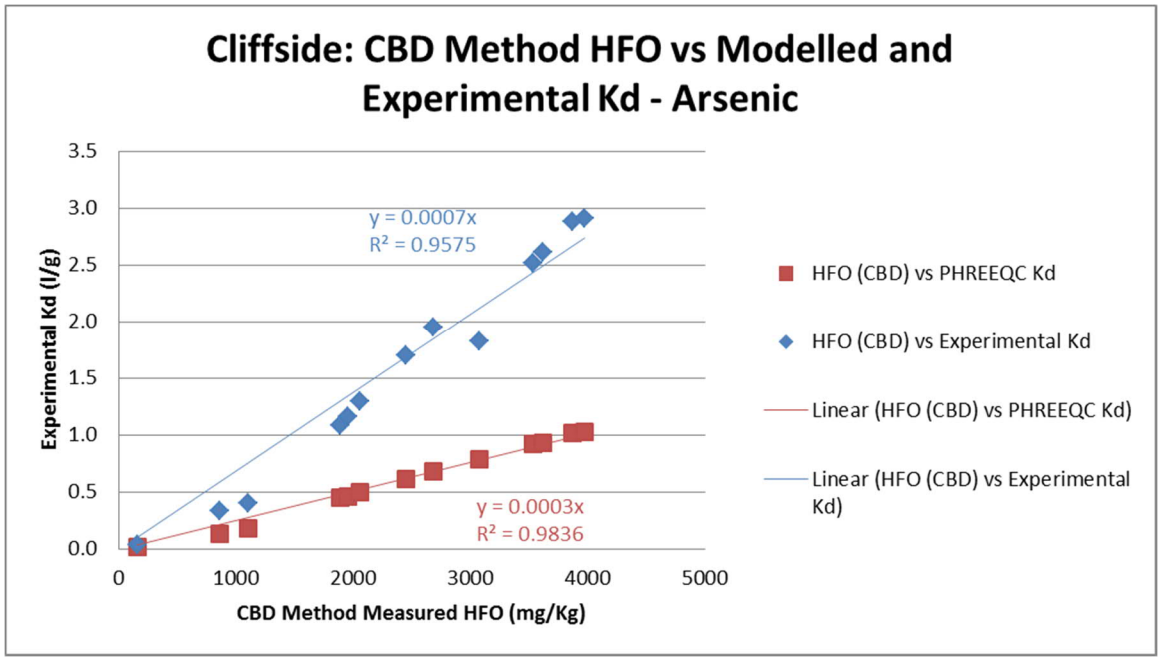

Figure 32: Experimental and model CBD method HFO vs As Kd plot - Cliffside

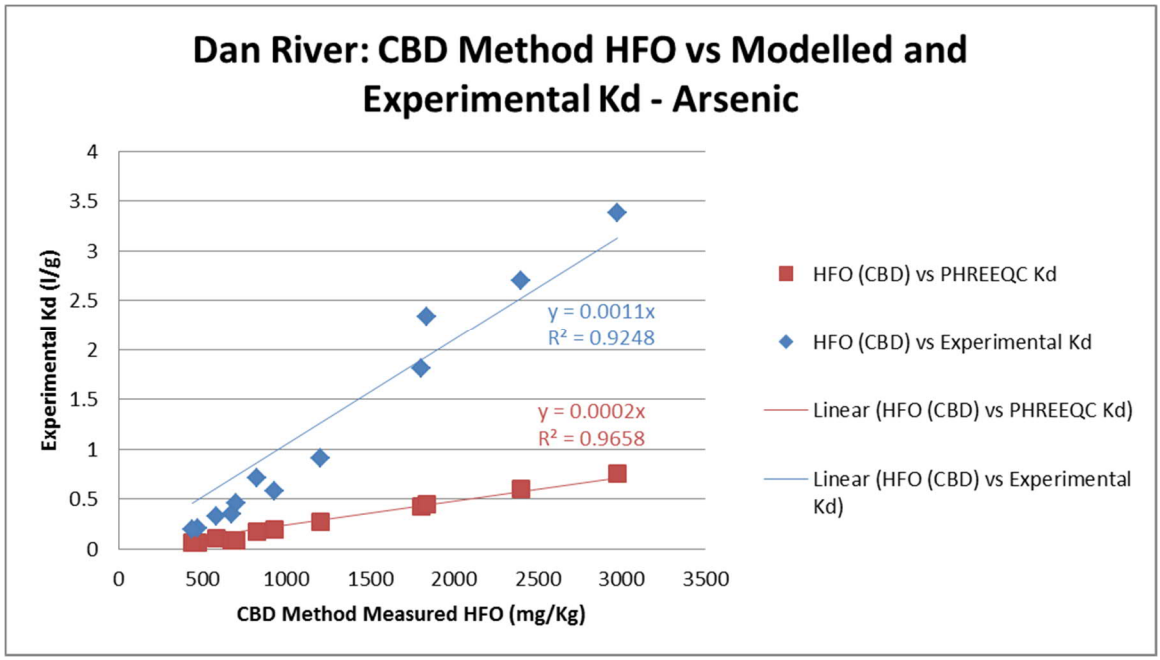

Figure 33: Experimental and model CBD method HFO vs As Kd plot - Dan River

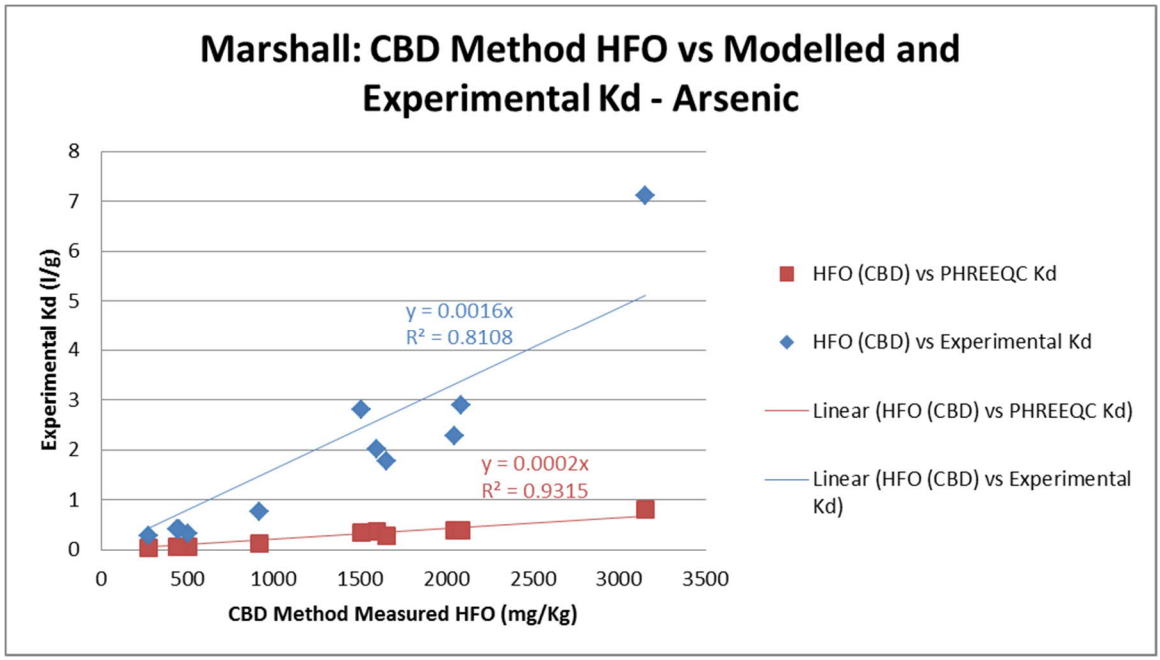

Figure 34: Experimental and model CBD method HFO vs As Kd plot - Marshall

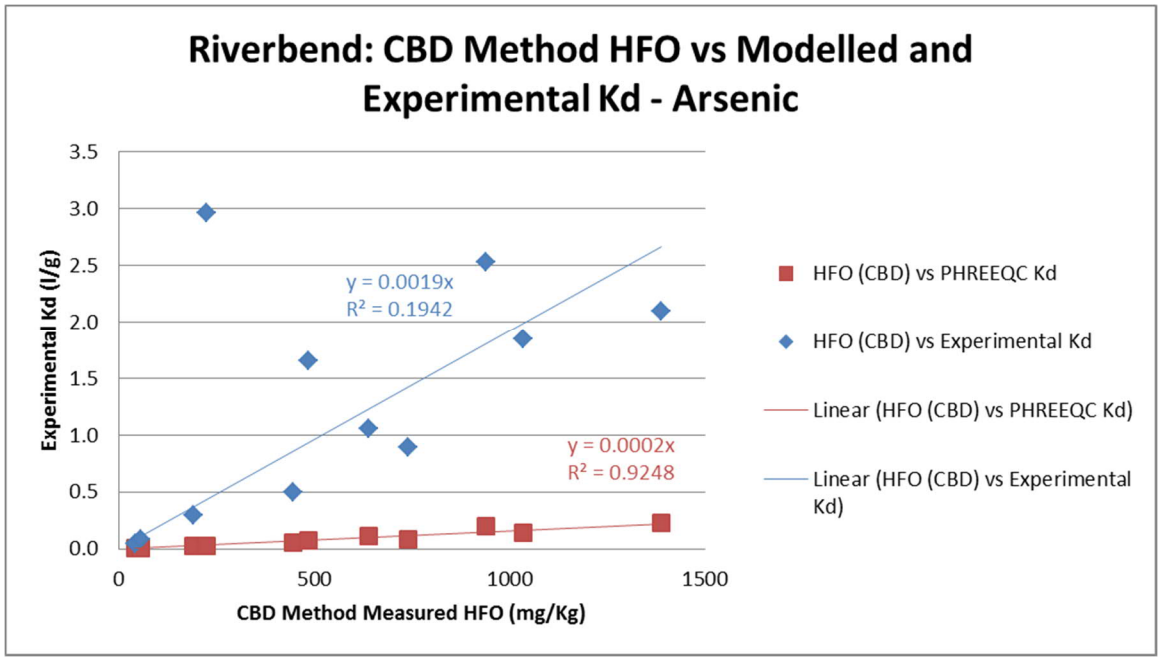

Figure 35: Experimental and model CBD method HFO vs As Kd plot - Riverbend

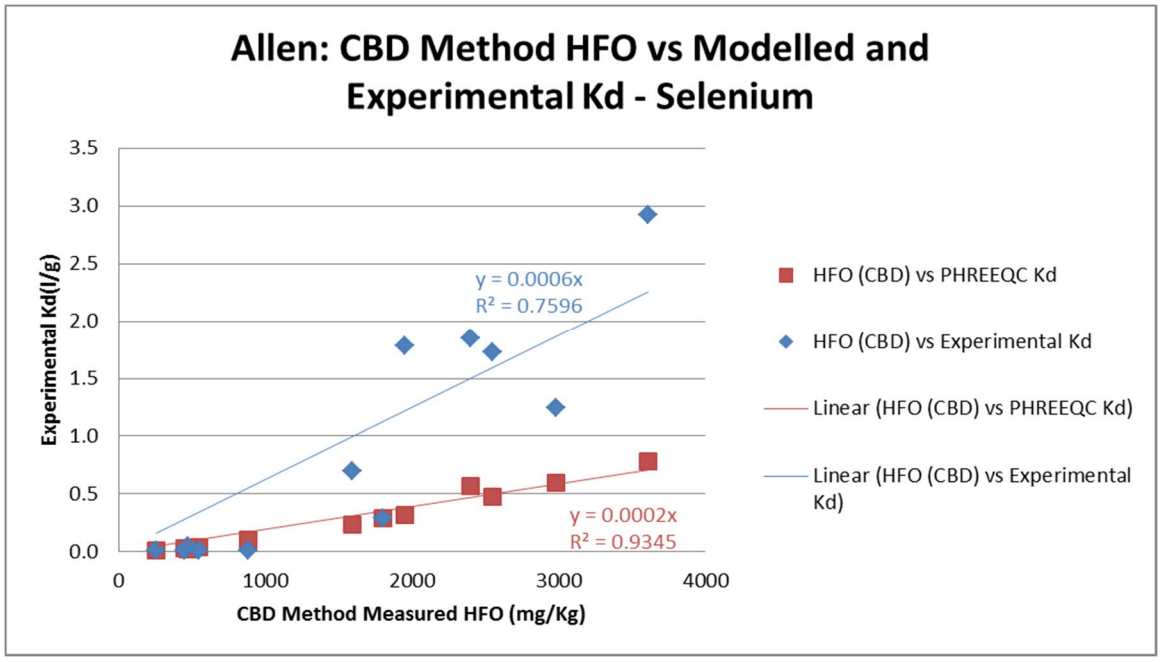

Figure 36: Experimental and model CBD method HFO vs Se Kd plot - Allen

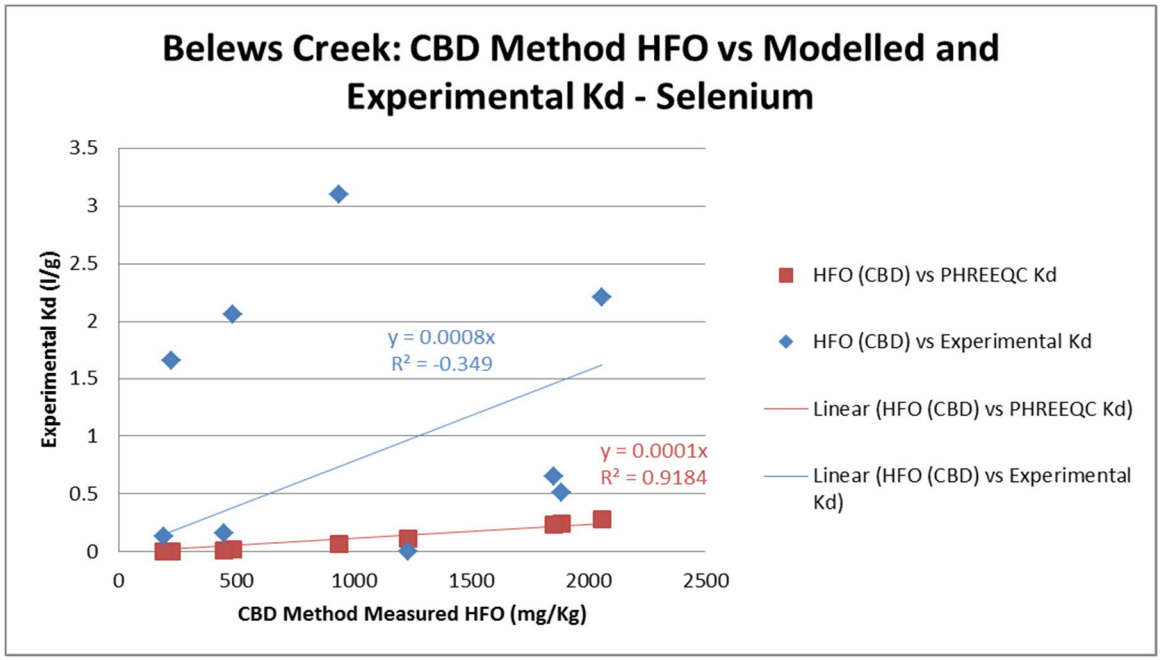

Figure 37: Experimental and model CBD method HFO vs Se Kd plot - Belews Creek

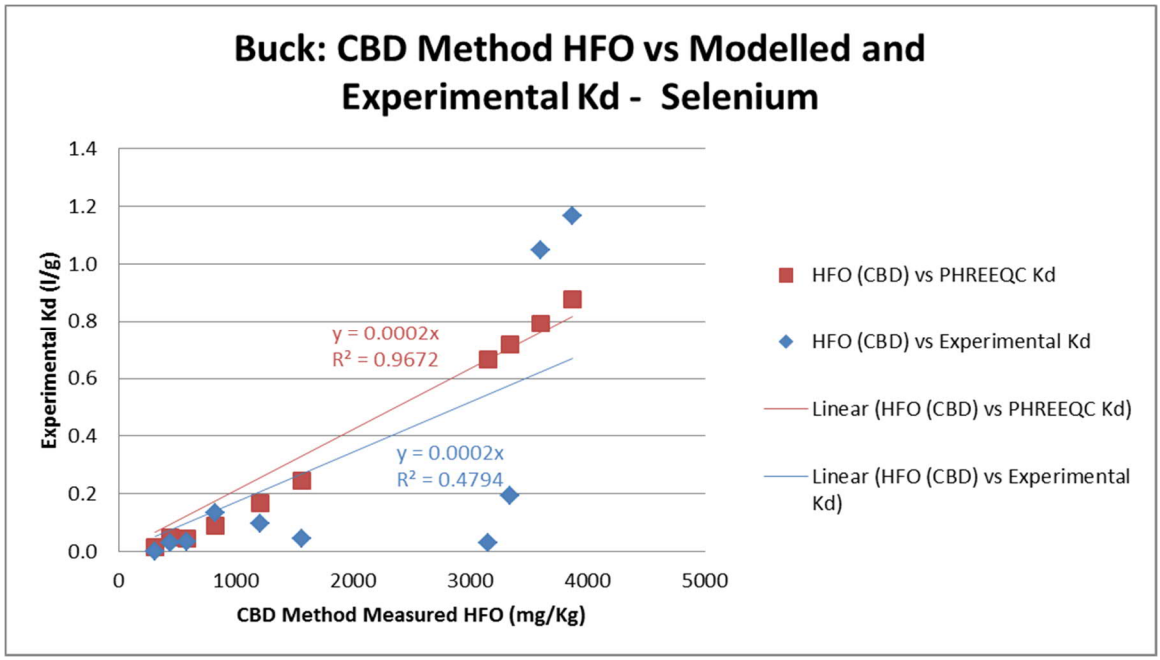

Figure 38: Experimental and model CBD method HFO vs Se Kd plot - Buck

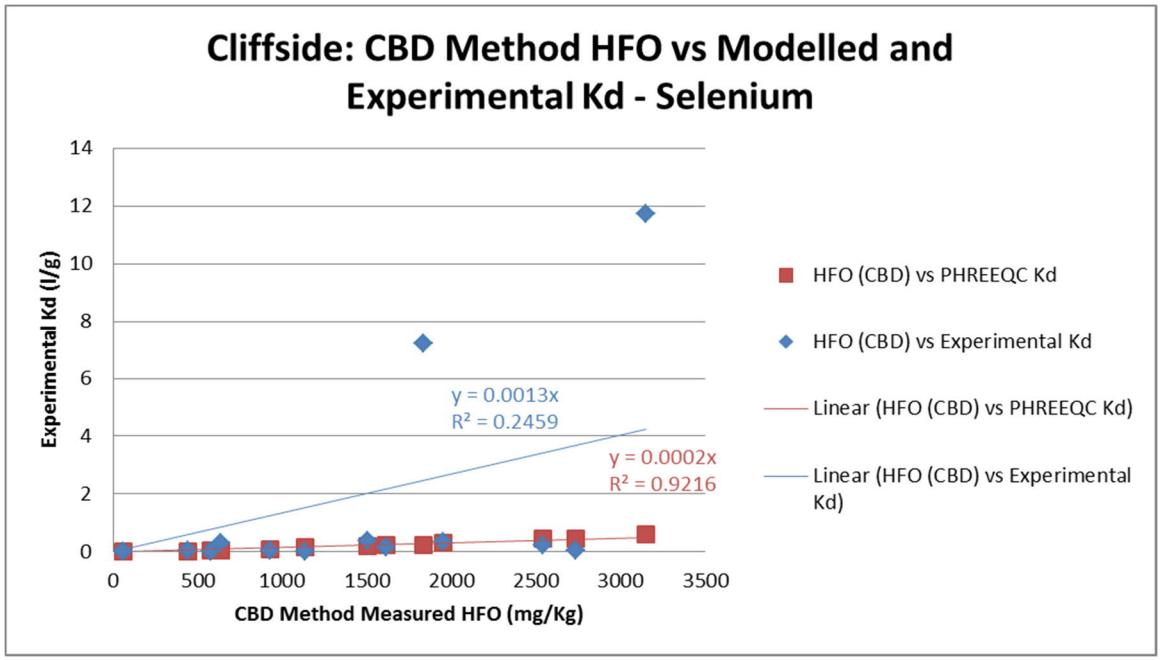

Figure 39: Experimental and model CBD method HFO vs Se Kd plot - Cliffside

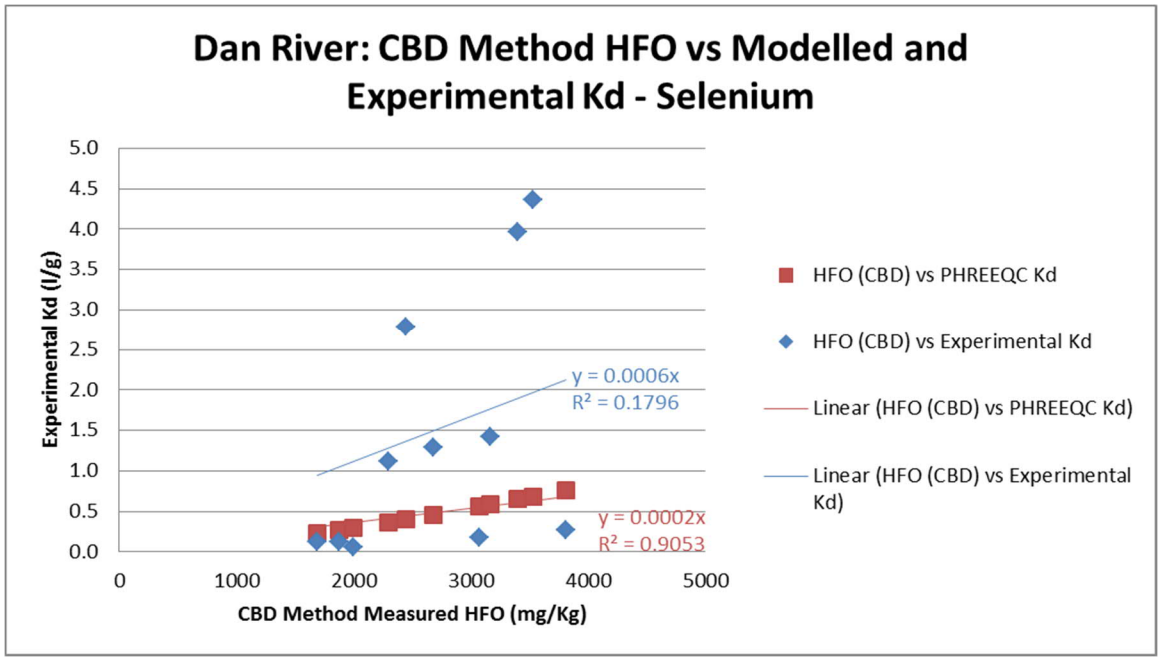

Figure 40: Experimental and model CBD method HFO vs Se Kd plot - Dan River

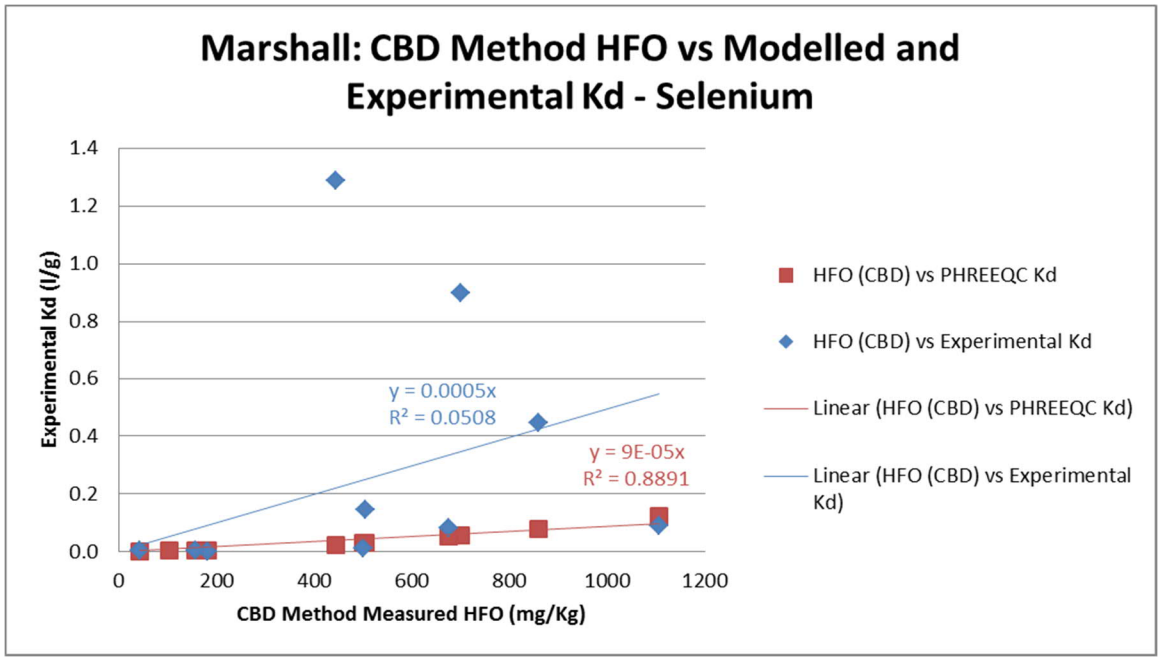

Figure 41: Experimental and model CBD method HFO vs Se Kd plot - Marshall

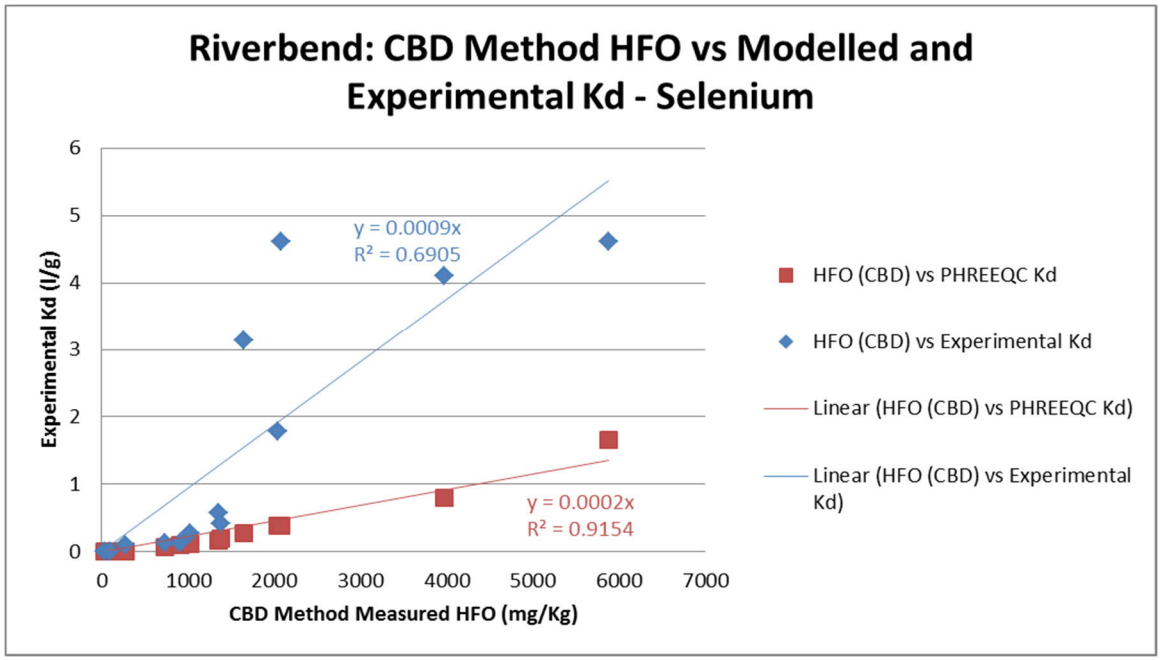

Figure 42: Experimental and model CBD method HFO vs Se Kd plot - Riverbend

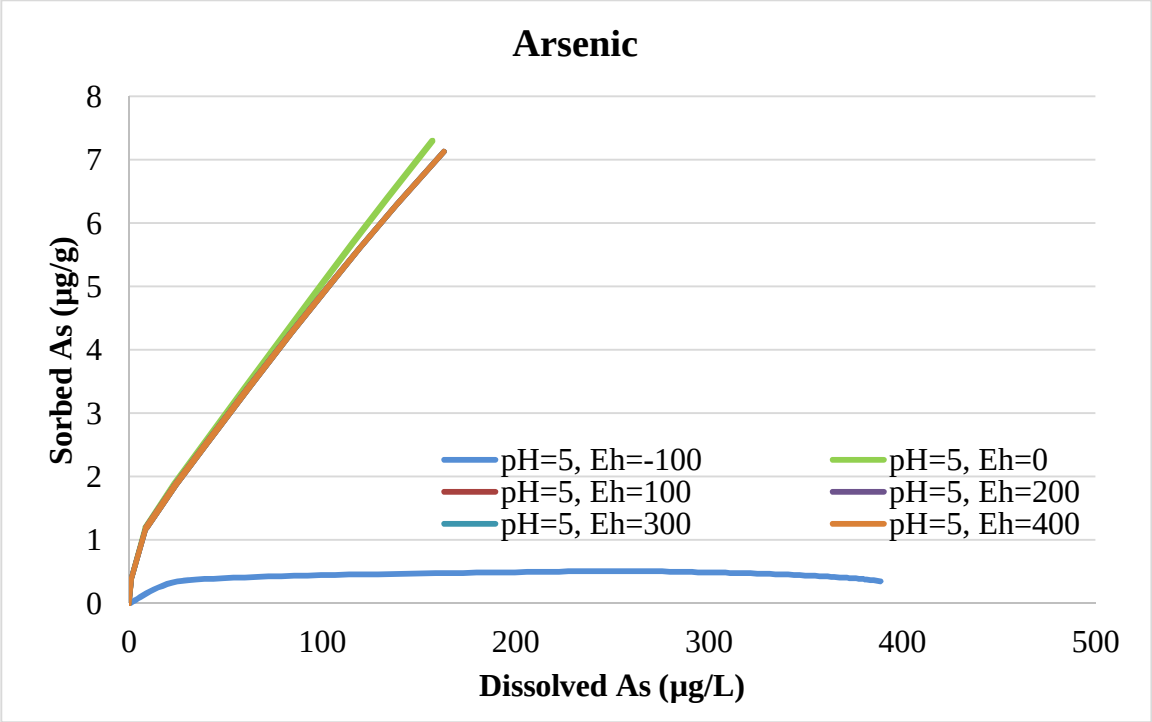

Figure 43: As sensitivity model with varied Eh and pH 5

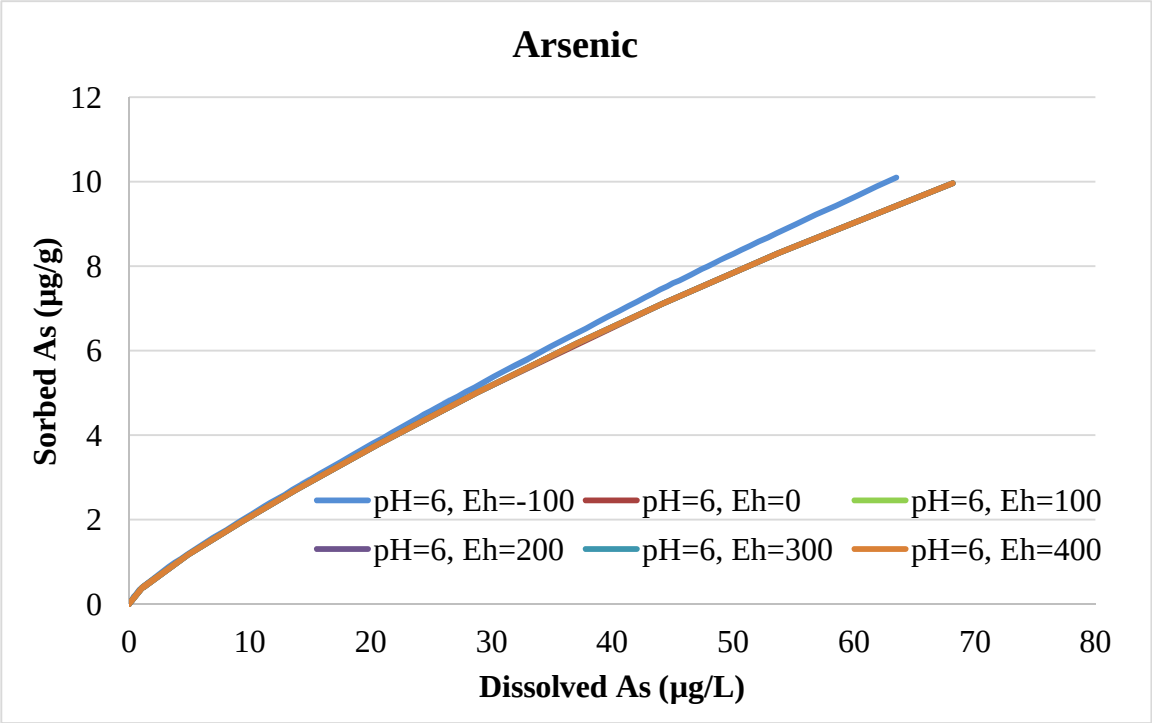

Figure 44: As sensitivity model with varied Eh and pH 6

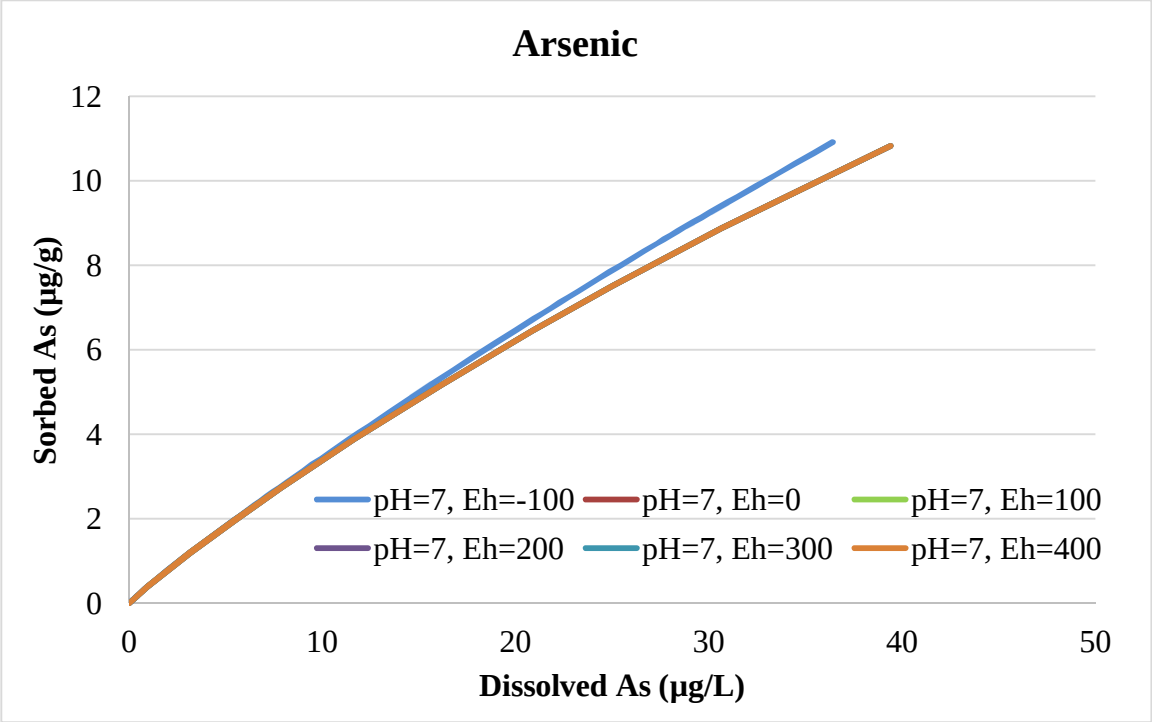

Figure 45: As sensitivity model with varied Eh and pH 7

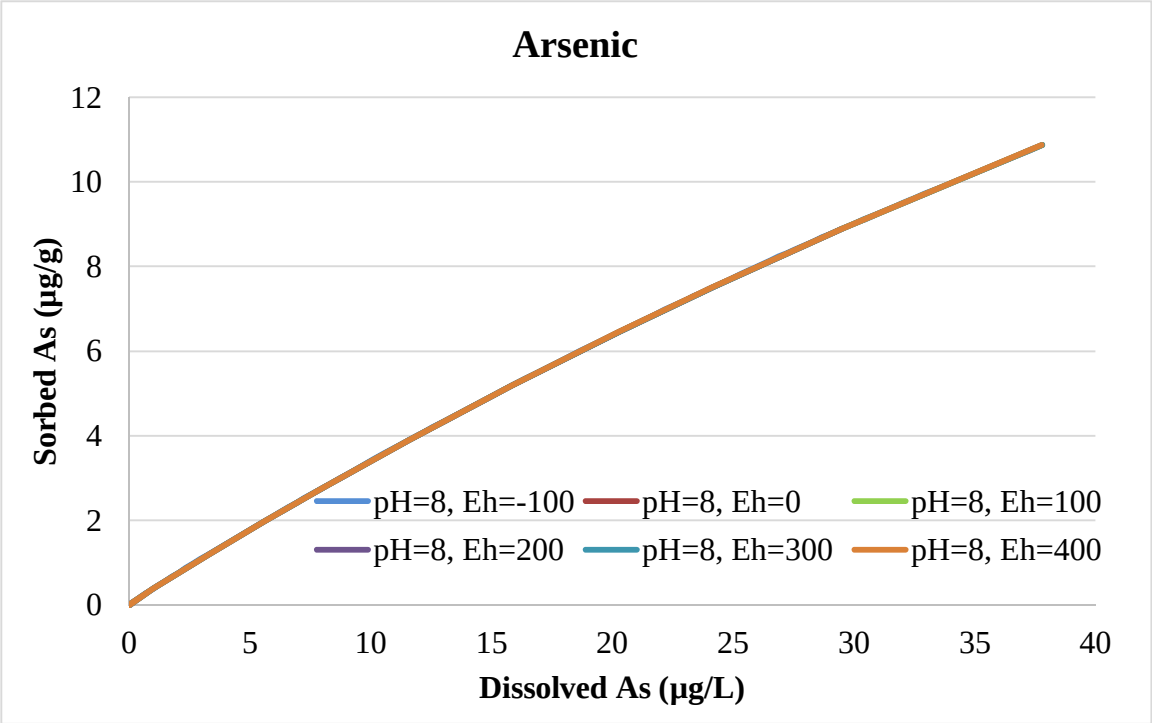

Figure 46: As sensitivity model with varied Eh and pH 8

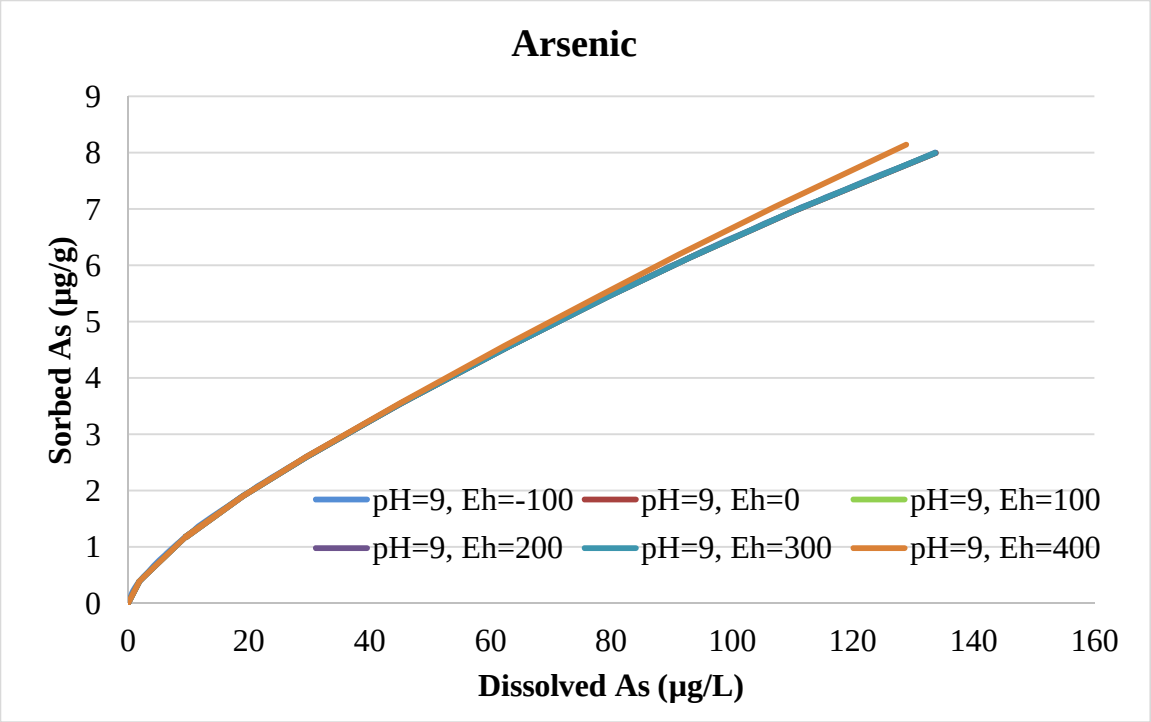

Figure 47: As sensitivity model with varied Eh and pH 9

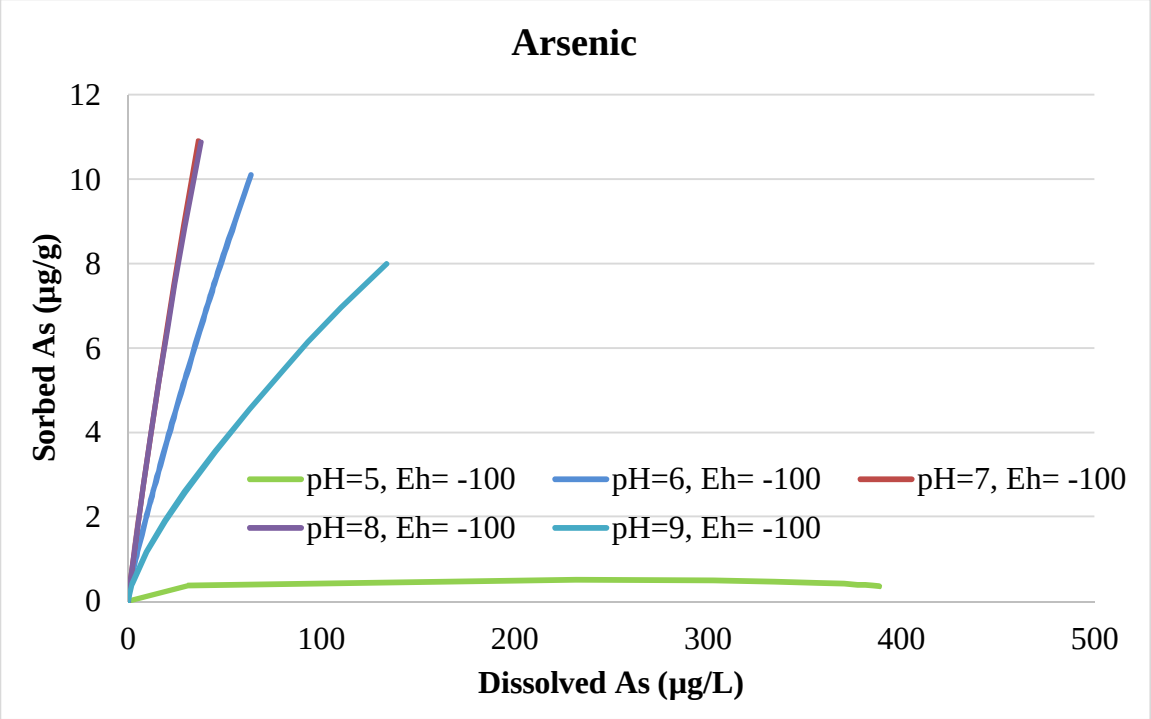

Figure 48: As sensitivity model with varied pH and Eh -100

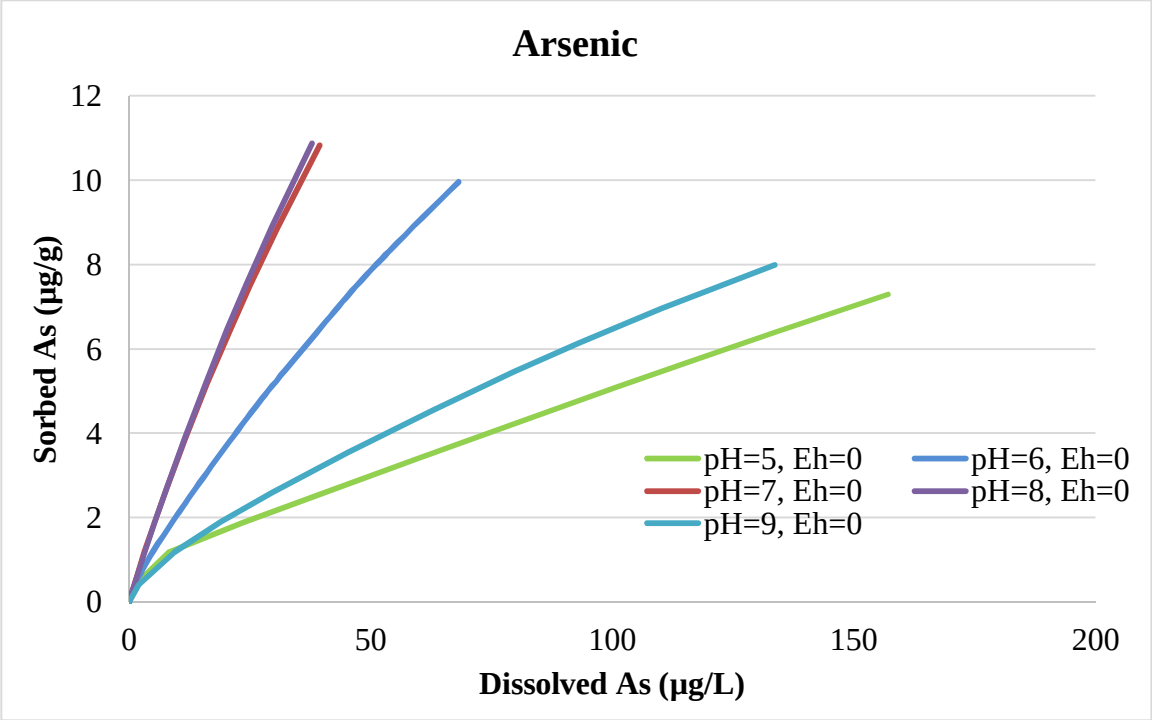

Figure 49: As sensitivity model with varied pH and Eh 0

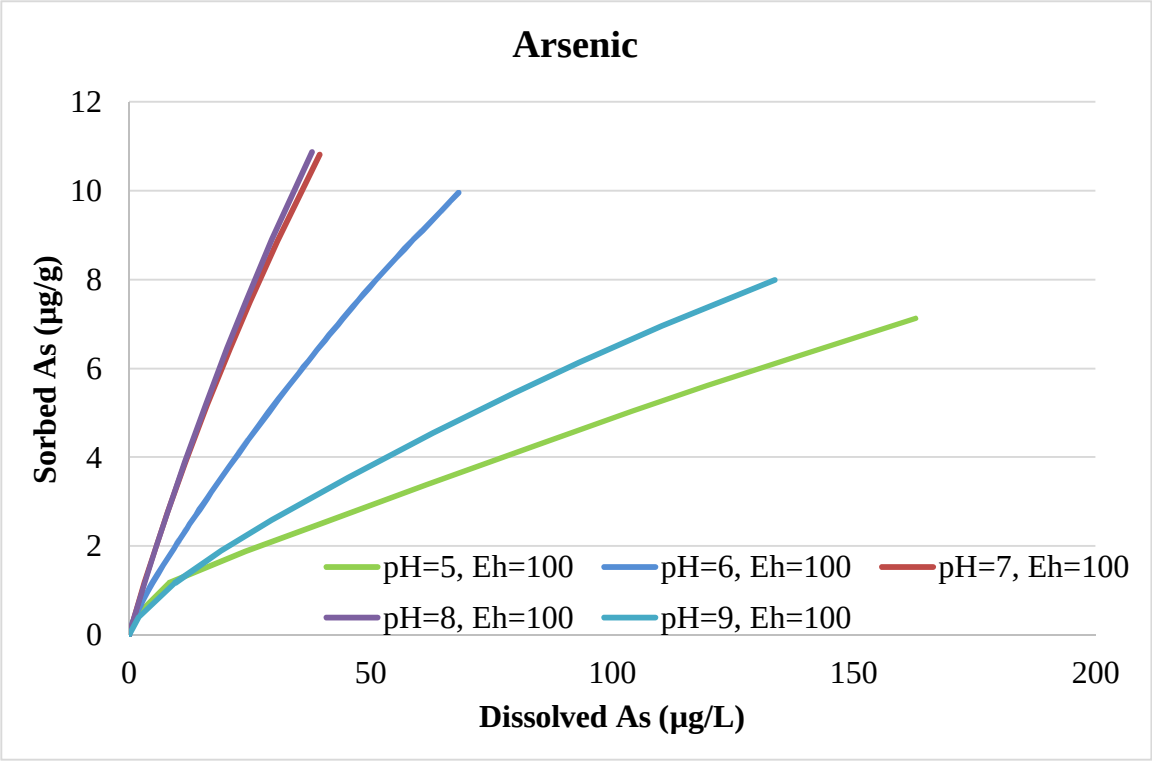

Figure 50: As sensitivity model with varied pH and Eh 100

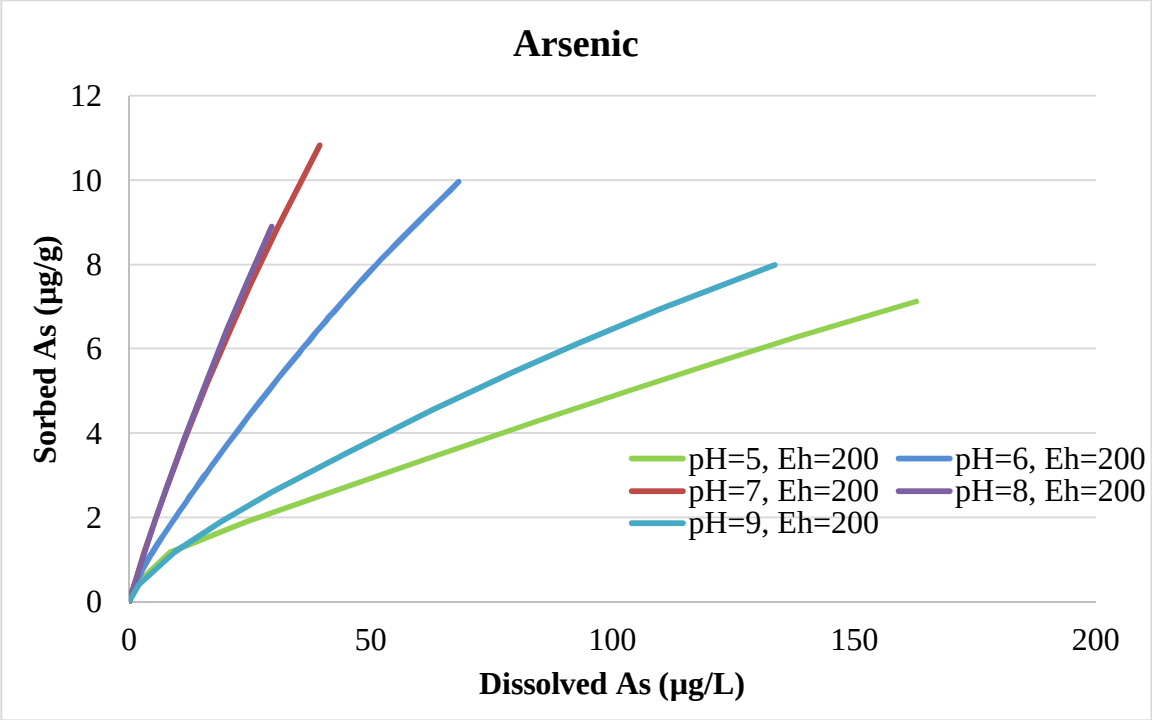

Figure 51: As sensitivity model with varied pH and Eh 200

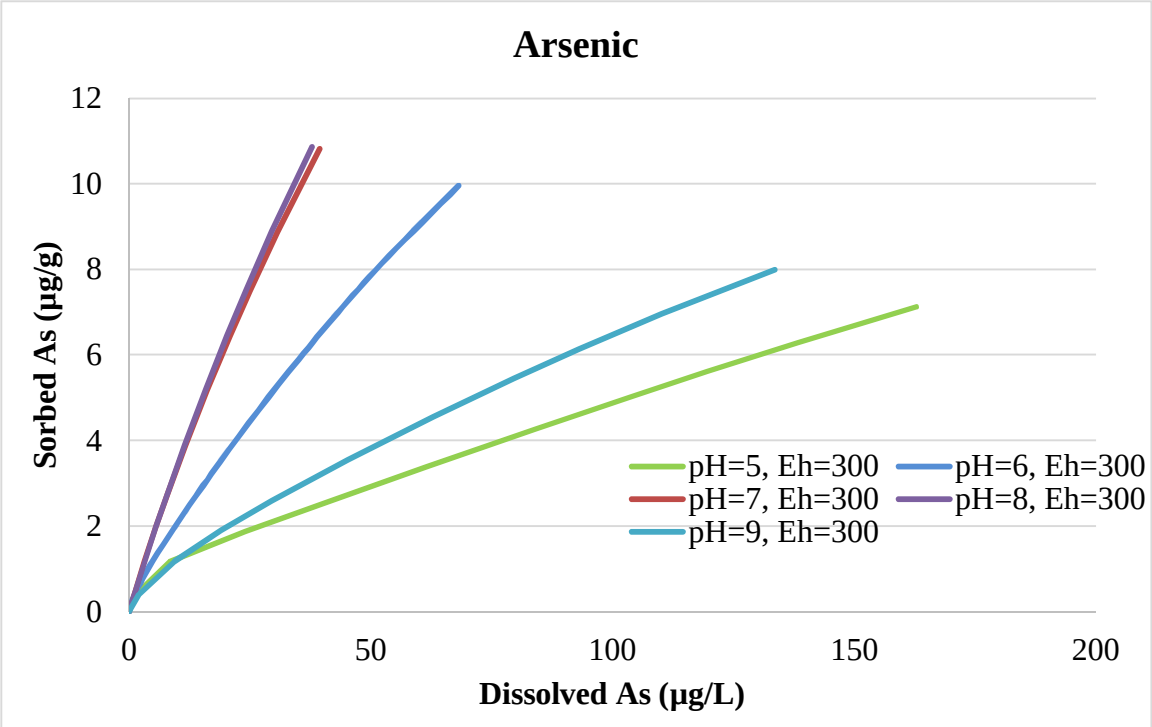

Figure 52: As sensitivity model with varied pH and Eh 300

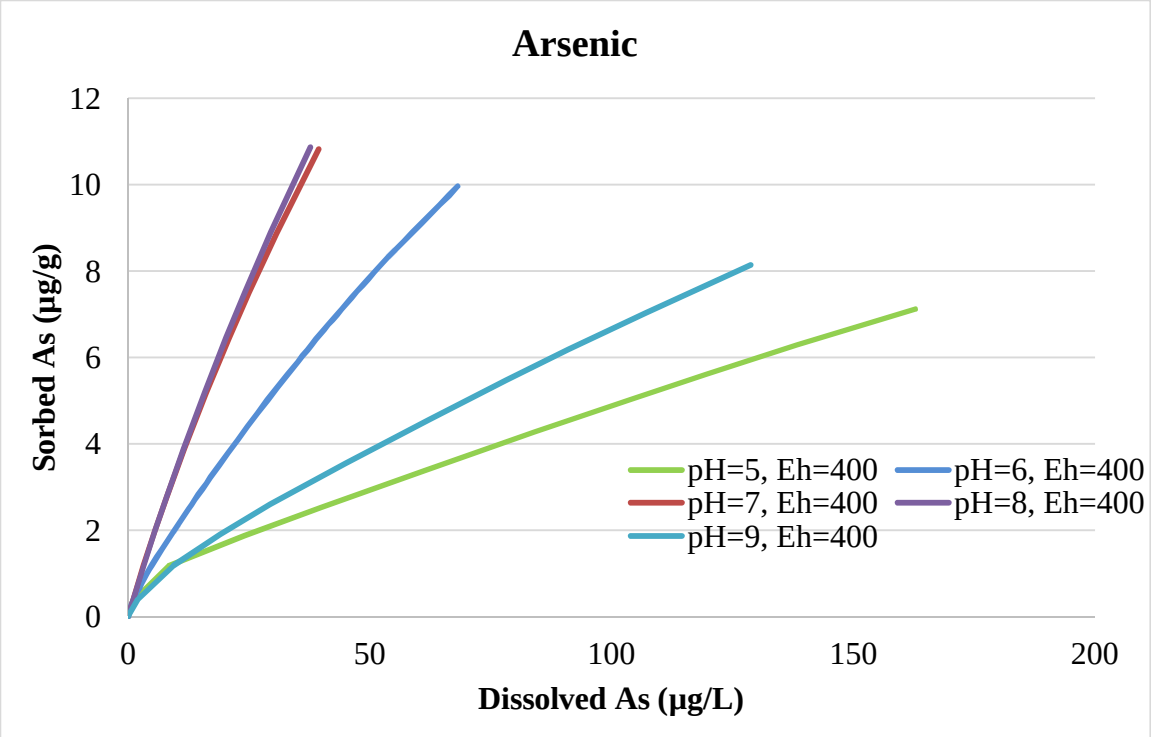

Figure 53: As sensitivity model with varied pH and Eh 400

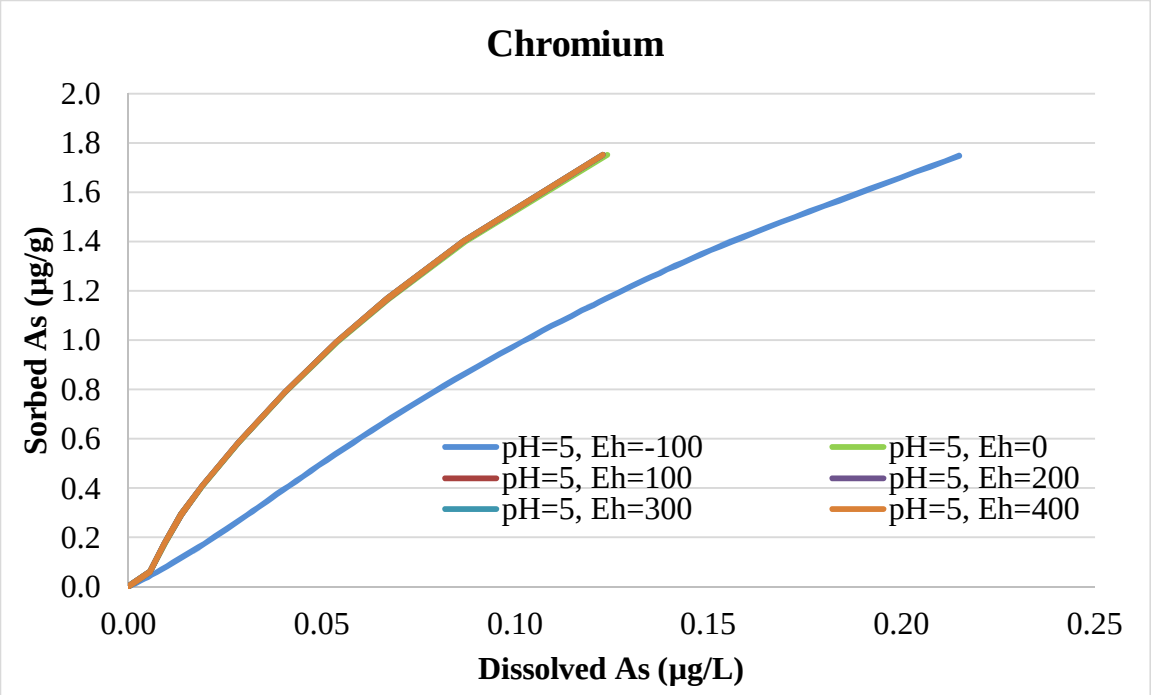

Figure 54: Cr sensitivity model with varied Eh and pH 5

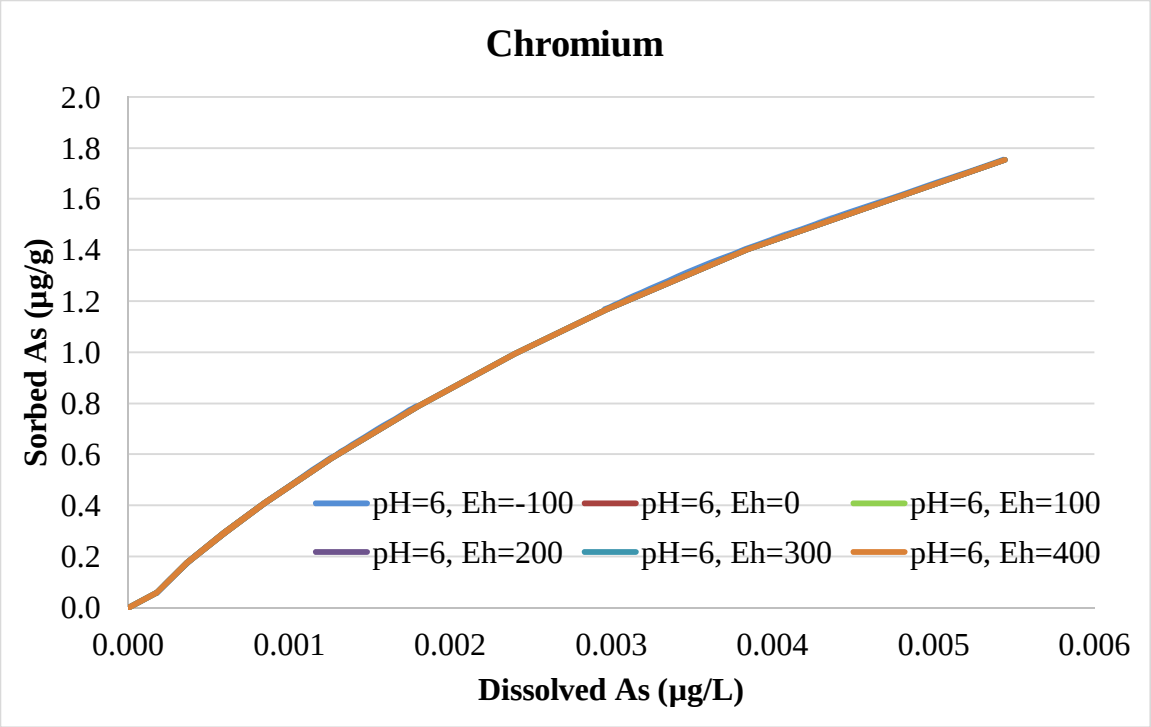

Figure 55: Cr sensitivity model with varied Eh and pH 6

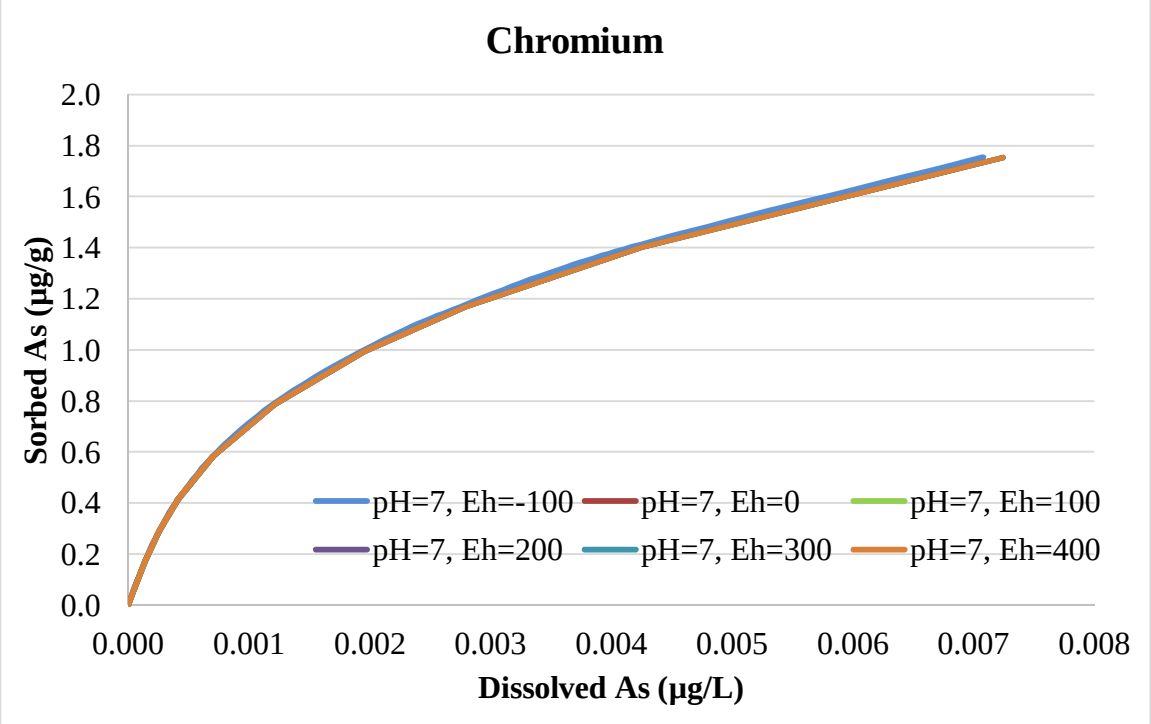

Figure 56: Cr sensitivity model with varied Eh and pH 7

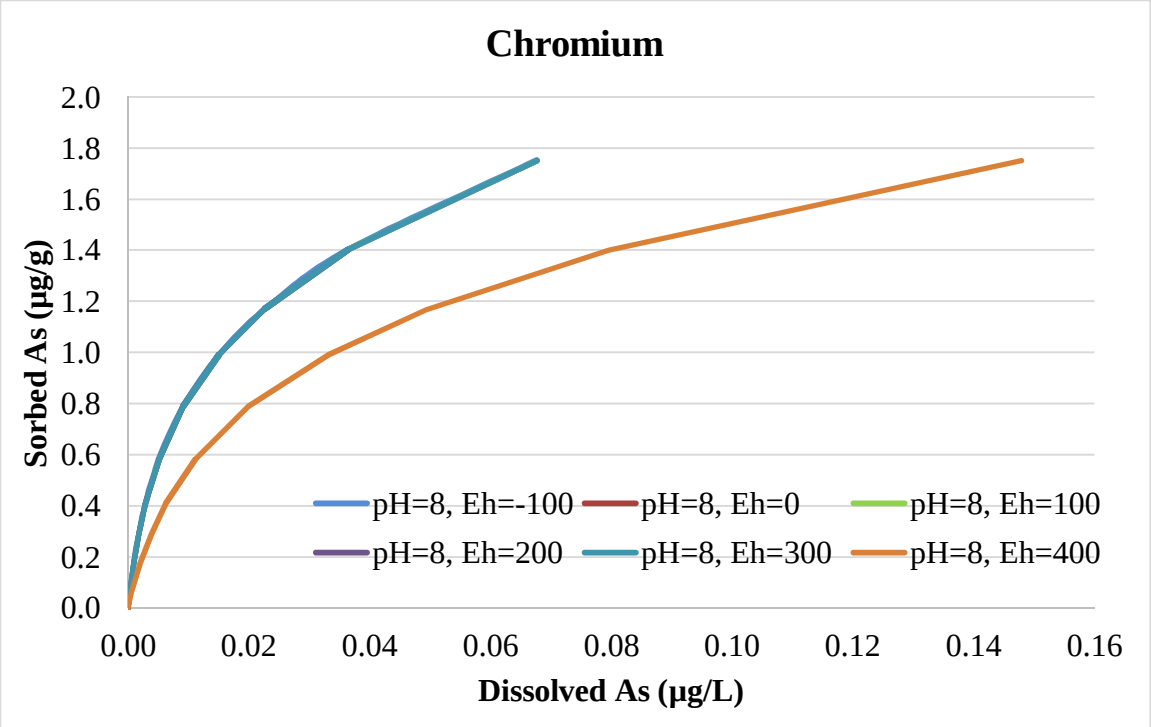

Figure 57: Cr sensitivity model with varied Eh and pH 8

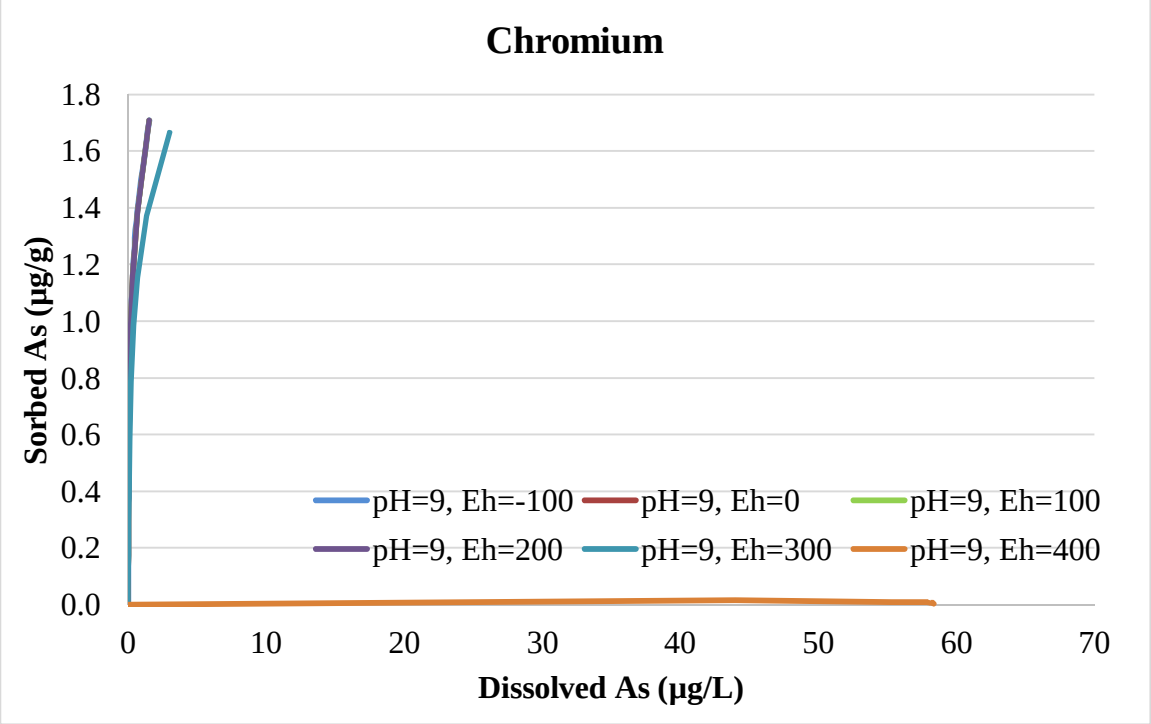

Figure 58: Cr sensitivity model with varied Eh and pH 9

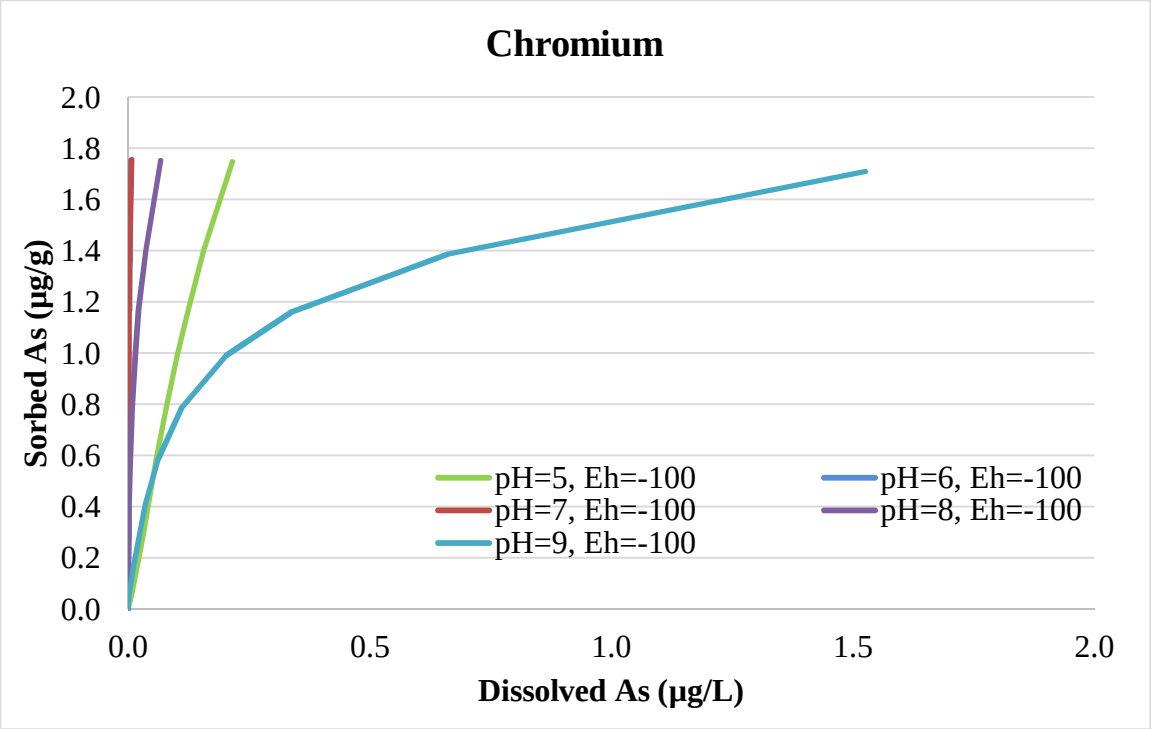

Figure 59: Cr sensitivity model with varied pH and Eh -100

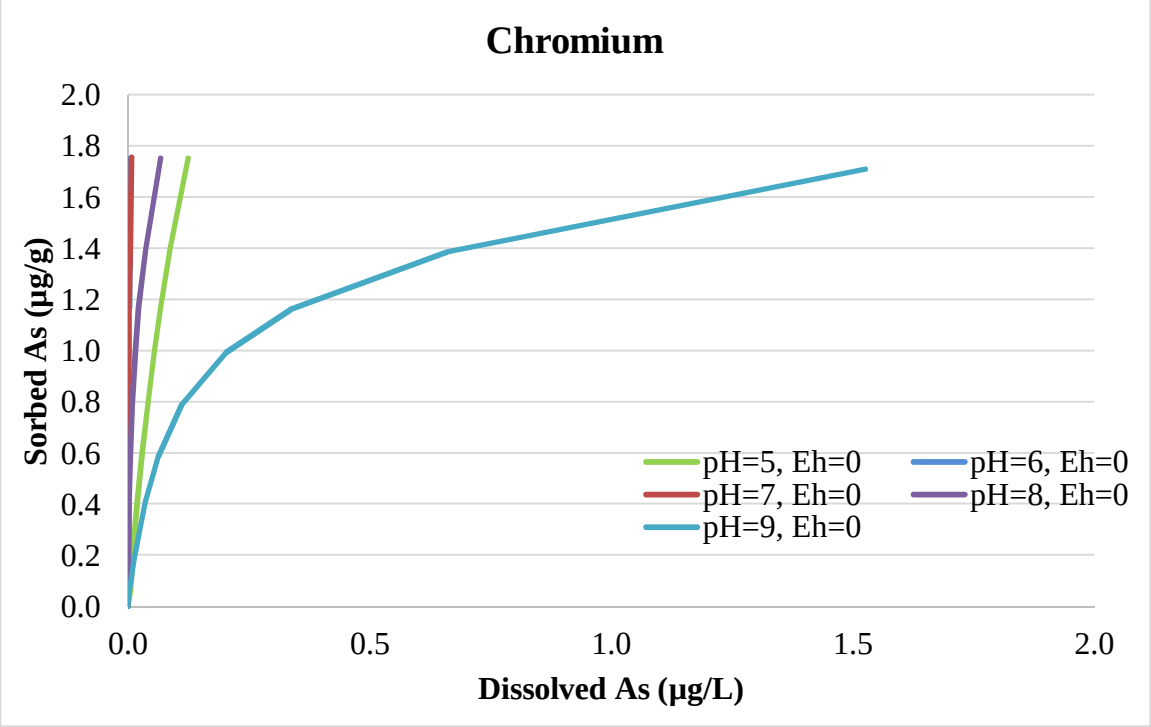

Figure 60: Cr sensitivity model with varied pH and Eh 0

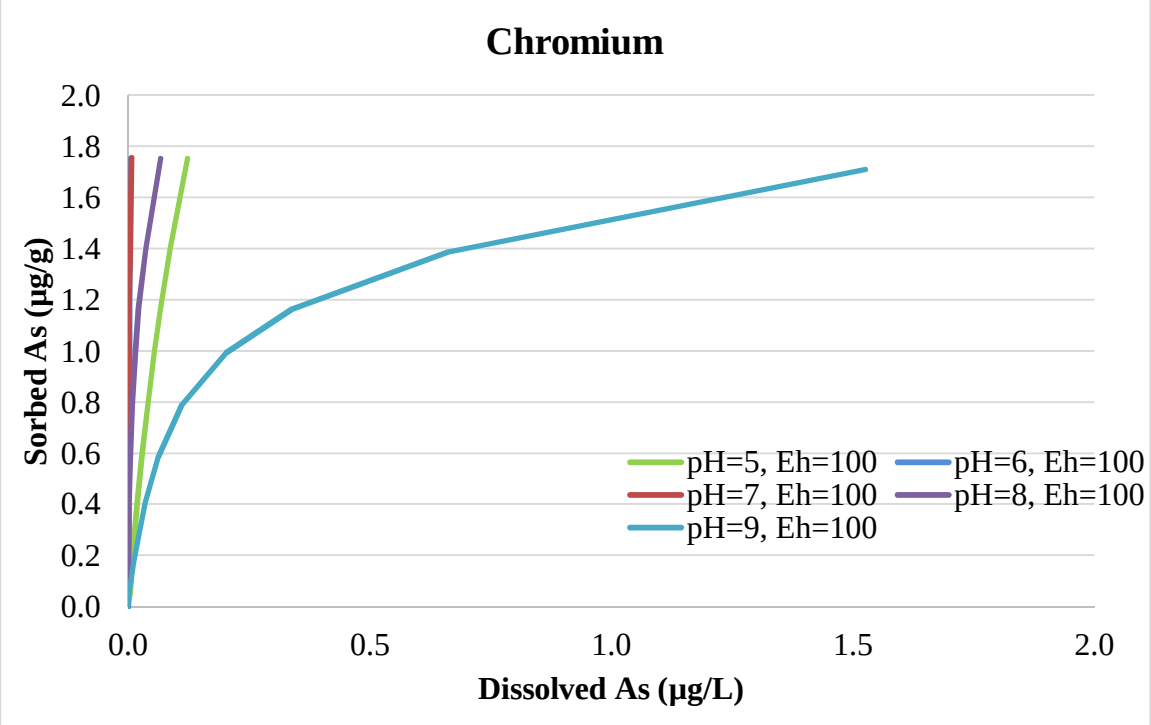

Figure 61: Cr sensitivity model with varied pH and Eh 100

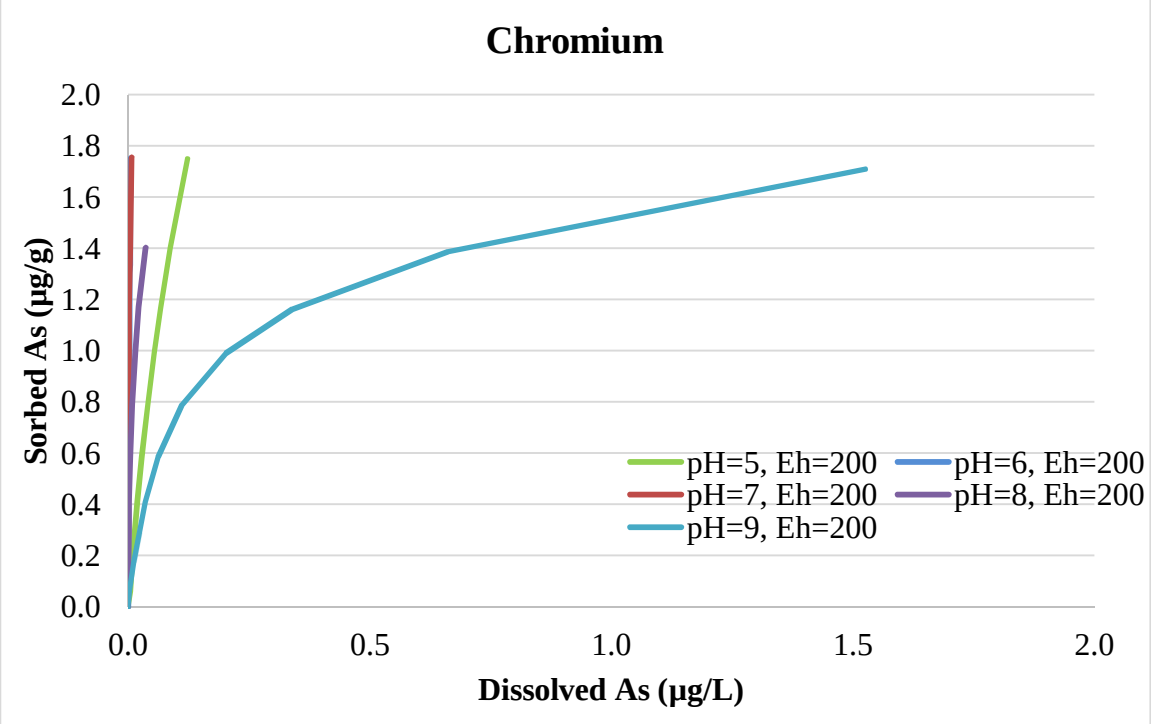

Figure 62: Cr sensitivity model with varied pH and Eh 200

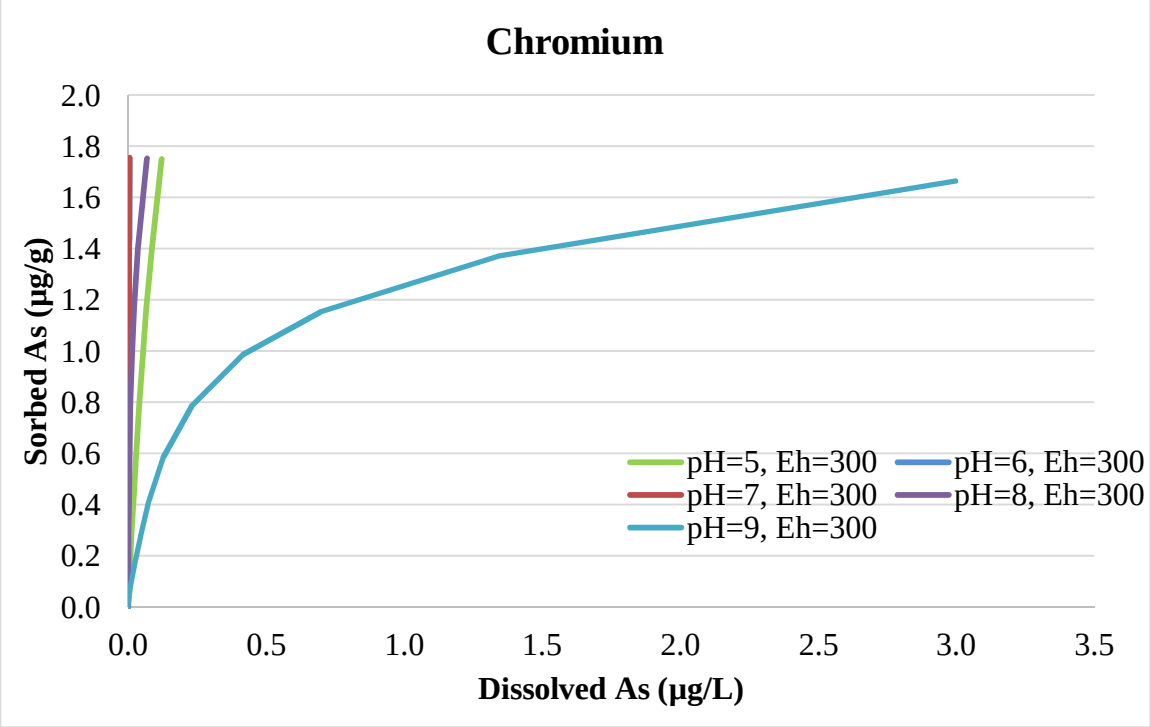

Figure 63: Cr sensitivity model with varied pH and Eh 300

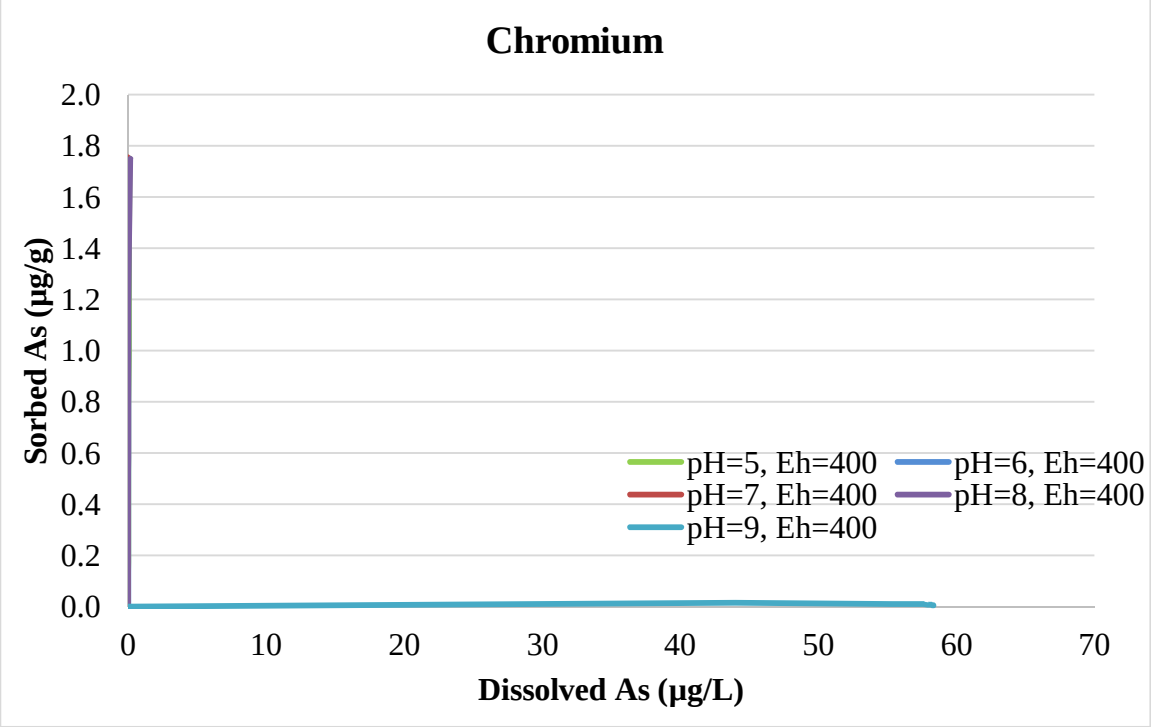

Figure 64: Cr sensitivity model with varied pH and Eh 400

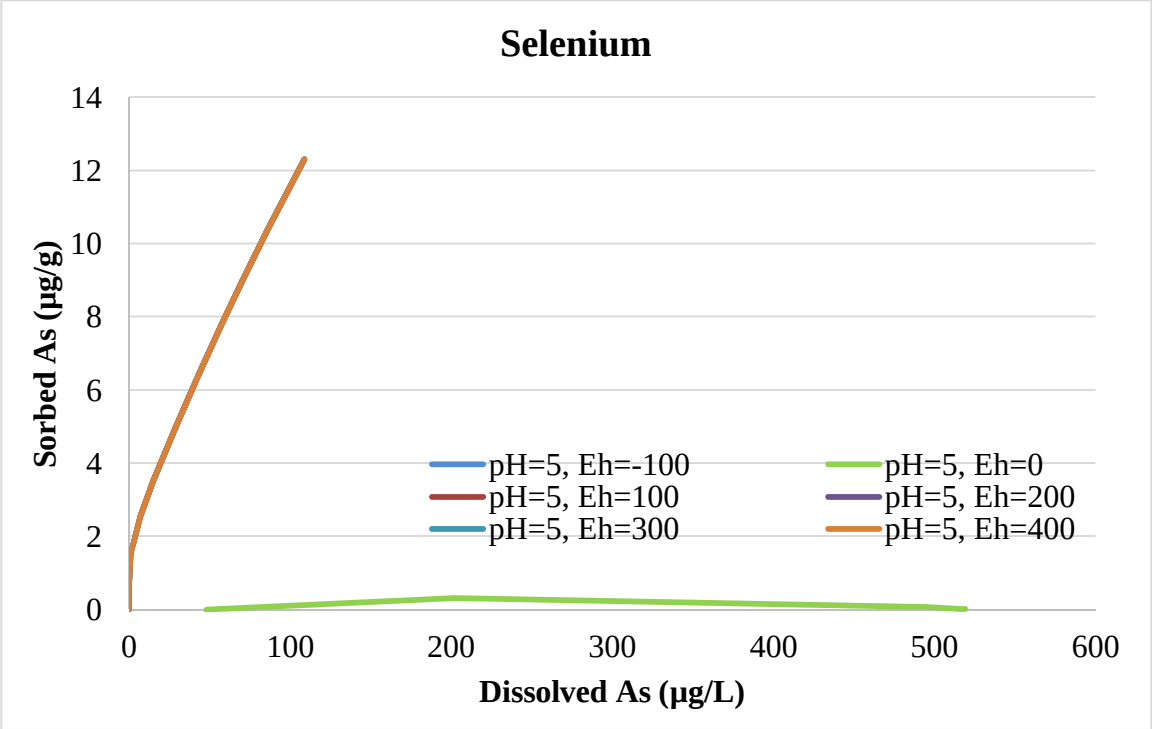

Figure 65: Se sensitivity model with varied Eh and pH 5

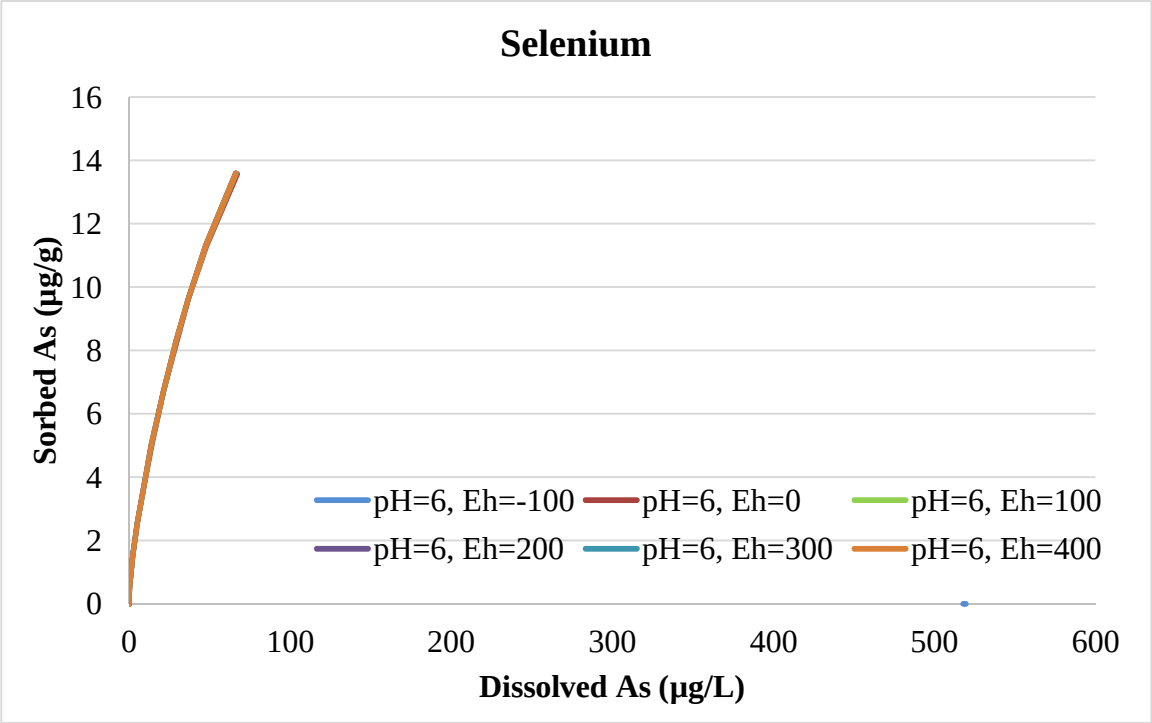

Figure 66: Se sensitivity model with varied Eh and pH 6

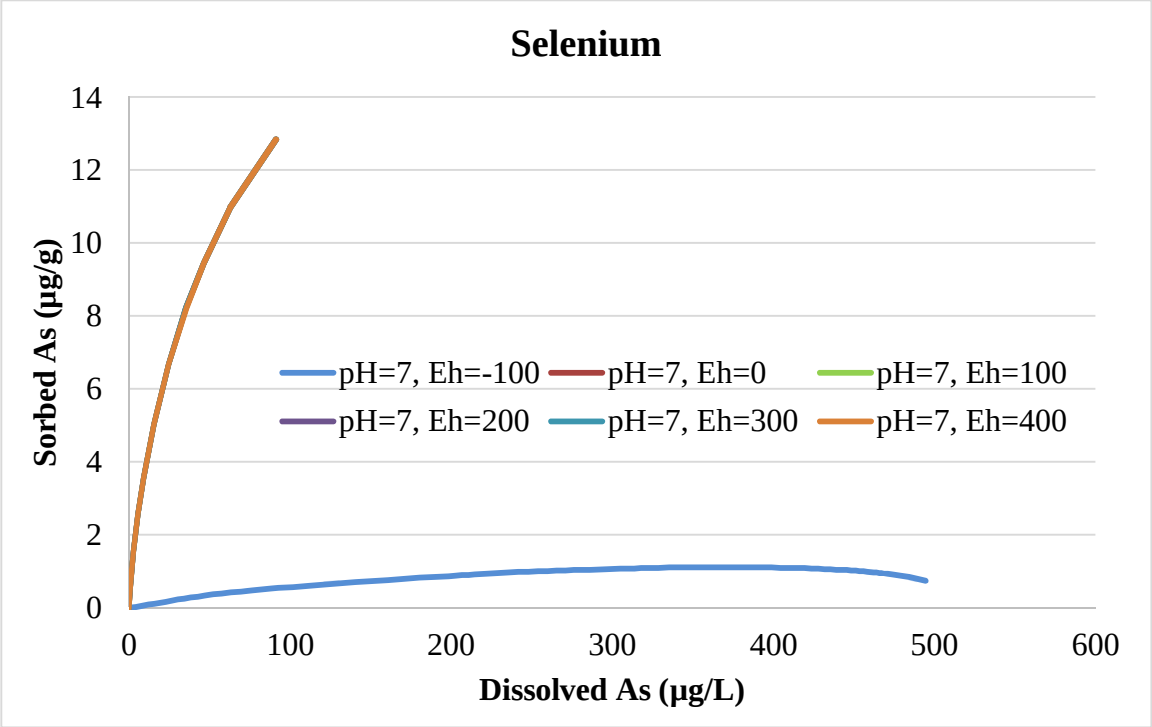

Figure 67: Se sensitivity model with varied Eh and pH 7

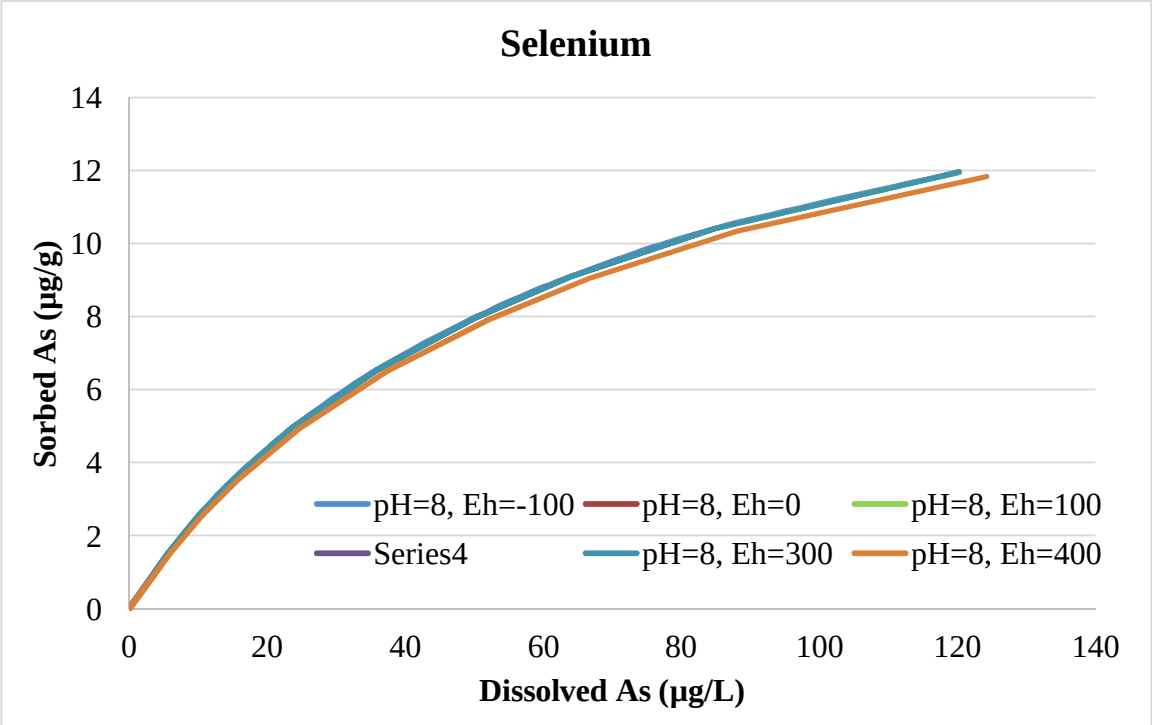

Figure 68: Se sensitivity model with varied Eh and pH 8

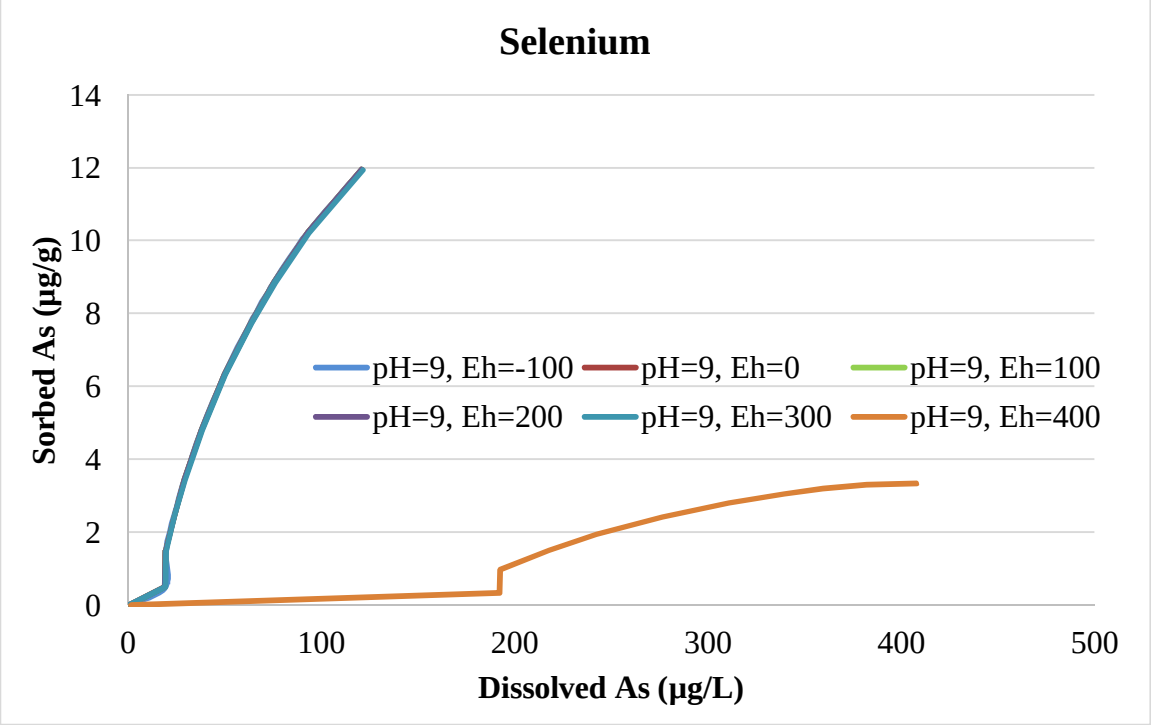

Figure 69: Se sensitivity model with varied Eh and pH 9

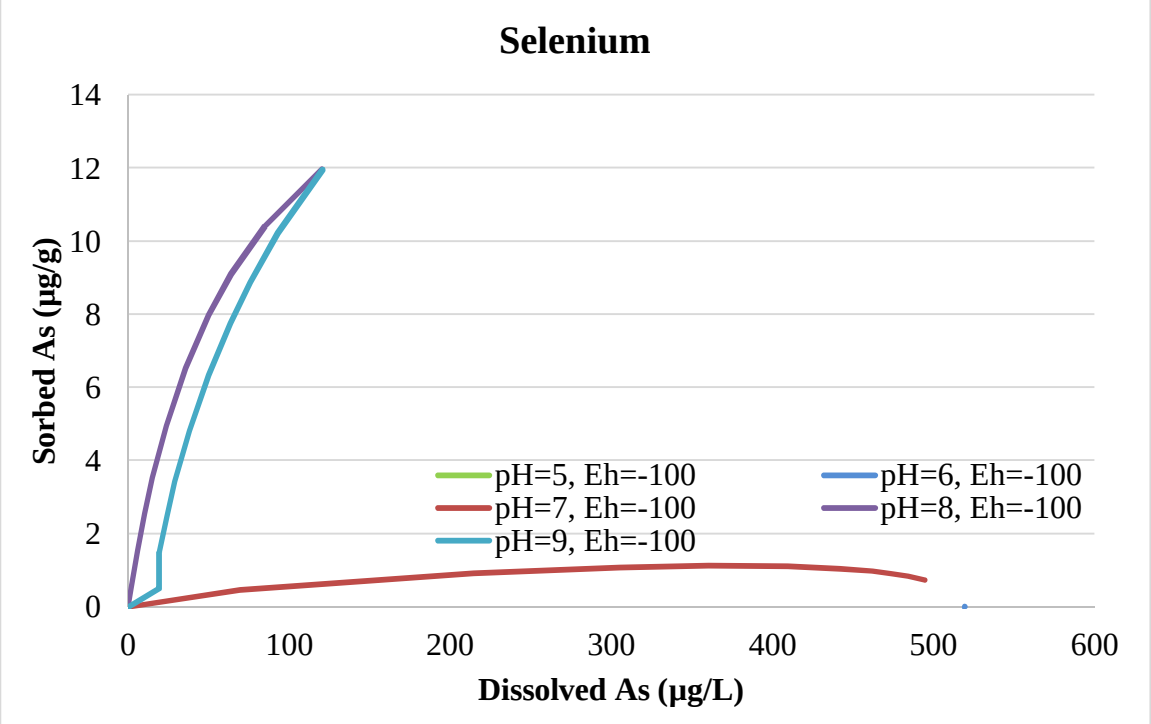

Figure 70: Se sensitivity model with varied pH and Eh -100

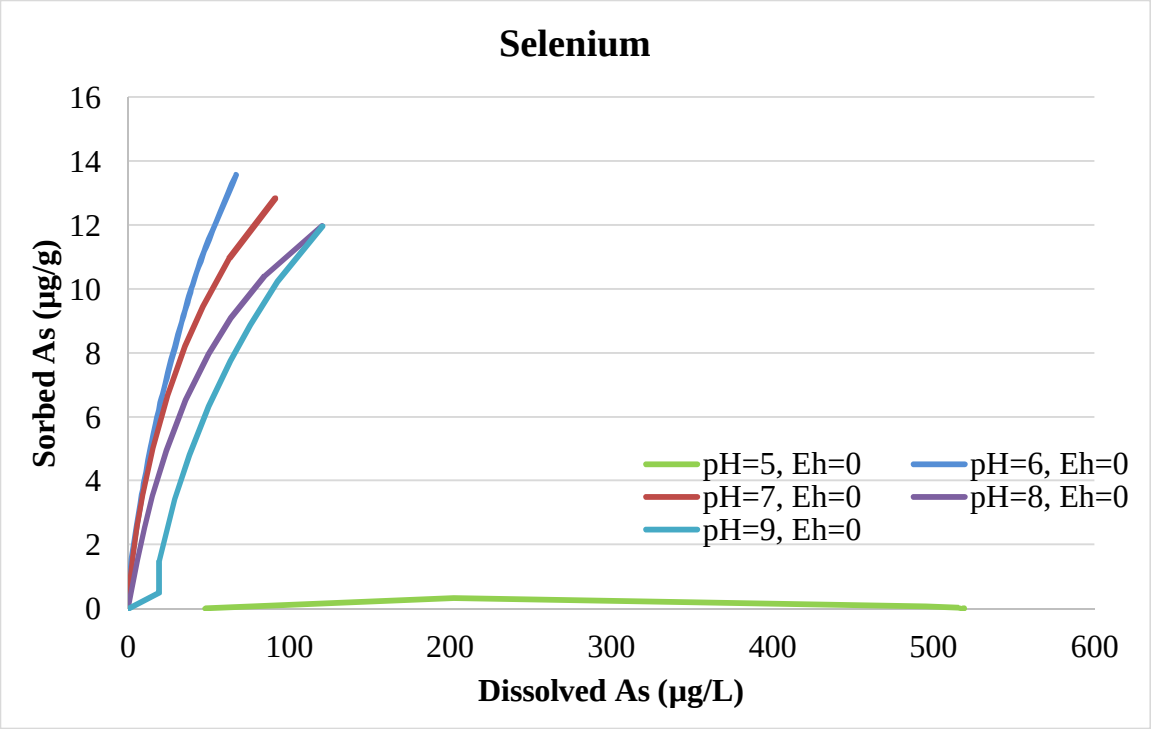

Figure 71: Se sensitivity model with varied pH and Eh 0

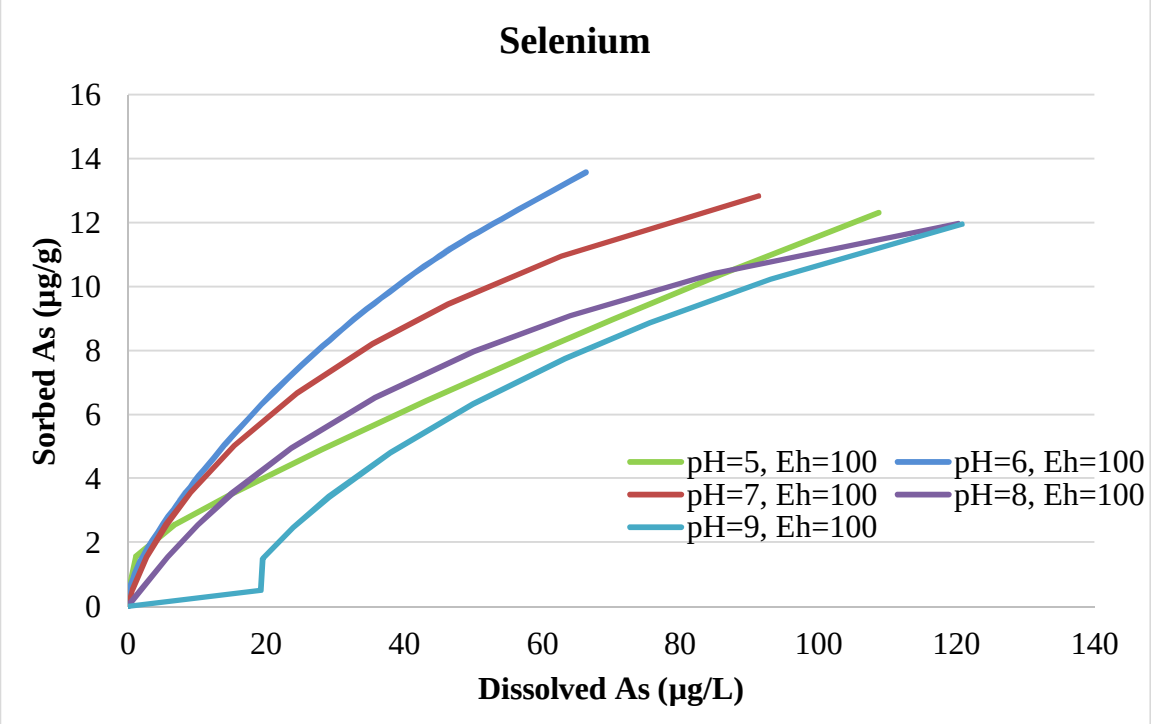

Figure 72: Se sensitivity model with varied pH and Eh 100

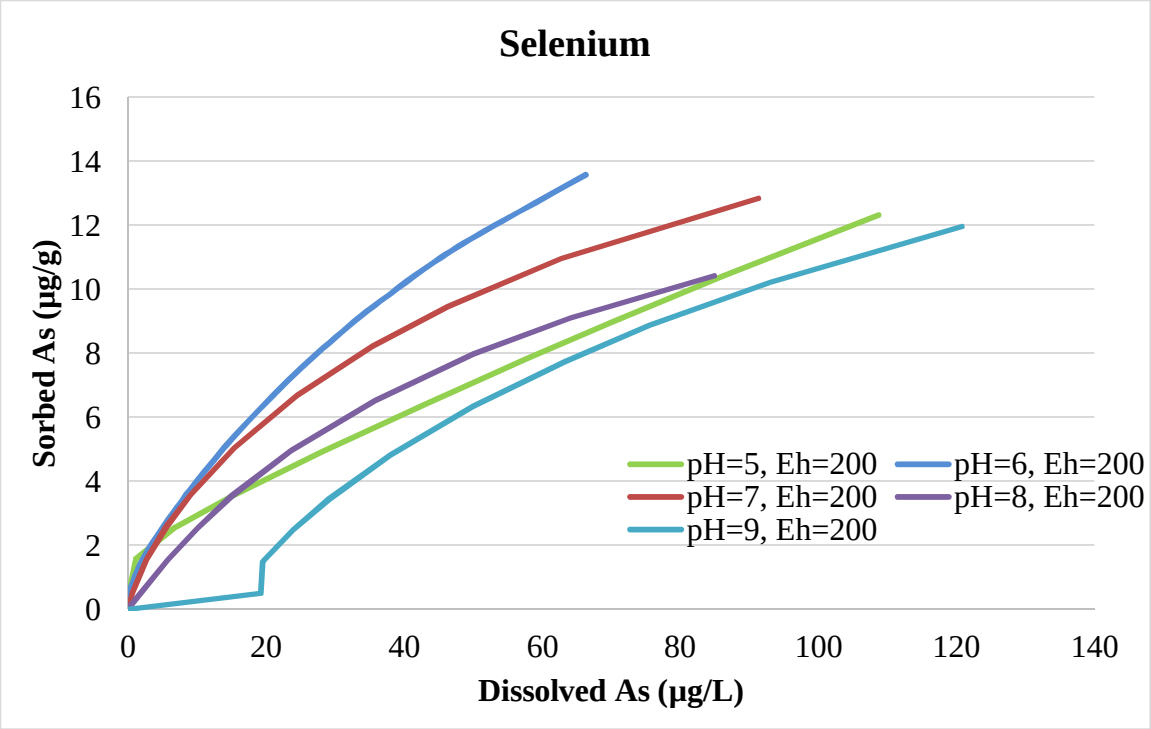

Figure 73: Se sensitivity model with varied pH and Eh 200

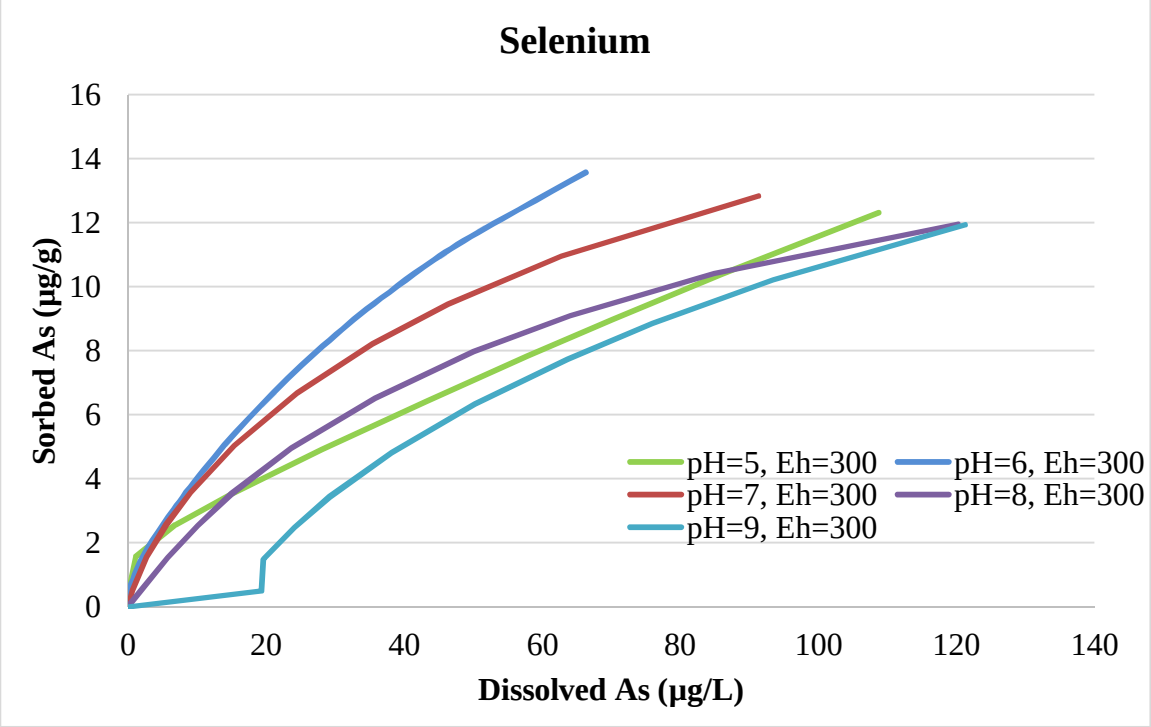

Figure 74: Se sensitivity model with varied pH and Eh 300

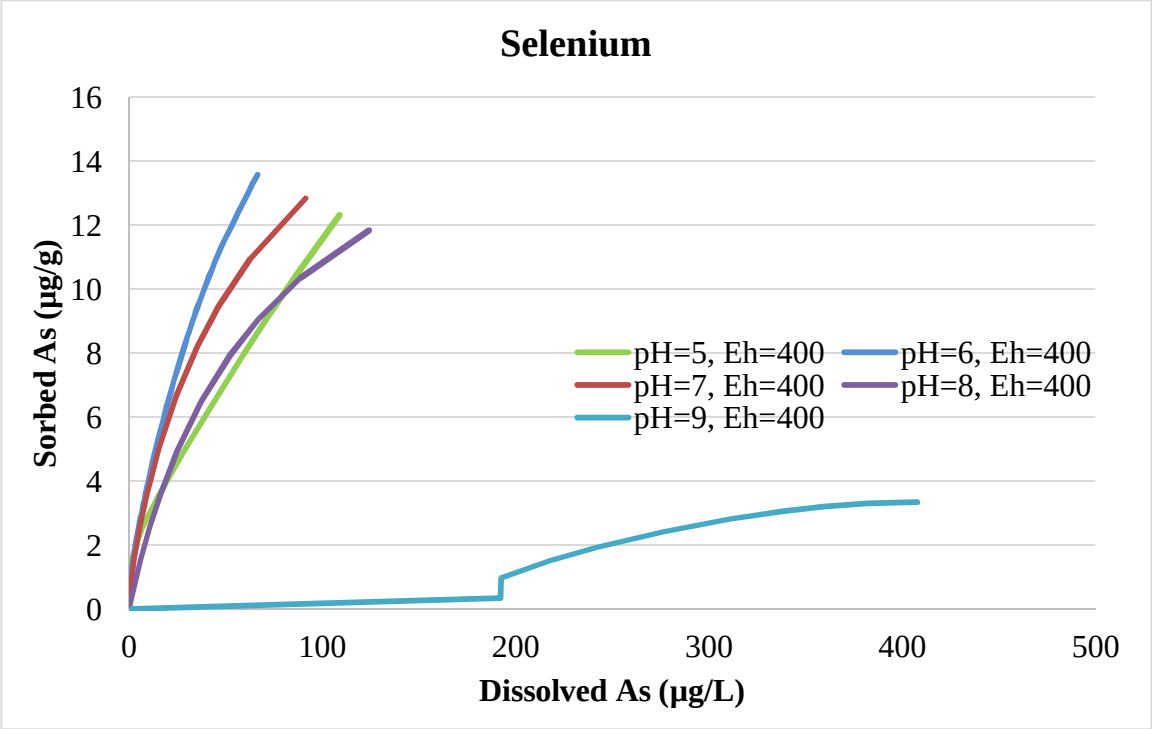

Figure 75: Se sensitivity model with varied pH and Eh 400

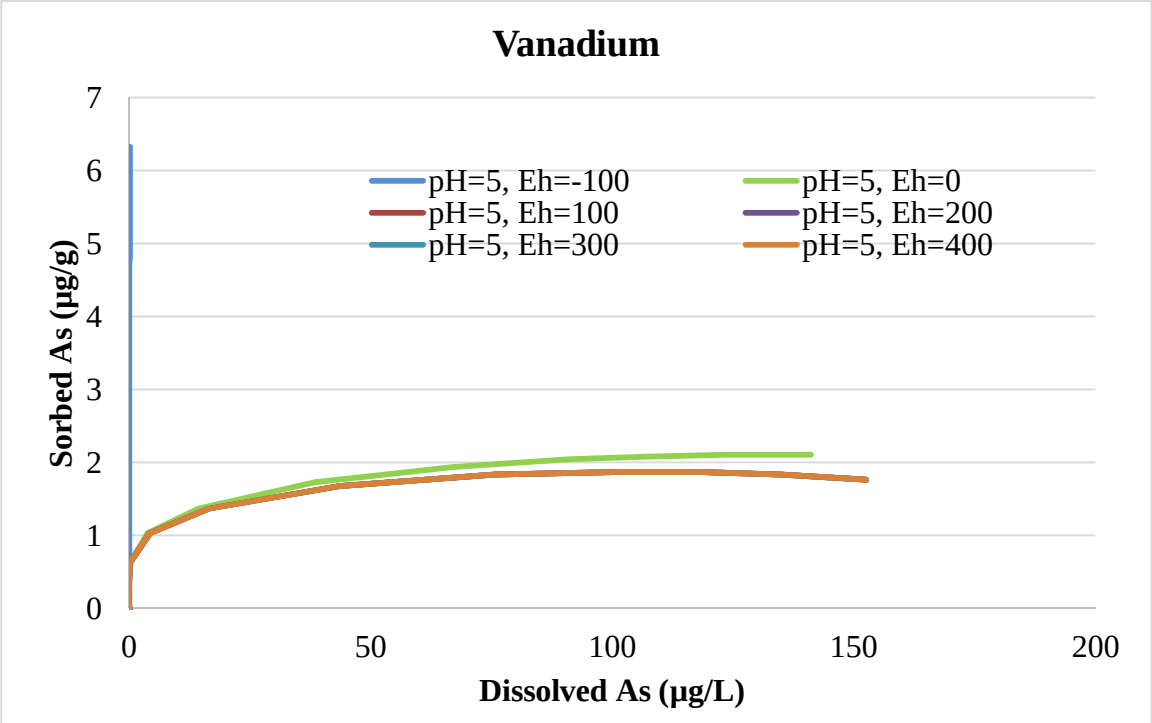

Figure 76: V sensitivity model with varied Eh and pH 5

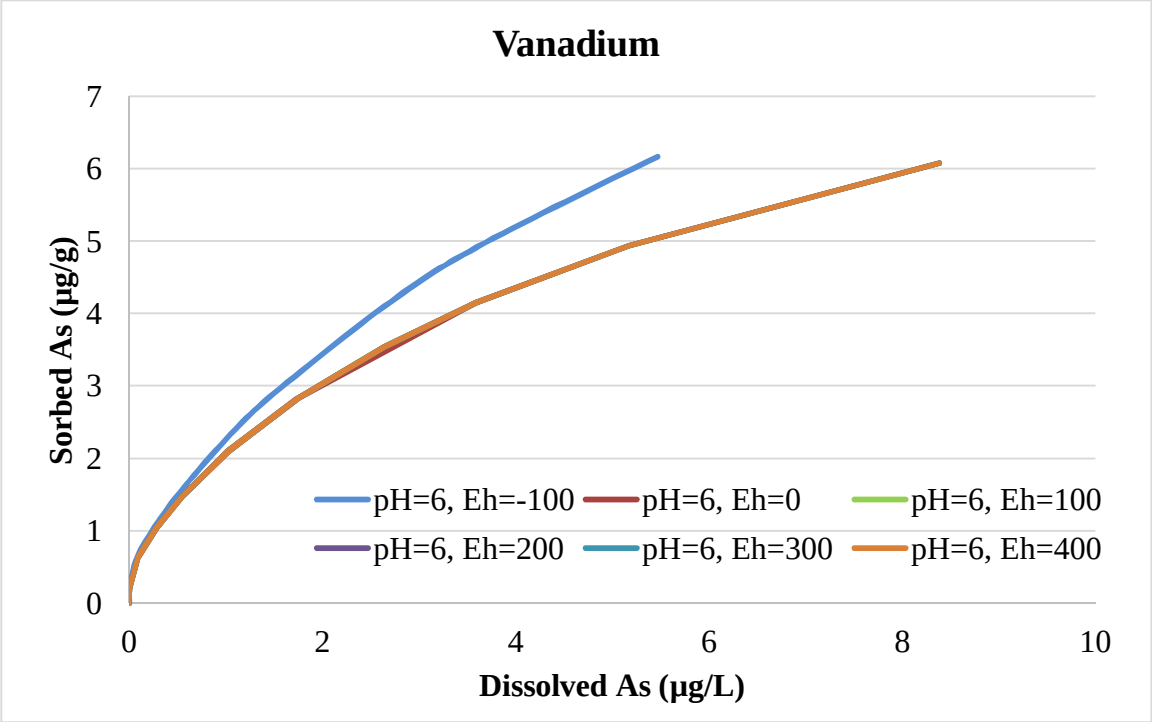

Figure 77: V sensitivity model with varied Eh and pH 6

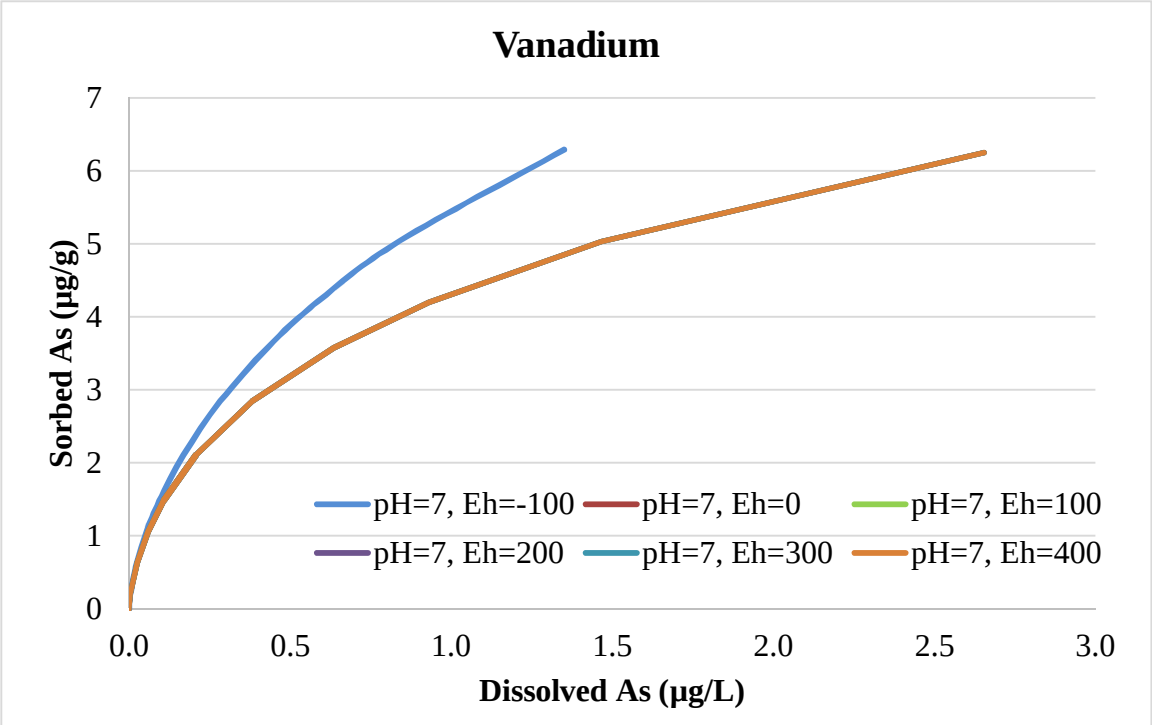

Figure 78: V sensitivity model with varied Eh and pH 7

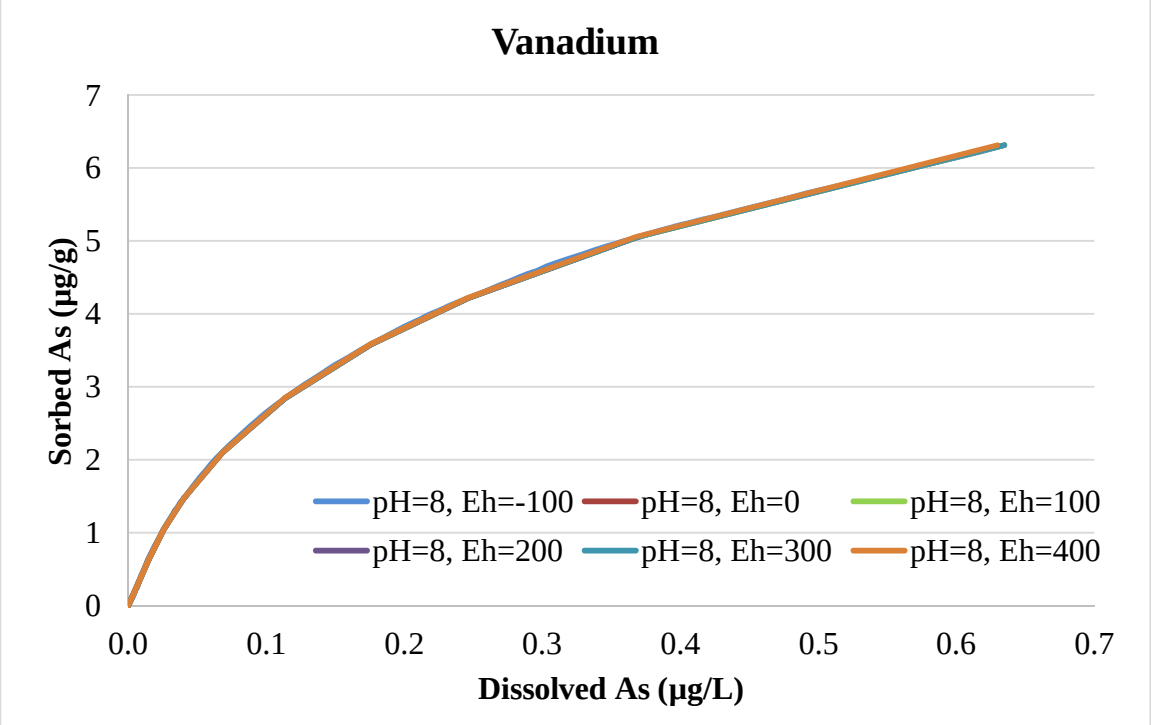

Figure 79: V sensitivity model with varied Eh and pH 8

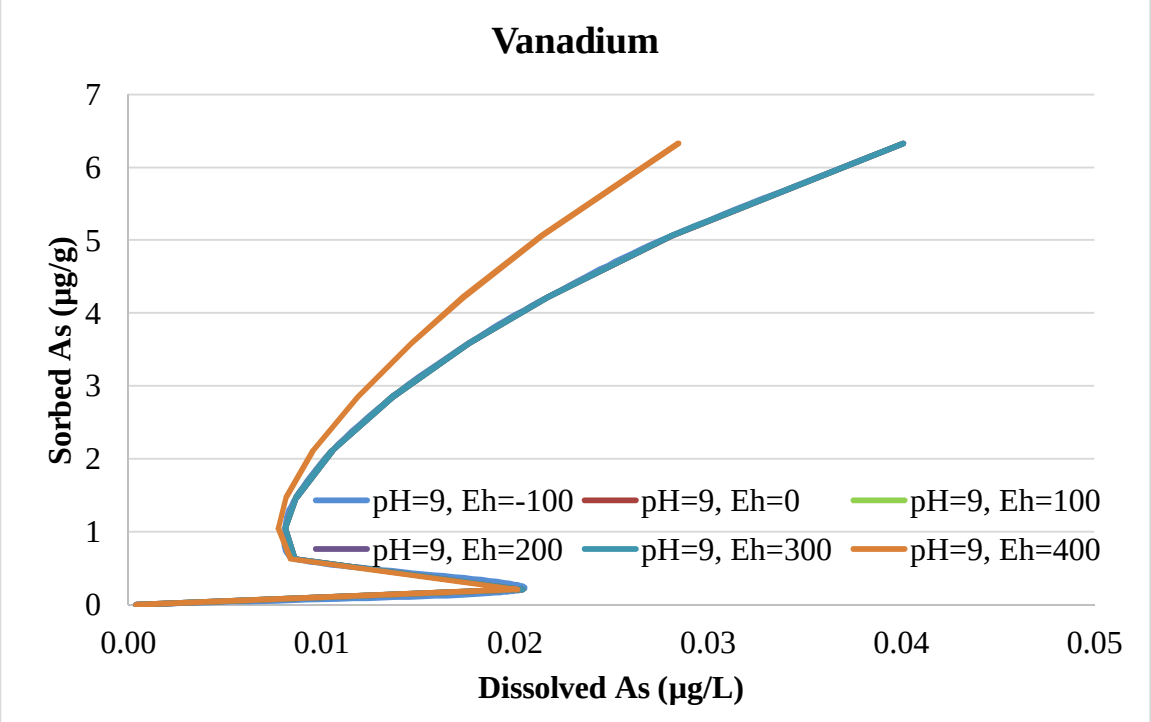

Figure 80: V sensitivity model with varied Eh and pH 9

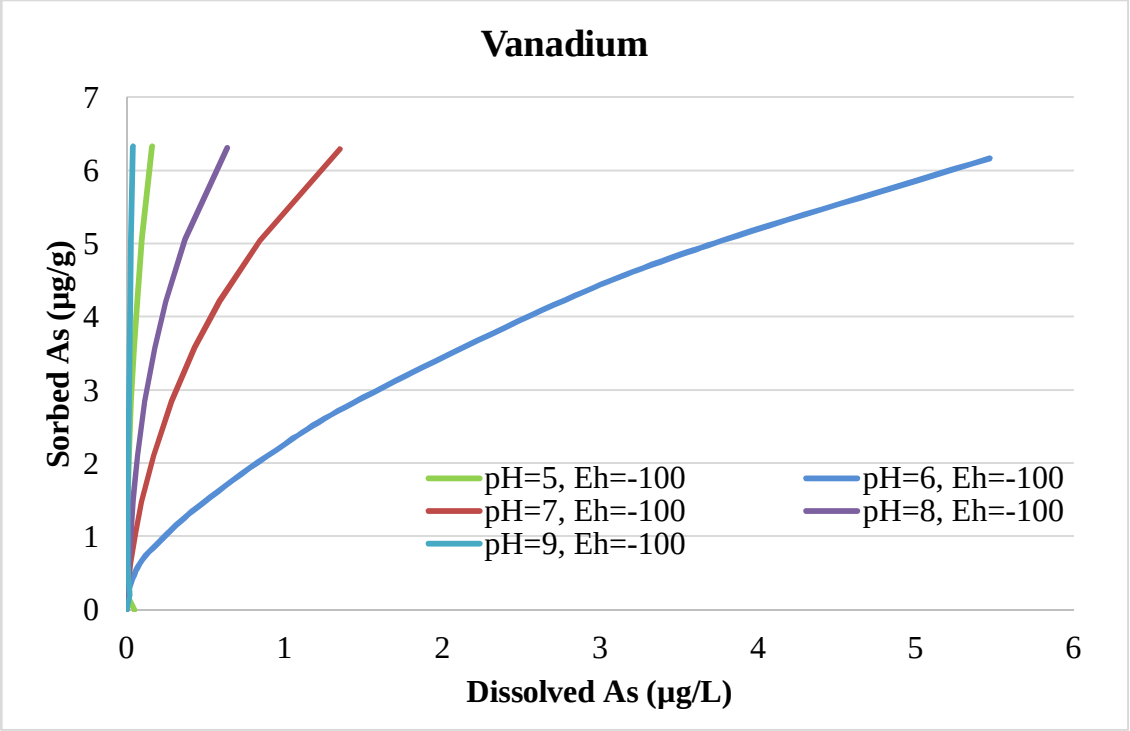

Figure 81: V sensitivity model with varied pH and Eh -100

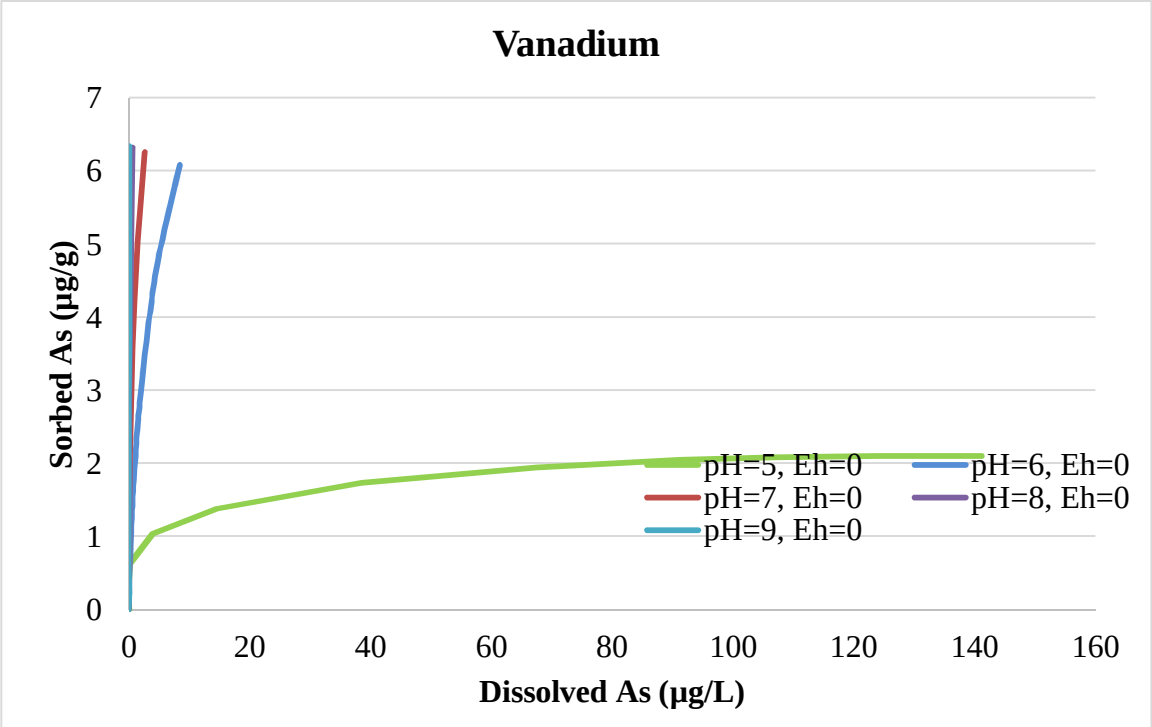

Figure 82: V sensitivity model with varied pH and Eh 0

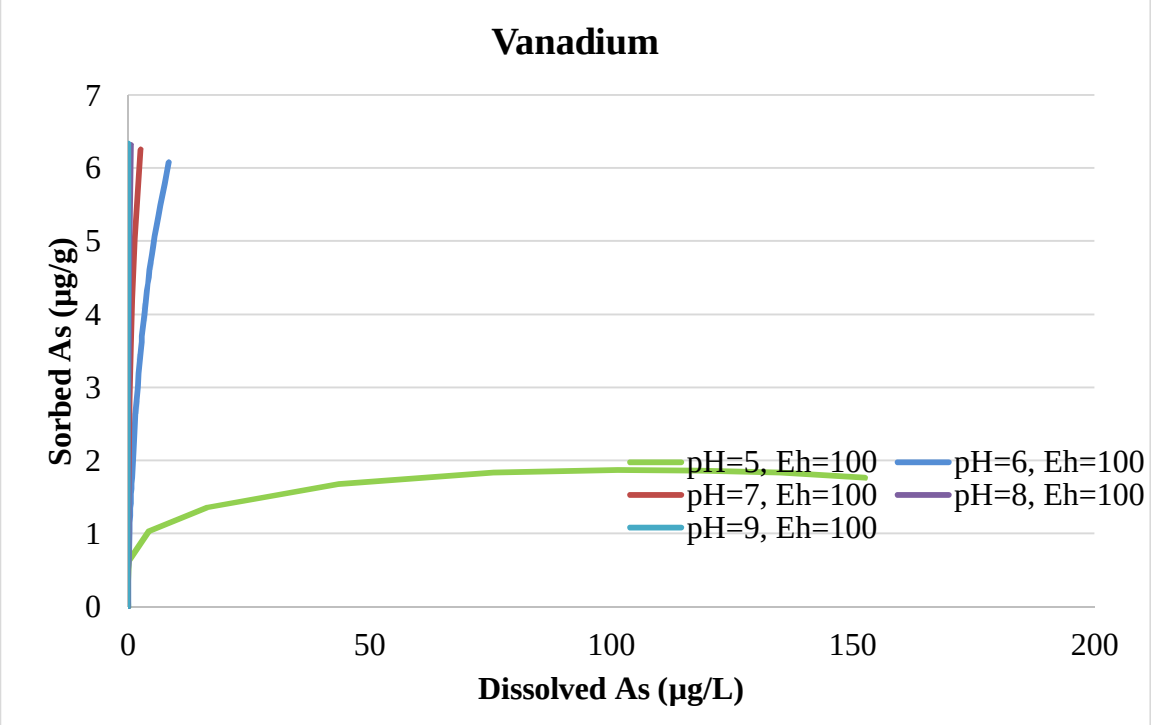

Figure 83: V sensitivity model with varied pH and Eh 100

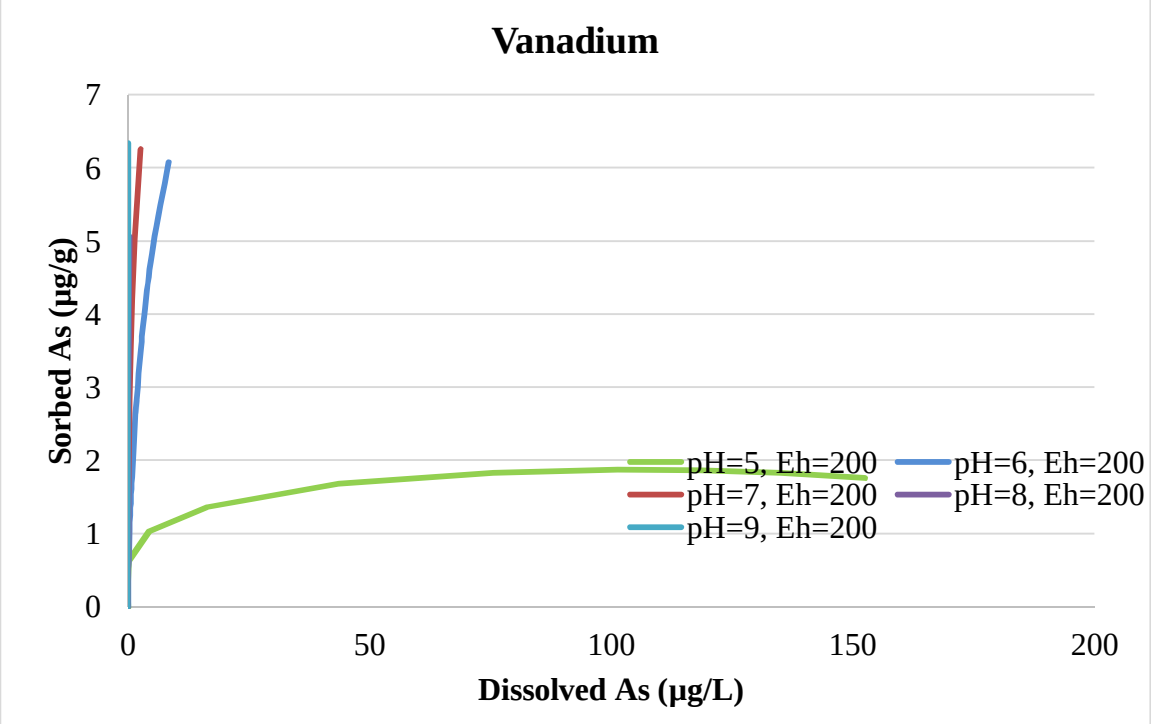

Figure 84: V sensitivity model with varied pH and Eh 200

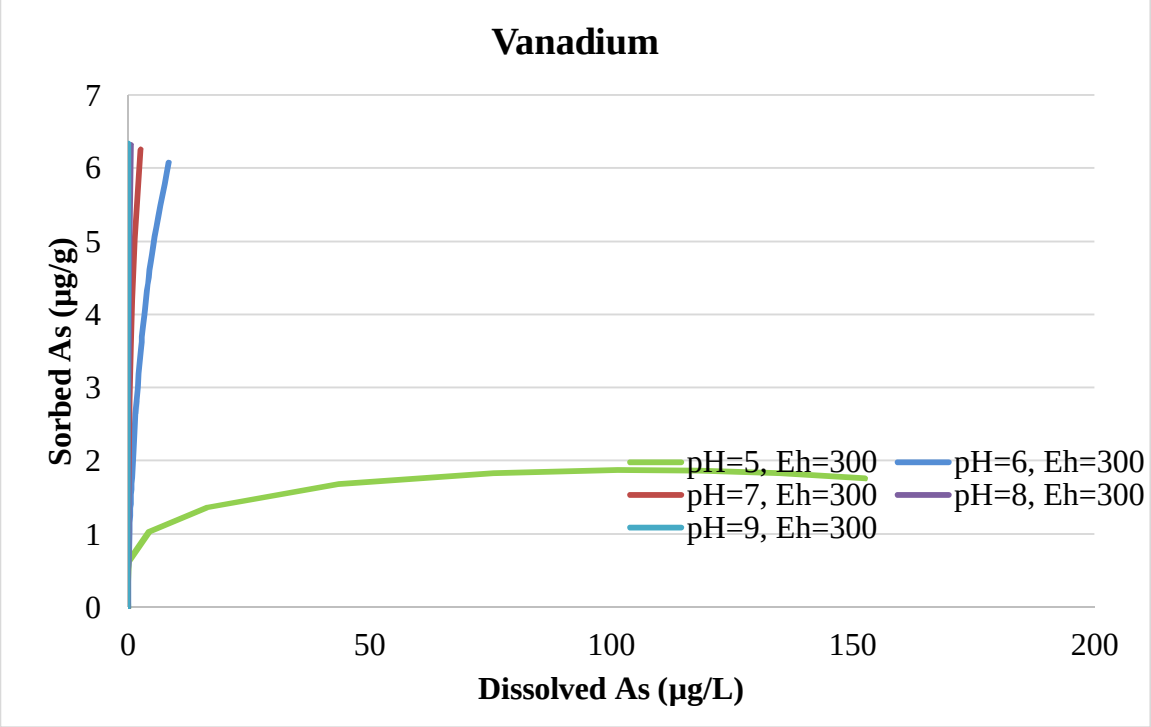

Figure 85: V sensitivity model with varied pH and Eh 300

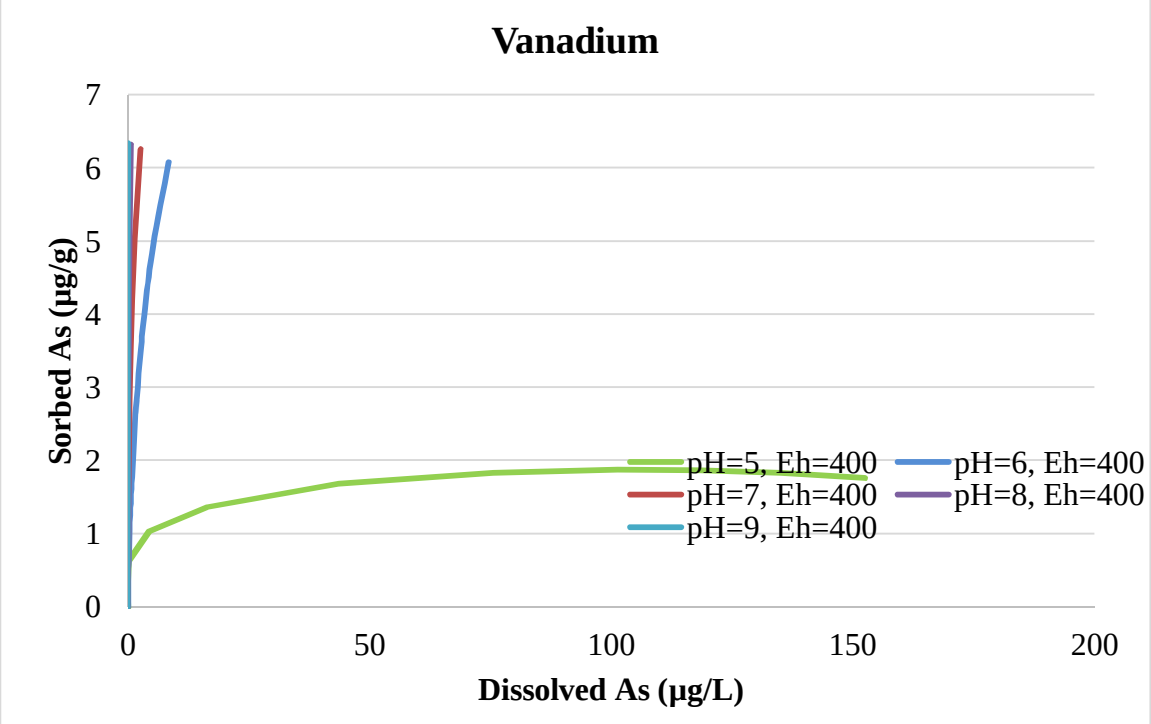

Figure 86: V sensitivity model with varied pH and Eh 400

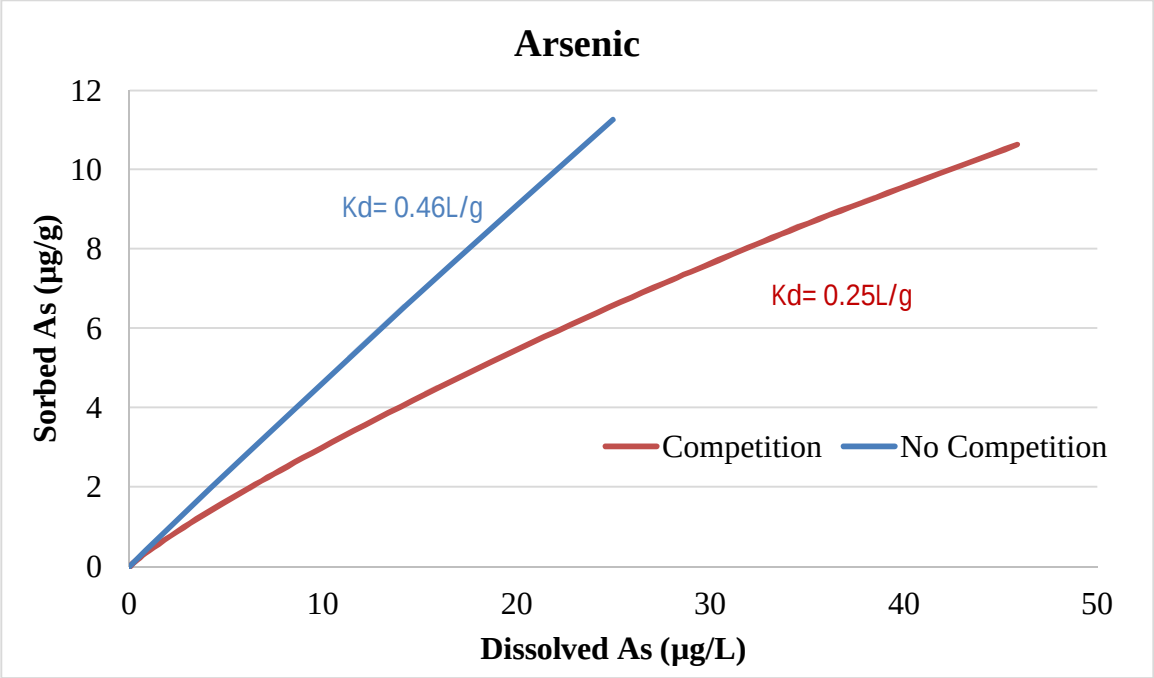

Figure 87: As adsorption competition sensitivity

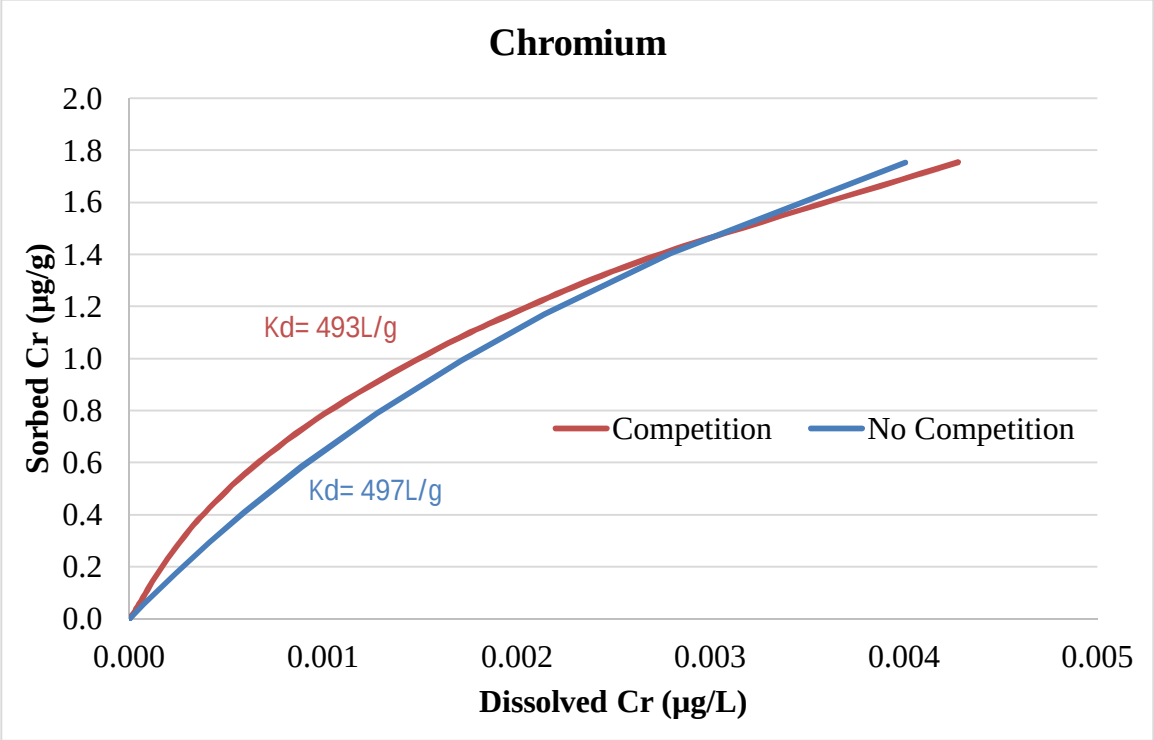

Figure 88: Cr adsorption competition sensitivity

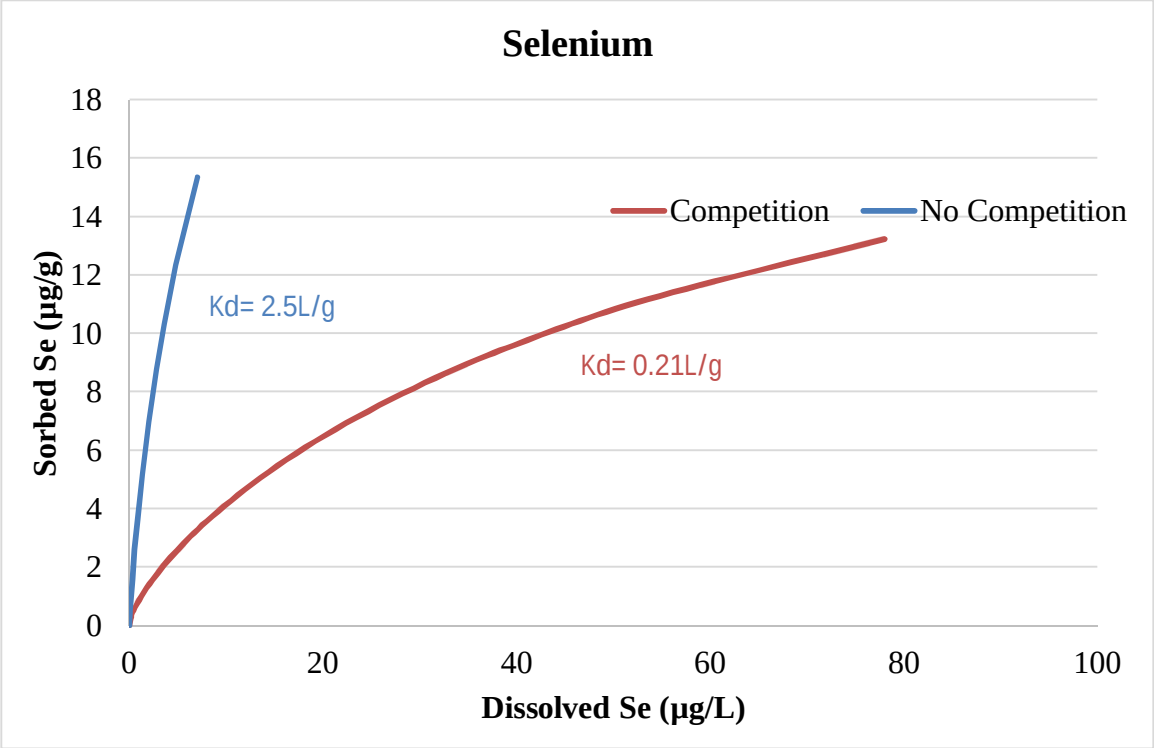

Figure 89: Se adsorption competition sensitivity

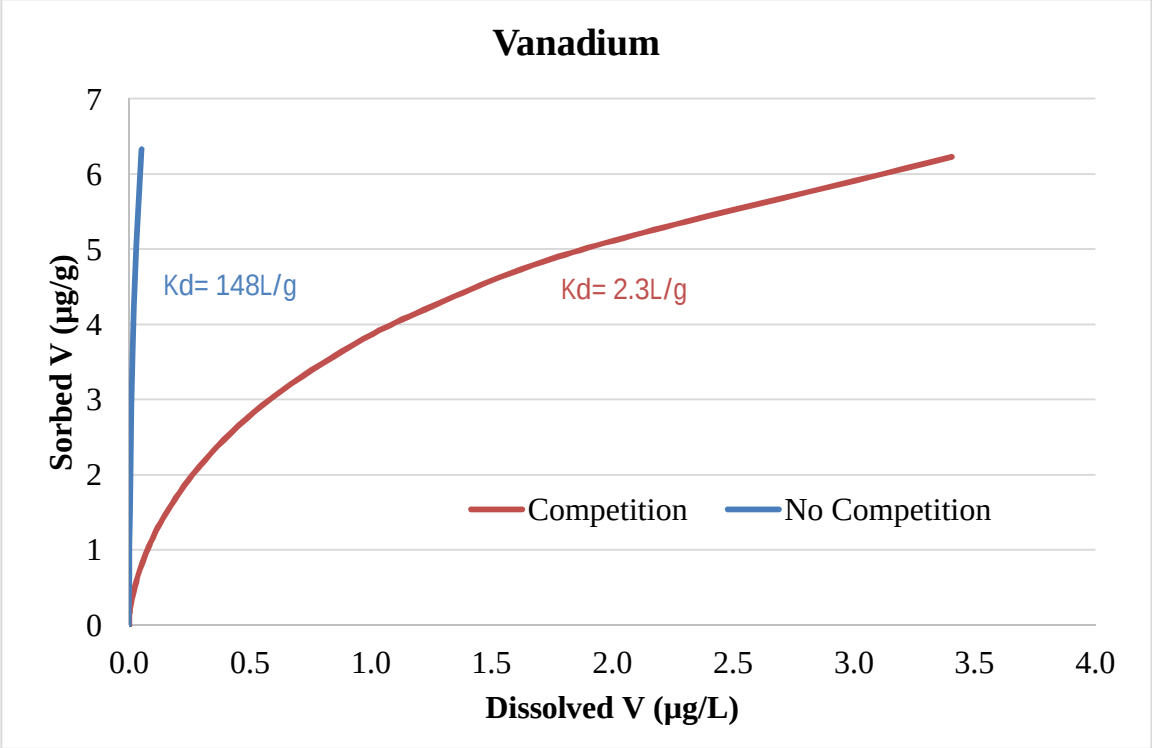

Figure 90: V adsorption competition sensitivity

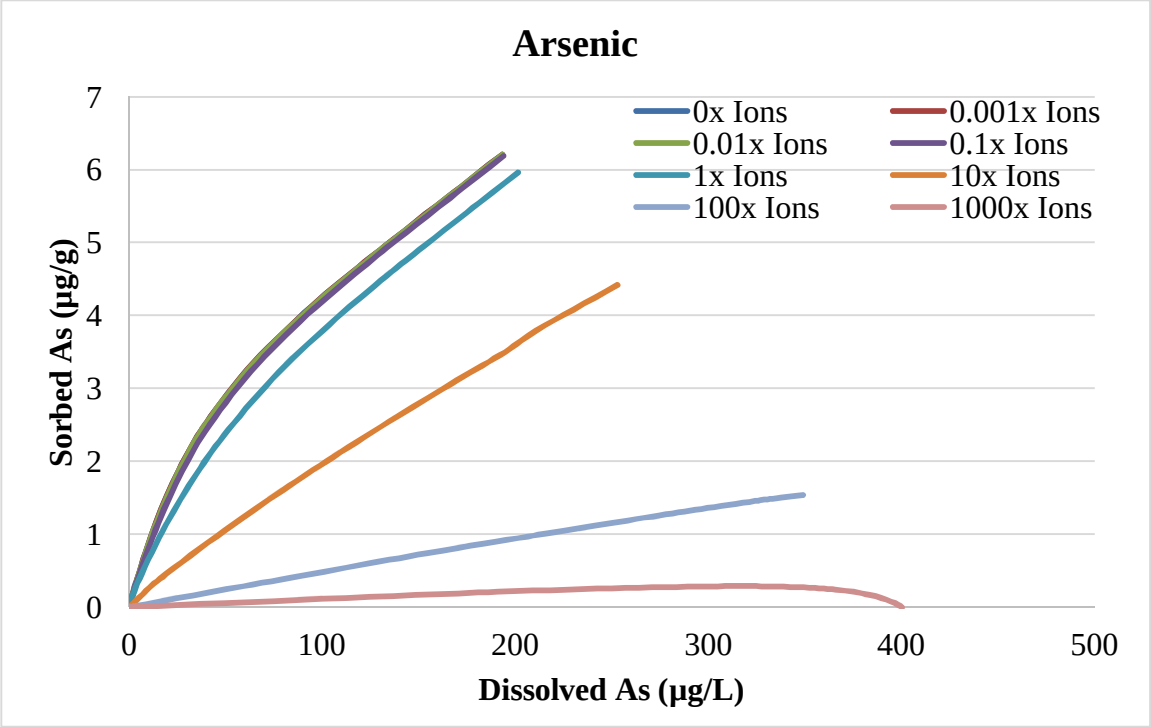

Figure 91: As adsorption sensitivity to variations in background constituents

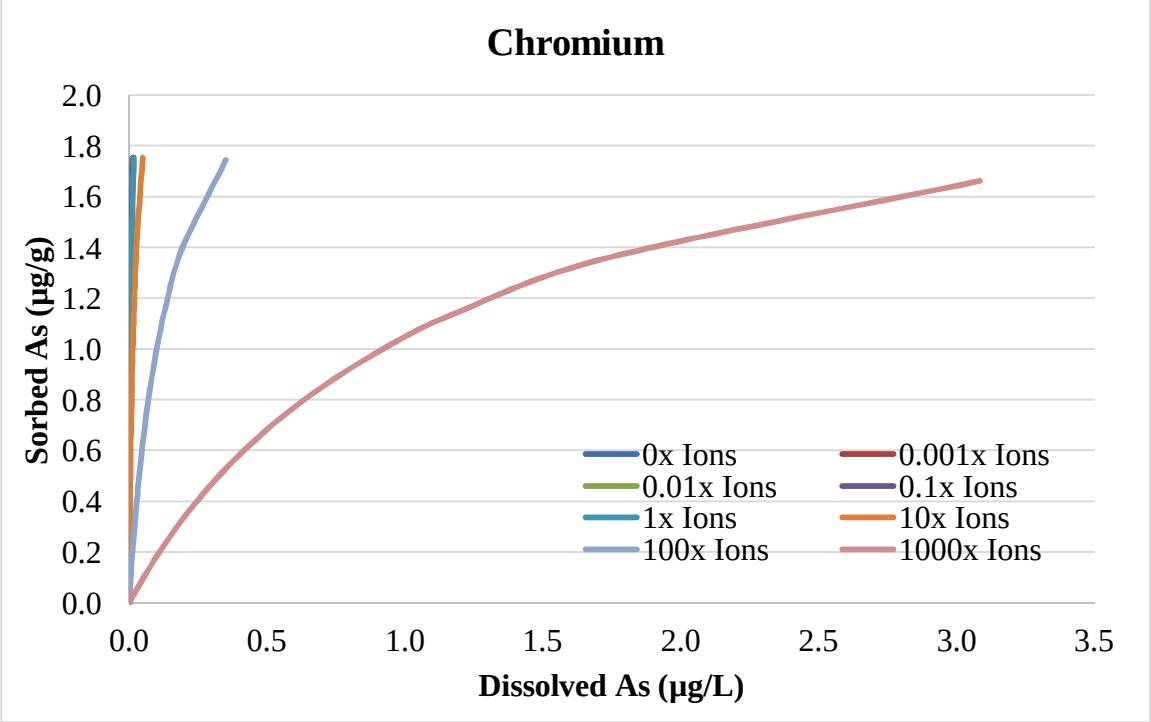

Figure 92: Cr adsorption sensitivity to variations in background constituents

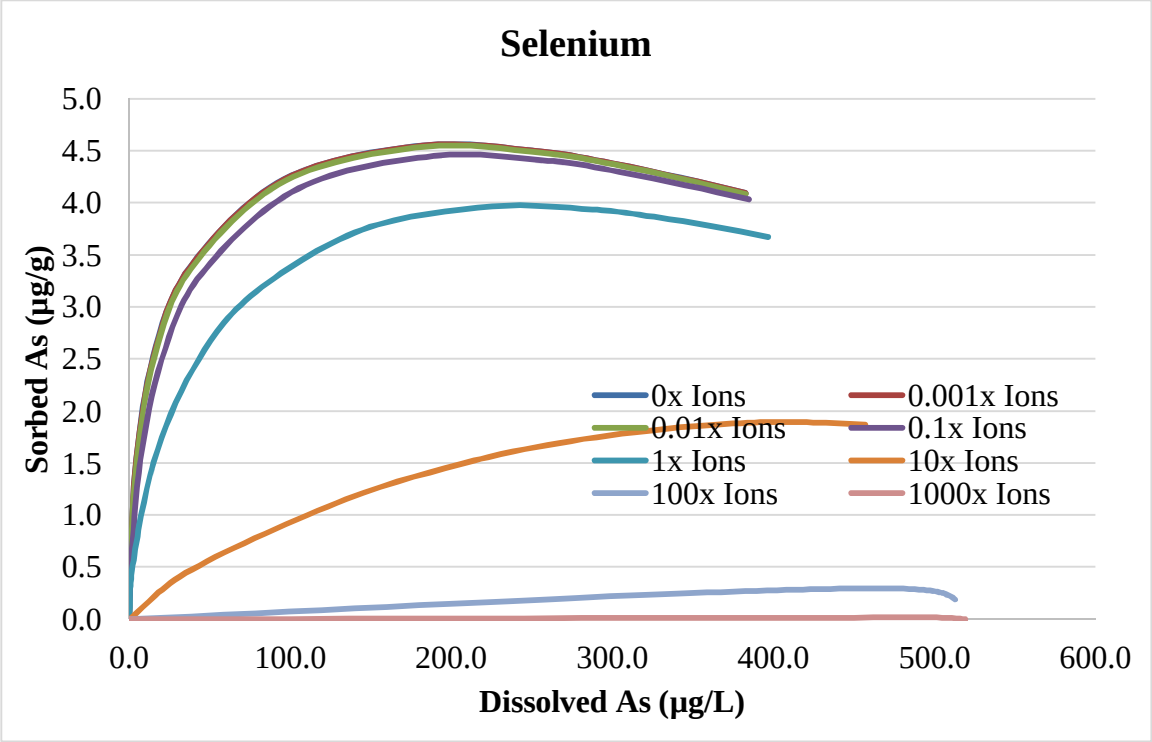

Figure 93: Se adsorption sensitivity to variations in background constituents

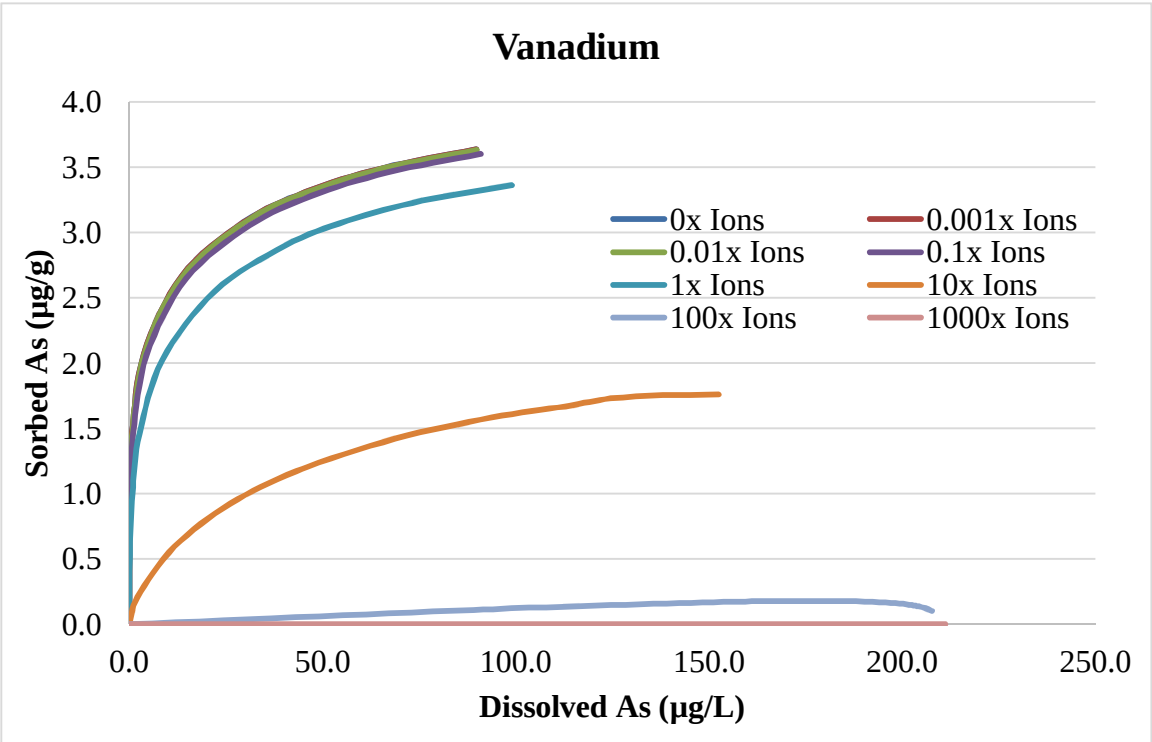

Figure 94: V adsorption sensitivity to variations in background constituents

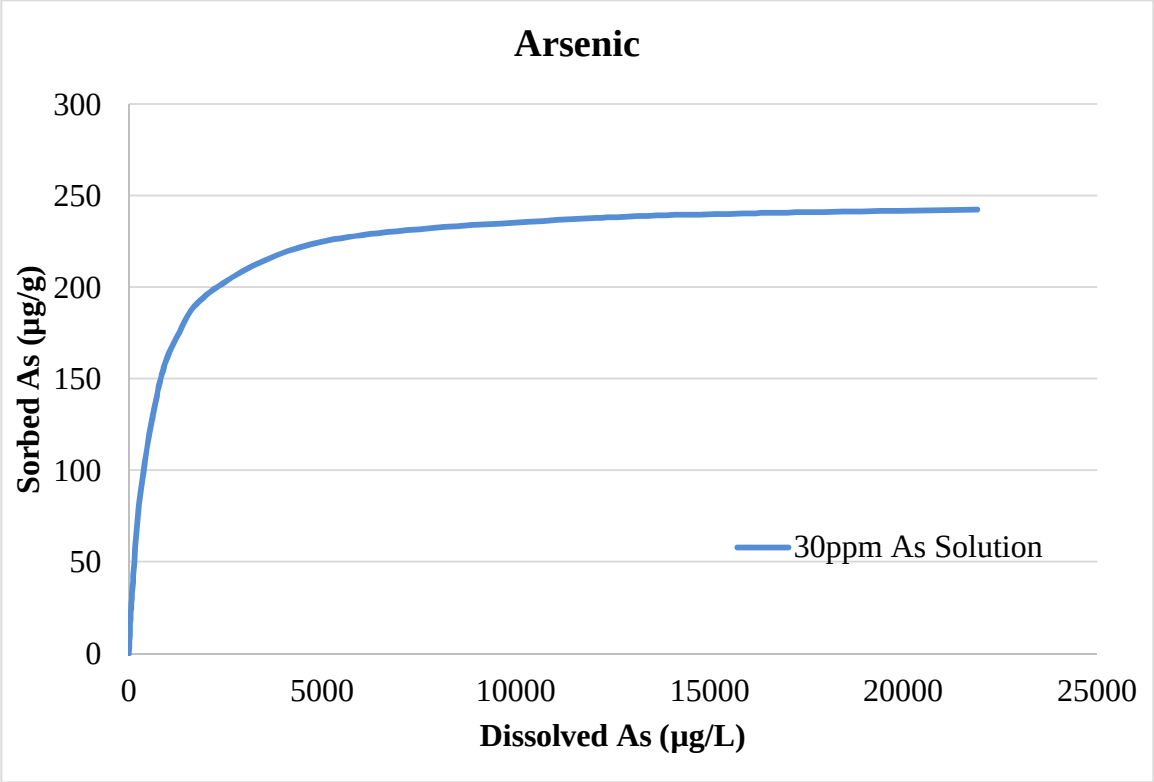

Figure 95: Adsorption capacity of As on HFO

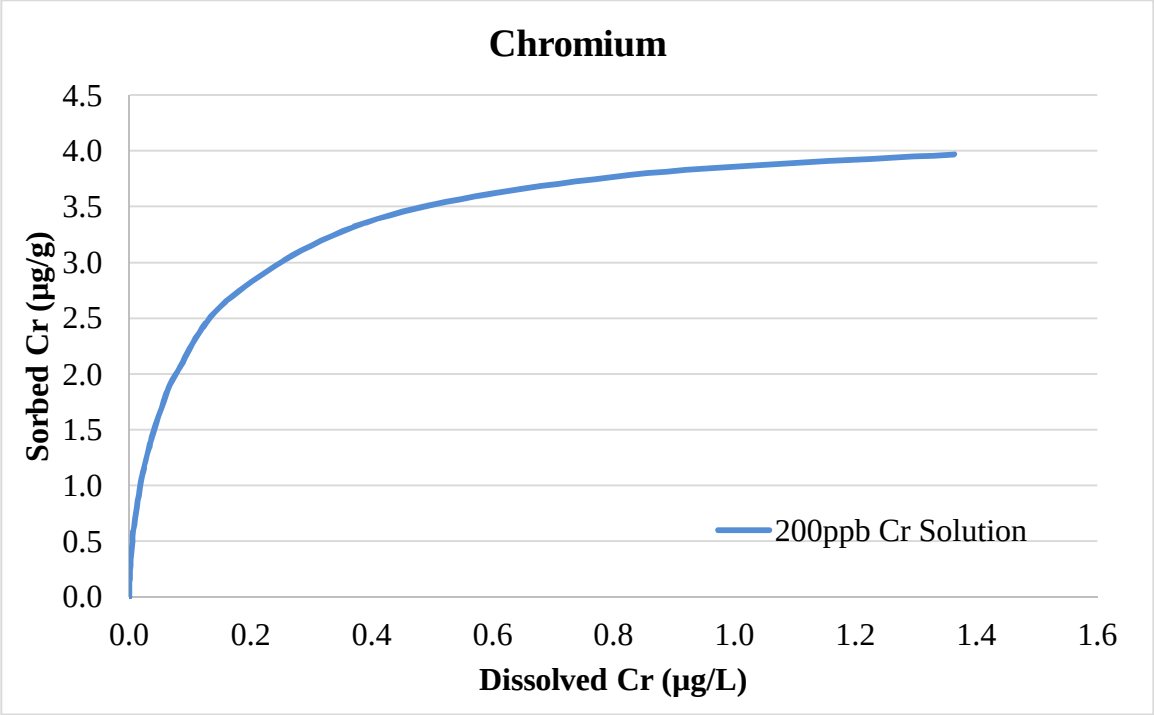

Figure 96: Adsorption capacity of Cr on HFO

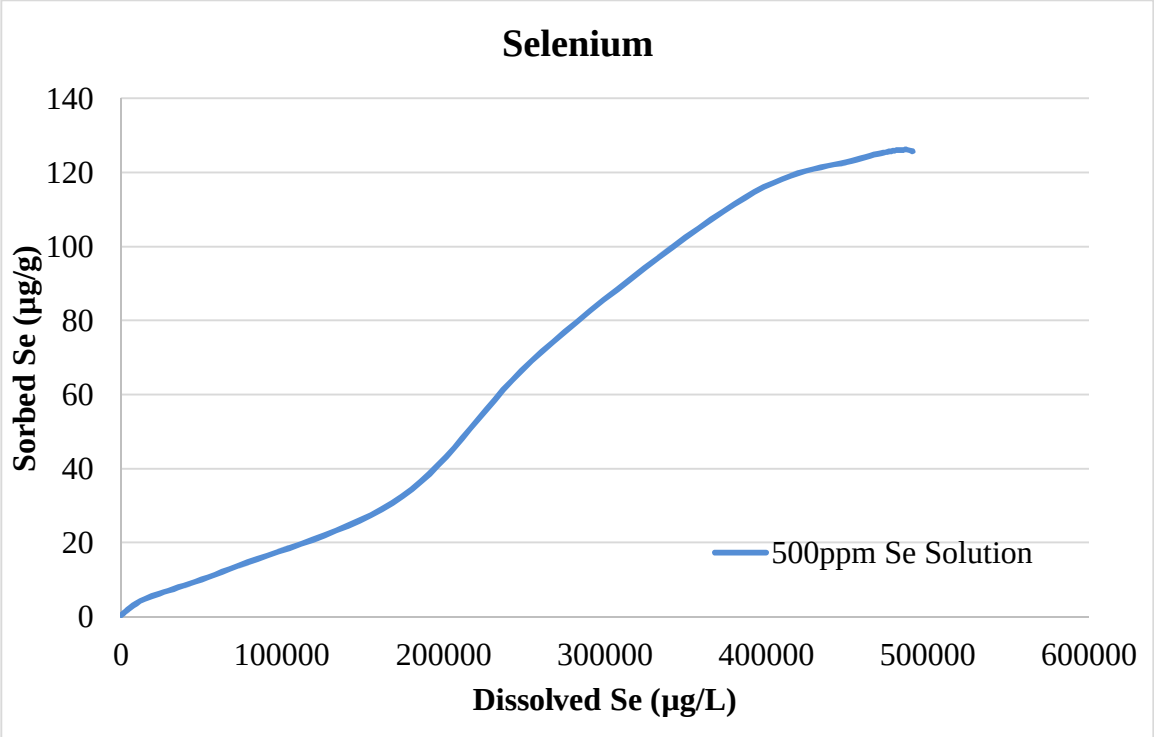

Figure 97: Adsorption capacity of Se on HFO

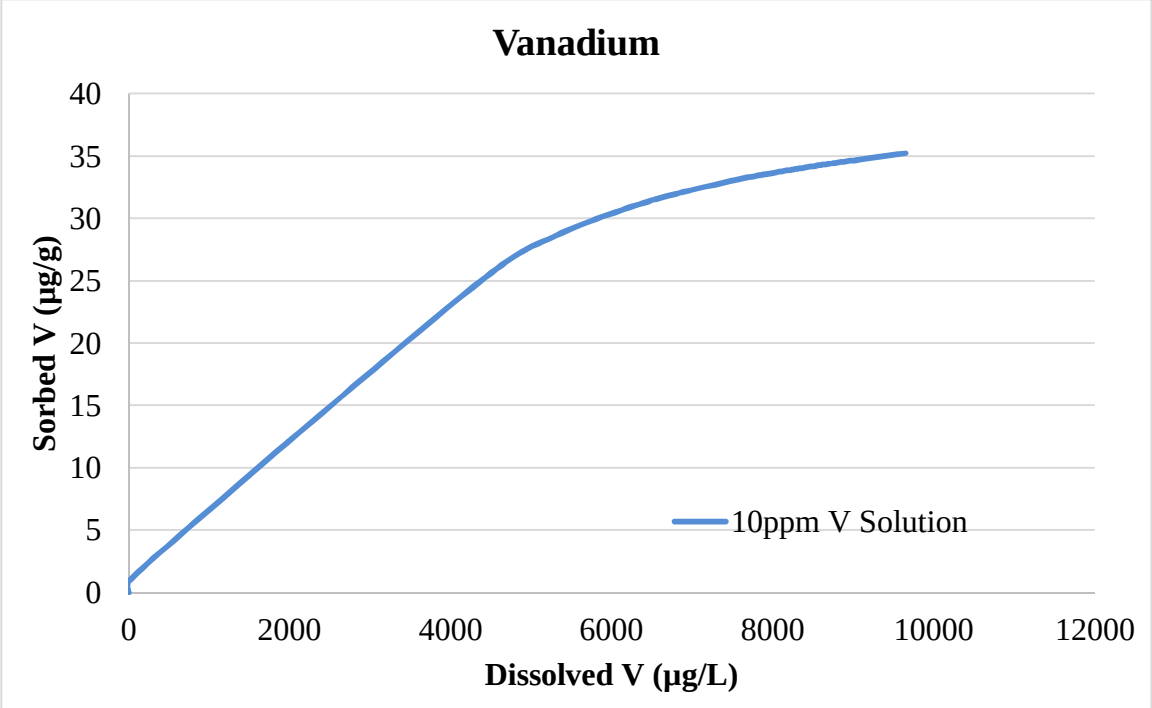

Figure 98: Adsorption capacity of V on HFO

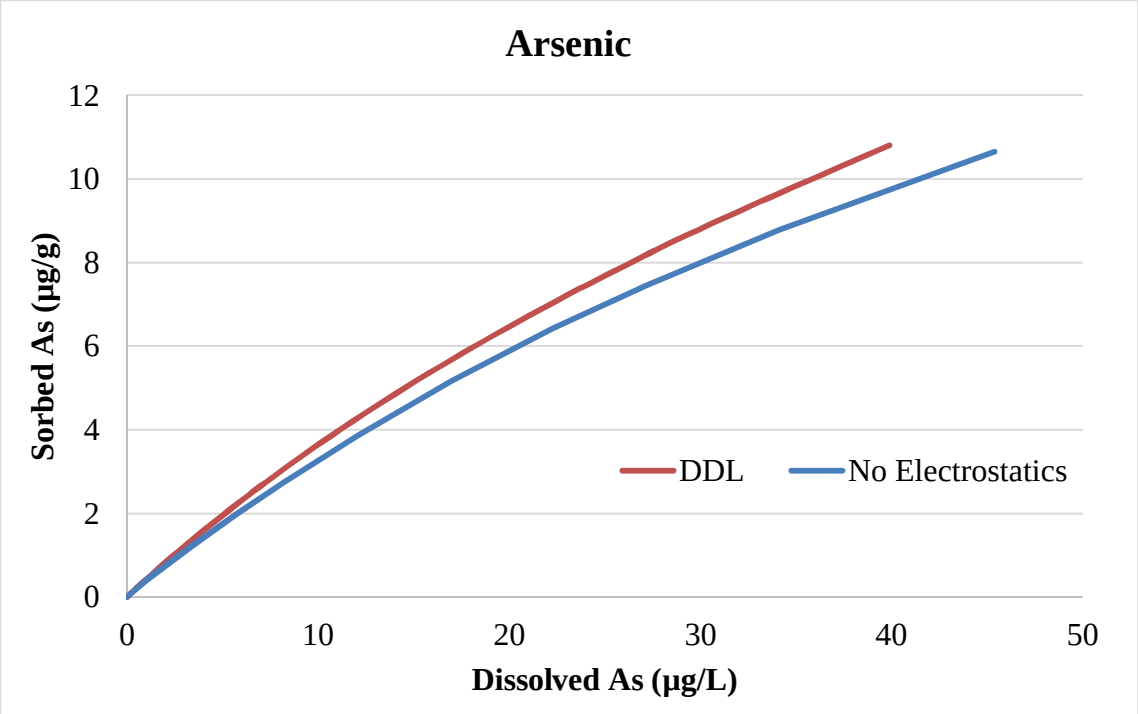

Figure 99: Base model with DDL vs base model without DDL – As

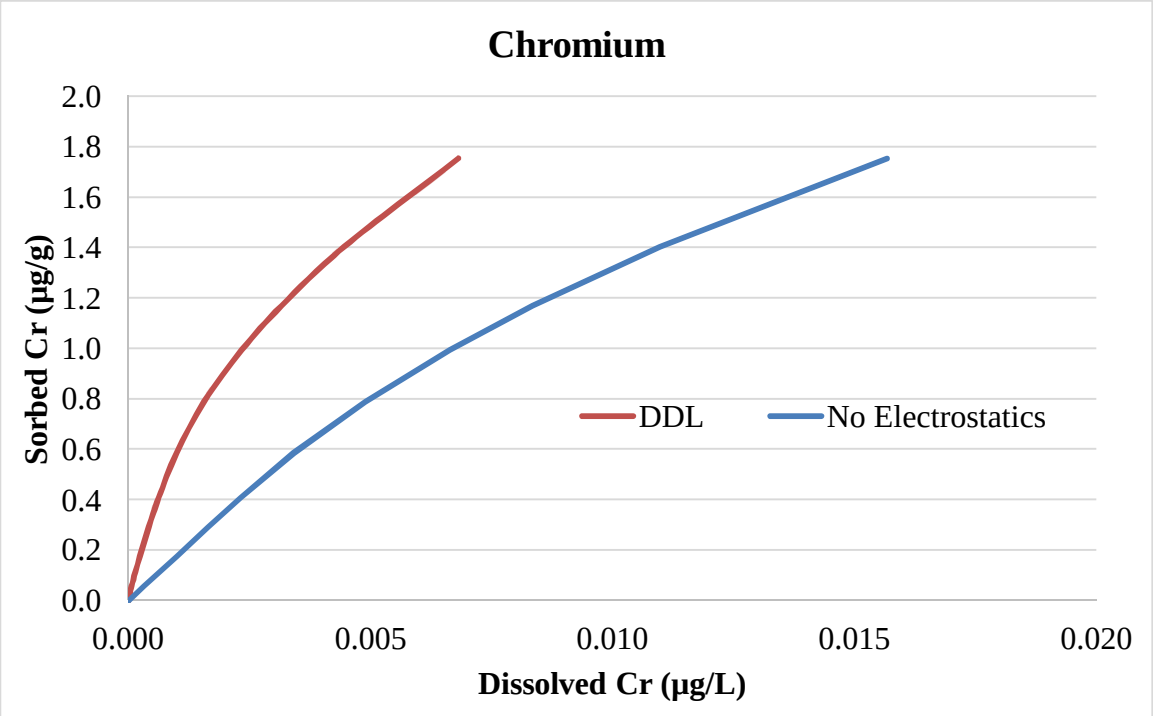

Figure 100: Base model with DDL vs base model without DDL - Cr

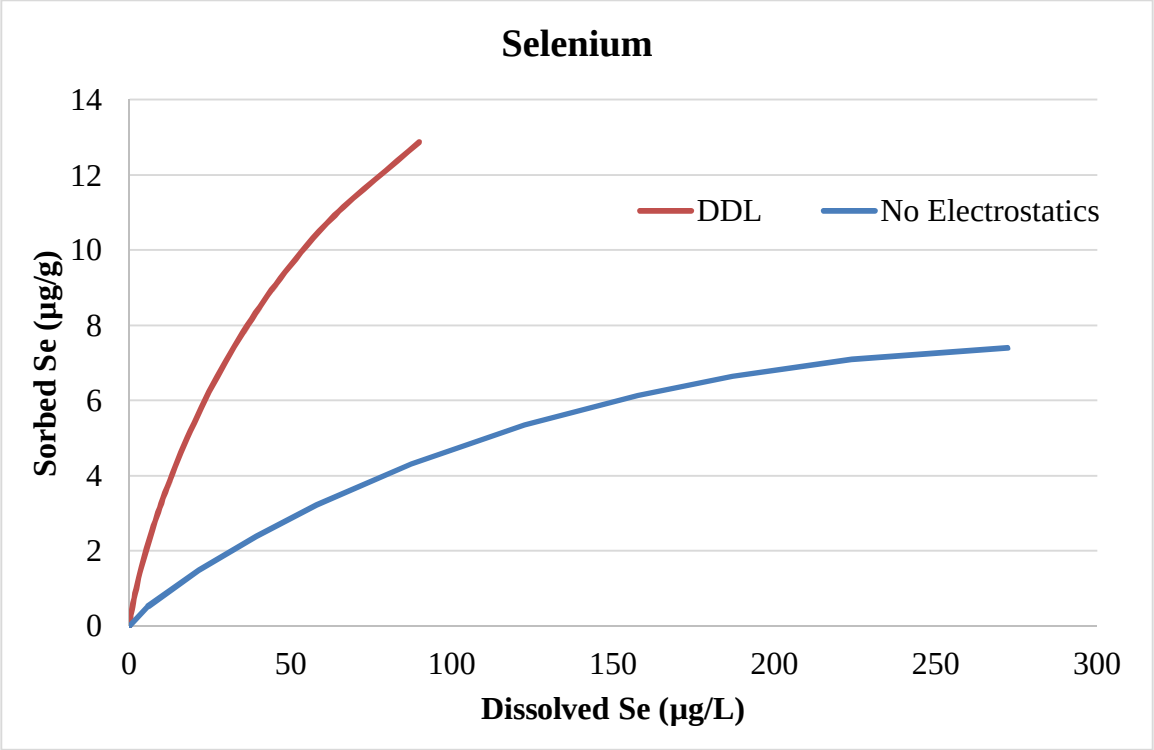

Figure 101: Base model with DDL vs base model without DDL – Se

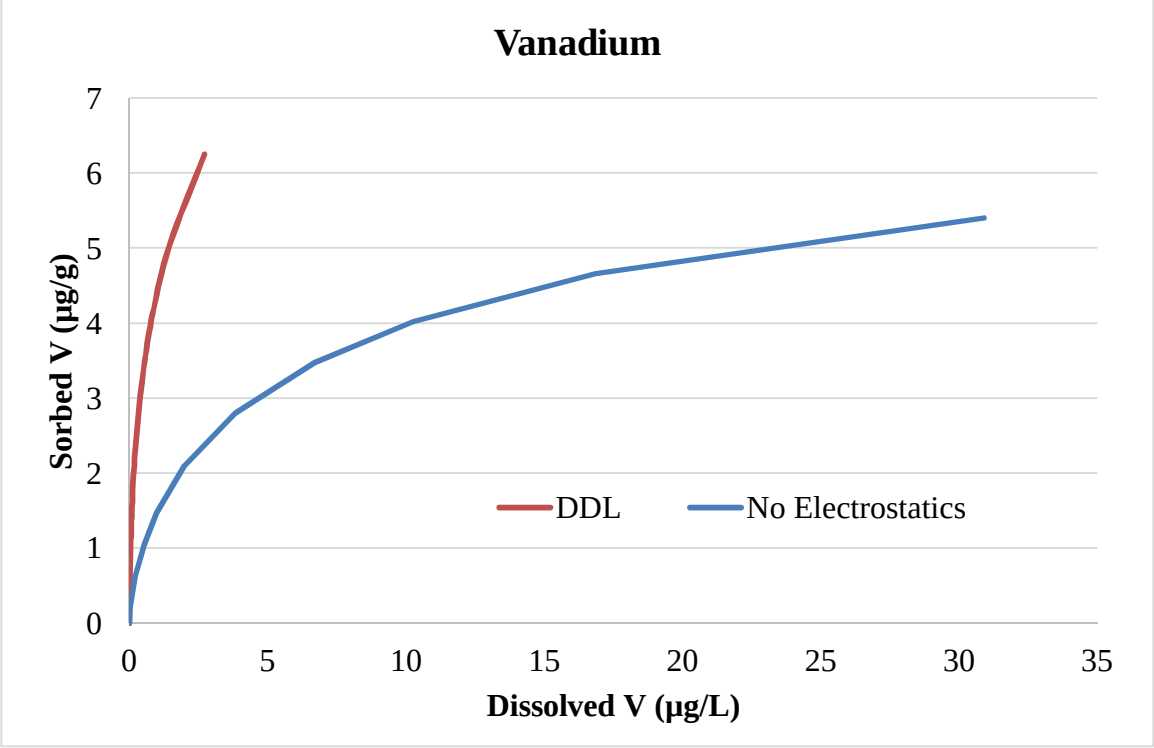

Figure 102: Base model with DDL vs base model without DDL - V

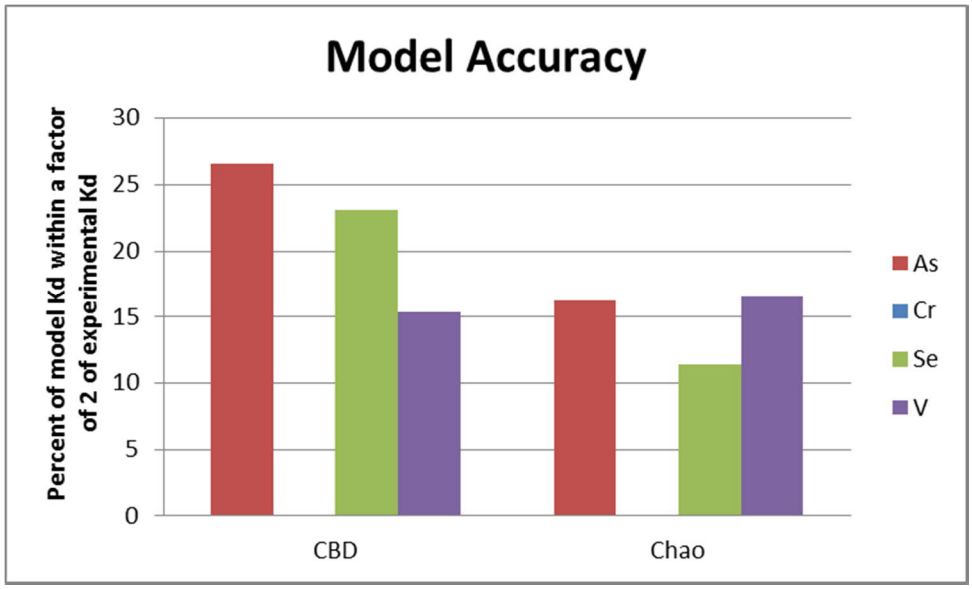

Figure 103: Percent model K_d values within a factor of 2 of experimental K_d values

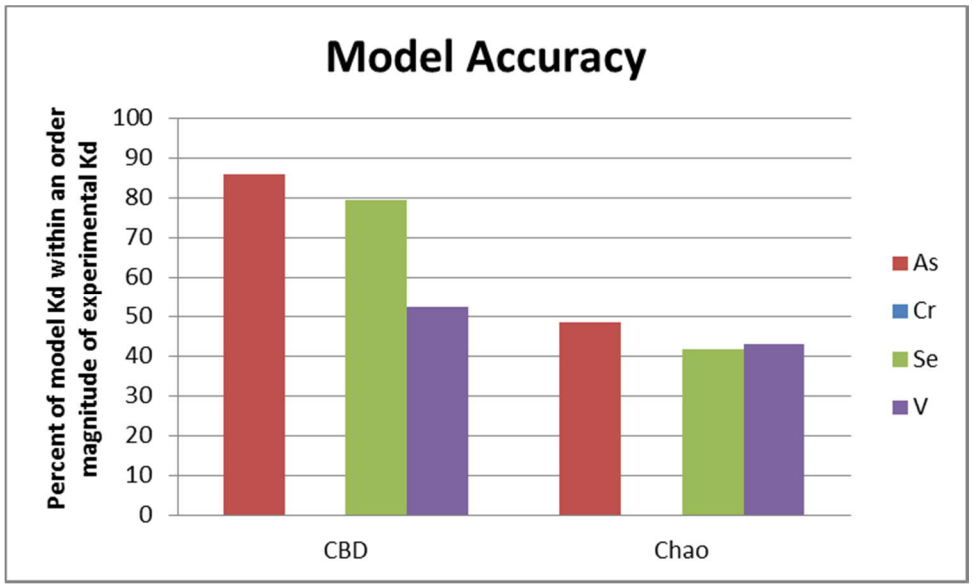

Figure 104: Percent model Kd values within a factor of 10 of experimental K_d values

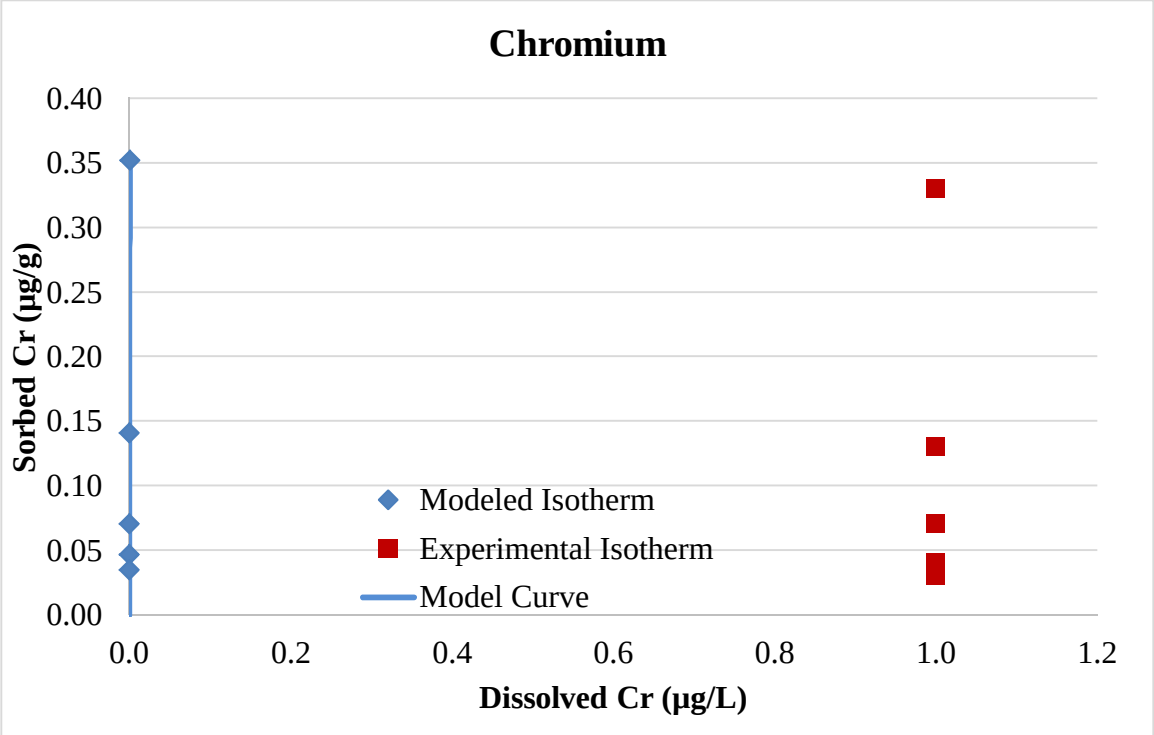

Figure 105: Allen AB-20S CBD model and experimental isotherms

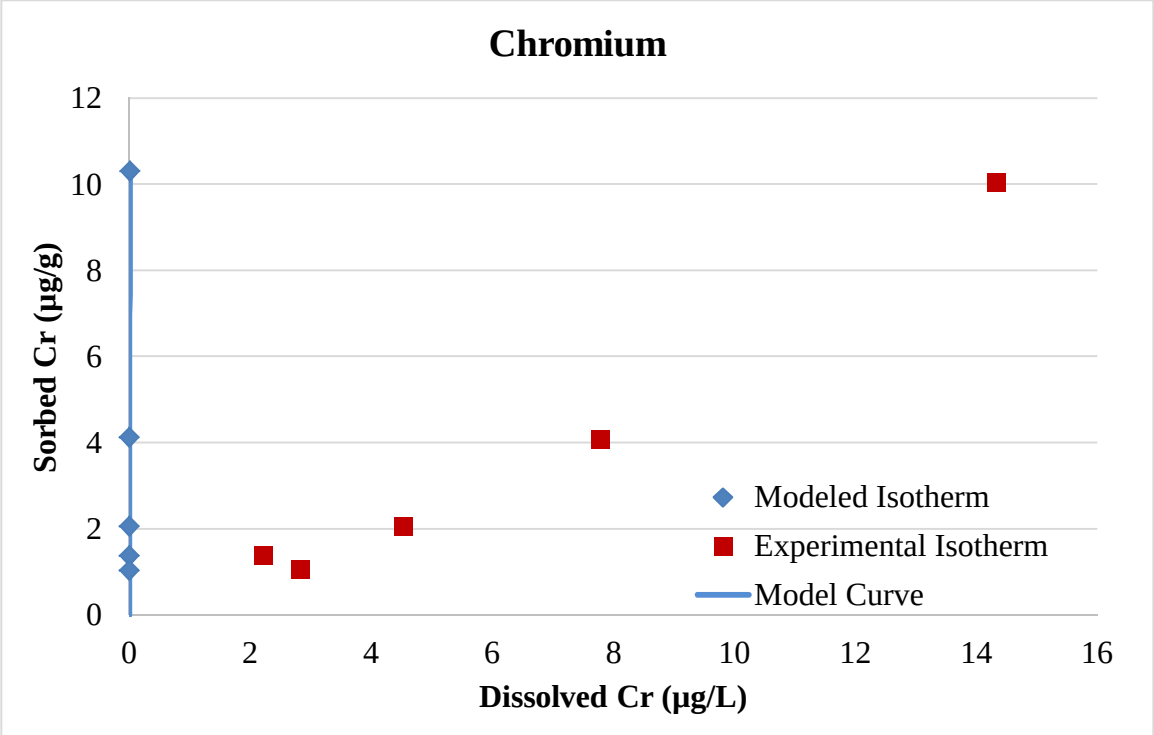

Figure 106: Allen AB-20D CBD model and experimental isotherms

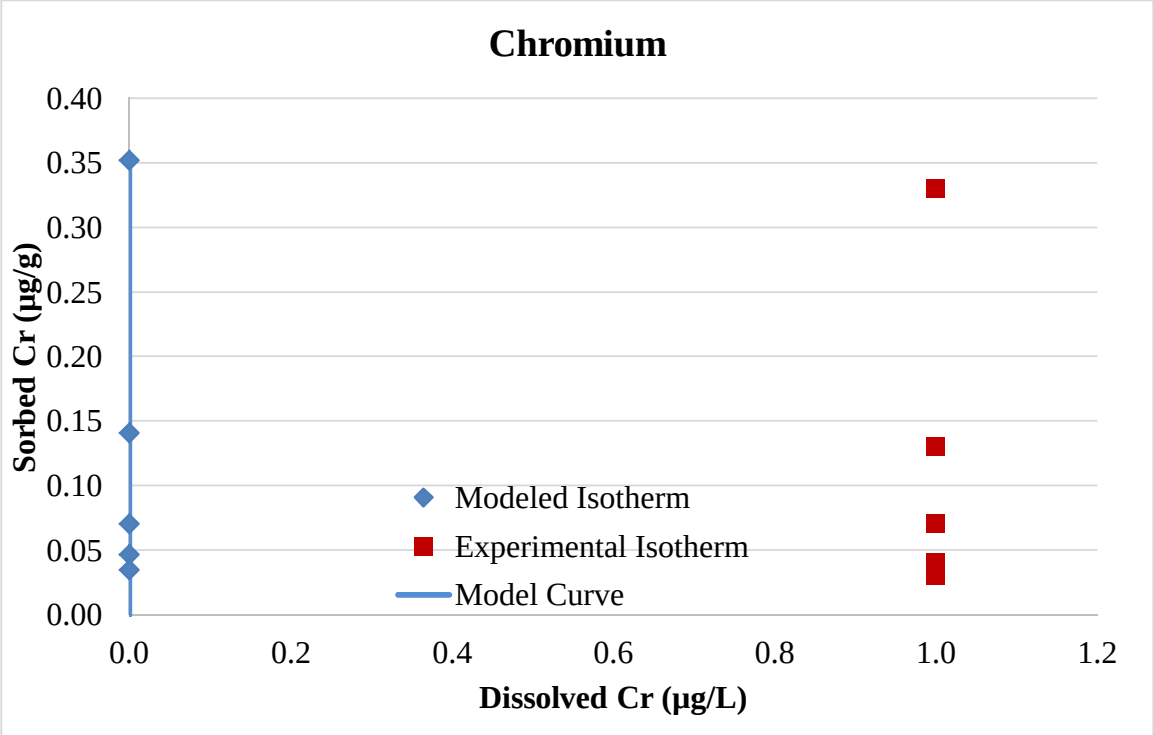

Figure 107: Allen AB-20S Chao model and experimental isotherms

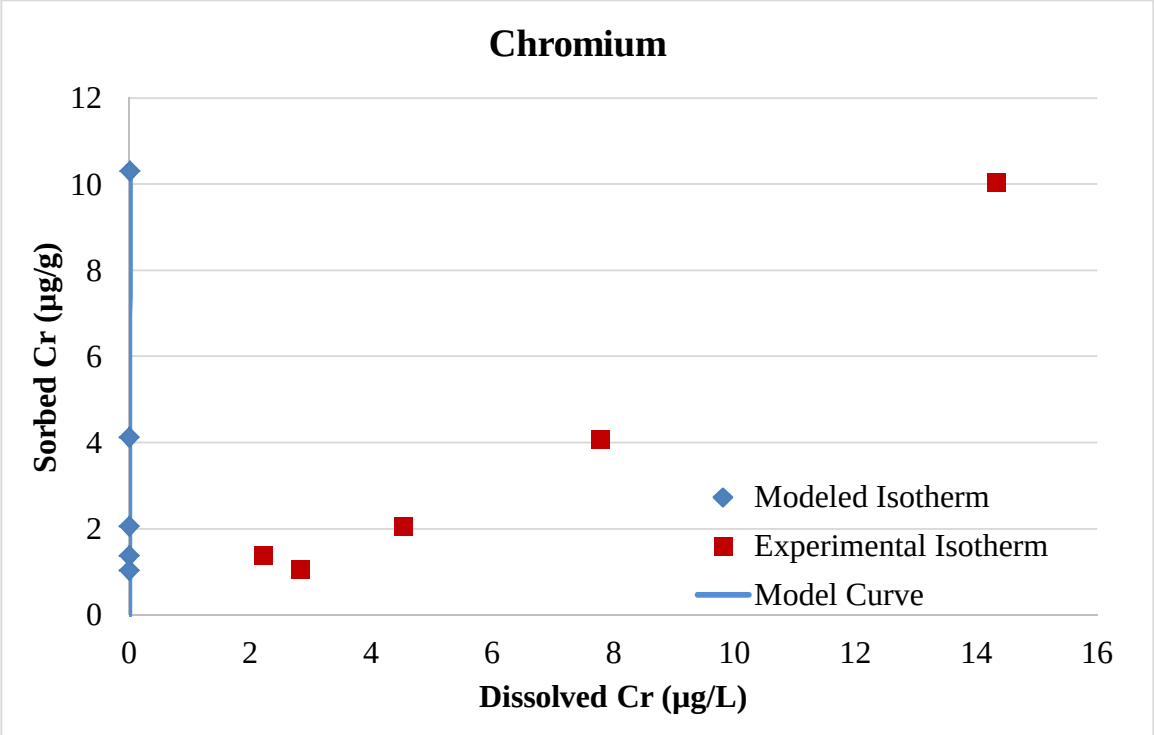

Figure 108: Allen AB-20D Chao model and experimental isotherms

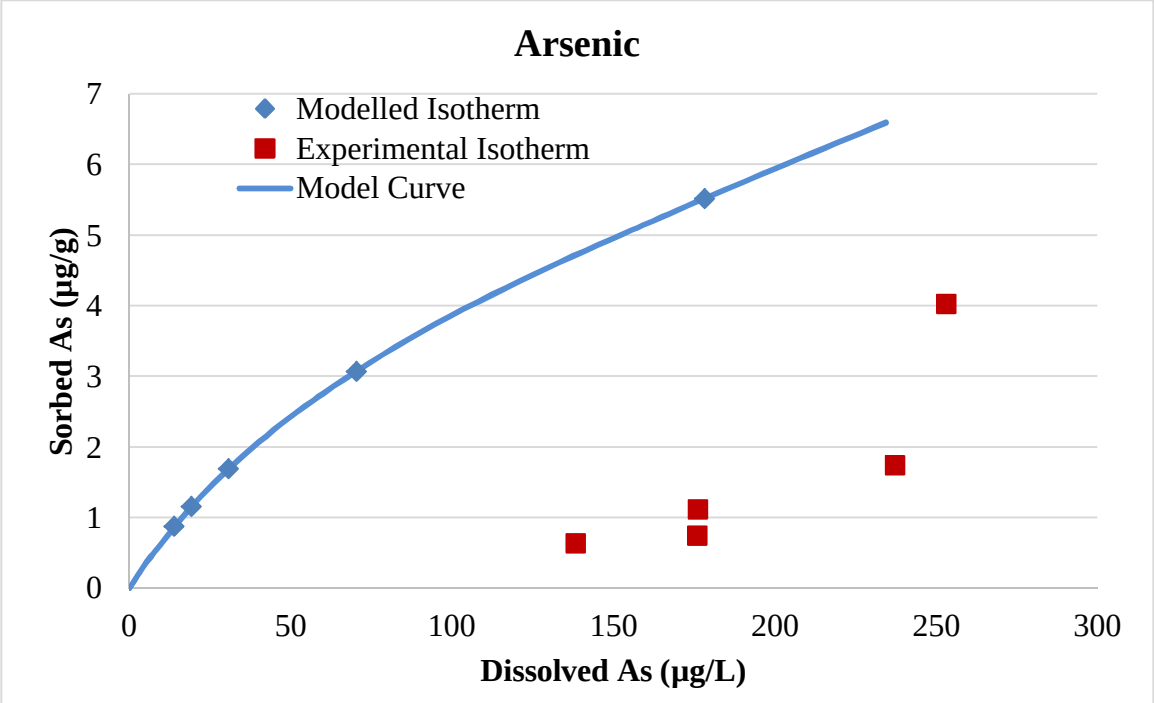

Figure 109: Allen AB-35R CBD method isotherm – As

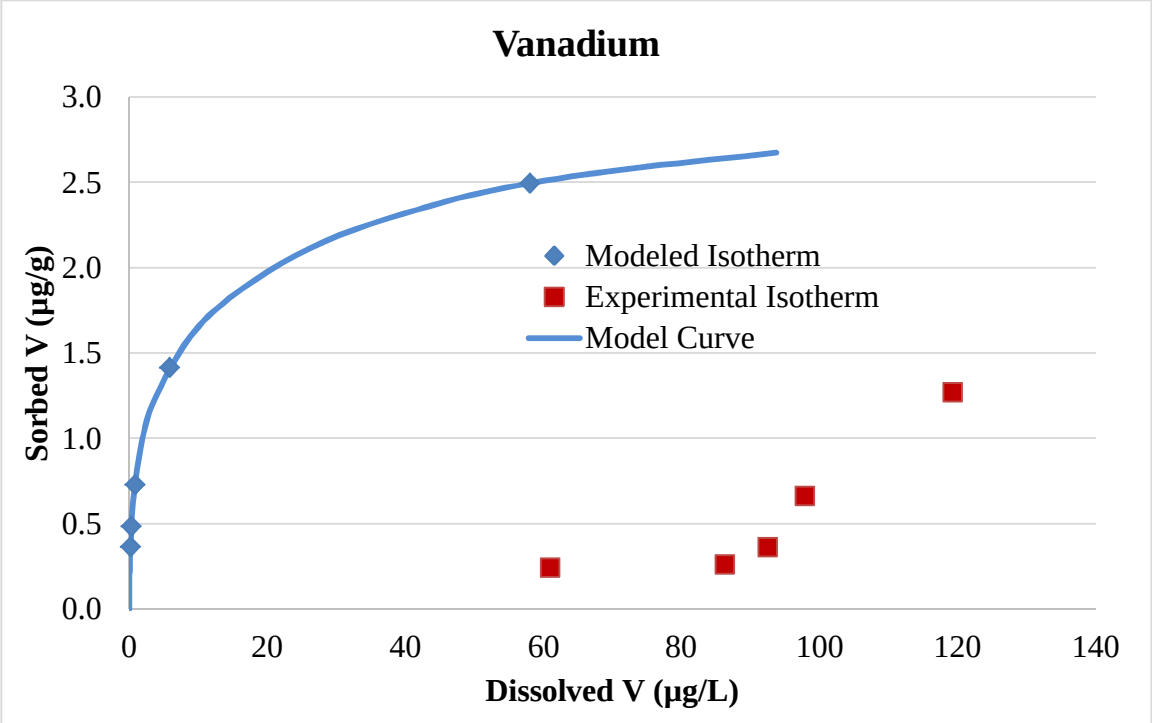

Figure 110: Allen AB-35R CBD method isotherm – V

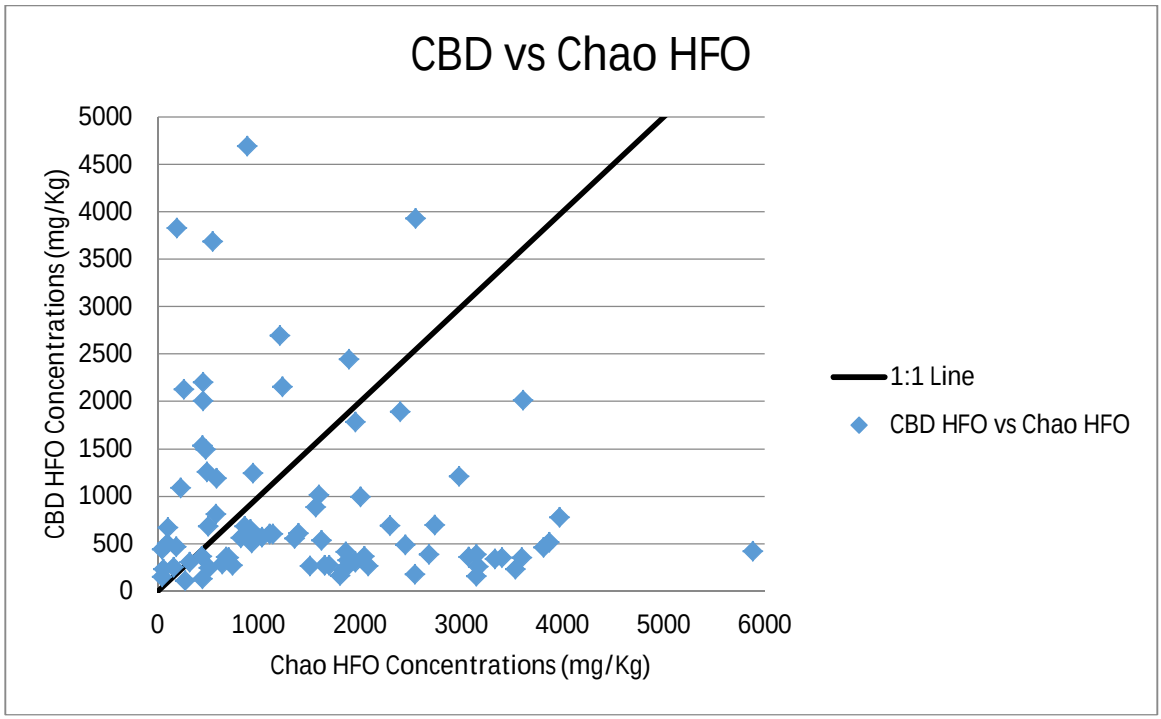

Figure 111: CBD vs Chao method HFO concentrations

APPENDIX C: PHREEQC SUPPLEMENTAL FILES AND ISOTHERMS

PHREEQC input, output, and database files are included in this work and are available through ProQuest at https://www.proquest.com/, and through the University of North Carolina at Charlotte J. Murrey Atkins Library. Supplemental files contained within in this submission include:

Name	File Type	Size	Software
CBD Batch Model	.pqi	111KB	PHREEQC
CBD Batch Model	.pqo	43.3MB	PHREEQC
CBD Batch Model-Cr	.pqi	111KB	PHREEQC
CBD Batch Model-Cr	.pqo	43.3MB	PHREEQC
Chao Batch Model	.pqi	112KB	PHREEQC
Chao Batch Model	.pqo	43.8MB	PHREEQC
Chao Batch Model-Cr	.pqi	122KB	PHREEQC
Chao Batch Model-Cr	.pqo	43.8MB	PHREEQC
Sensitivity Analysis-pH & Eh	.pqi	112KB	PHREEQC
Sensitivity Analysis-pH & Eh	.pqo	14.7MB	PHREEQC
Phreeqcmaster_2016	.txt	140KB	Notepad
Allen PHREEQC Batch Isotherms(CBD)	.xlsx	966KB	Excel
Allen PHREEQC Batch Isotherms(Chao)	.xlsx	969KB	Excel
Belews Creek PHREEQC Batch Isotherms(CBD)	.xlsx	731KB	Excel
Belews Creek PHREEQC Batch Isotherms(Chao)	.xlsx	679KB	Excel
Buck PHREEQC Batch Isotherms(CBD)	.xlsx	738KB	Excel
Buck PHREEQC Batch Isotherms(Chao)	.xlsx	737KB	Excel
Cliffside PHREEQC Batch Isotherms(CBD)	.xlsx	965KB	Excel
Cliffside PHREEQC Batch Isotherms(Chao)	.xlsx	964KB	Excel
Dan River PHREEQC Batch Isotherms(CBD)	.xlsx	795KB	Excel
Dan River PHREEQC Batch Isotherms(Chao)	.xlsx	852KB	Excel
Marshall PHREEQC Batch Isotherms(CBD)	.xlsx	795KB	Excel
Marshall PHREEQC Batch Isotherms(Chao)	.xlsx	795KB	Excel
Riverbend PHREEQC Batch Isotherms(CBD)	.xlsx	909KB	Excel
Riverbend PHREEQC Batch Isotherms(Chao)	.xlsx	908KB	Excel